IDENTIFICATION OF REGIONAL SHALE GAS SWEET SPOTS AND UNCONVENTIONAL RESERVOIRS USING WELL LOGS AND SEISMIC DATA

By

ABUDRAHIM ELKASEH

A dissertation submitted in partial fulfillment of the requirements for the degree of Doctor of Philosophy

Faculty of Engineering and Science

School of Earth and Planetary Sciences

Curtin University

Supervisors:

January 2022

Abstract

The integral motivation of this research is to postulate a novel approach to determining the correlation between static and dynamic rock elastic parameters by utilizing a total of five core samples taken from five wells (Fruitcake-1, Missing-1, Looma-1, and Canopus-1), in the Canning Basin, Australia. The ability to rapidly transform in situ dynamic rock elastic properties to their static counterparts heavily relies on the accuracy of the predictive equations computed to achieve this correlation. The rapid determination of static properties is fundamental to achieve fast reservoir characterization for an immediate direction of reservoir development and management. Fracking jobs and consequent reservoir fracture management is dependent on the accuracy of the predictive correlation equations linking dynamic to static rock elastic parameters. In the Canning Basin, there is a significantly small number of geomechanical tests conducted to acquire the necessary elastic properties data for optimum reservoir modeling and characterization. Correlating static and dynamic parameters, seven important rock elastic modulii fundamental were calculated towards reservoir characterization of shale gas including Young's modulus (E), Poisson's ratio (ν), brittleness index, shear modulus (k), bulk modulus (G), Lambda.Rho (λ.Rho) and Mu.Rho (μ.Rho). In this research, rock physics parameters are utilized to create geostatistical models mapping the in-situ spatial distribution of the aforementioned rock parameters. Acoustic waves (P and S waves) modeling (or inverse seismic modeling) of post-stack data was used as reference data to check the reliability of the predictive models determined from the seven rock elastic parameters.

The first set of research activities involved the determination of the predictive empirical correlation equations for the dynamic and static parameters estimations using the results of the

laboratory tests on the core samples. The simulation results indicated that the developed empirical correlation equations linking static to dynamic rock elastic parameters have high predictive ability. In particular, a high correlation (R^2 of 0.69 to 0.97) between the modeled and the predicted rock elastic parameters was achieved. The results are important in shale gas exploration activities as they meet reliable criteria to rapidly predict the in situ reservoir characteristics from a small number of well core samples. It should be noted that laboratory studies to accurately determine in situ rock strength and deformation parameters are expensive and time-consuming. Furthermore, the ability of the current research to model the in situ spatial distribution of brittle shale (especially areas adjacent to the Fruitcake-1 well) depicts the higher and lower ranges of mechanical properties throughout the formation. In summary, the results show an improved ability to compute correlation equations with higher predictive ability and capability at the understanding and spatial mapping of rock mechanical properties in shale gas reservoirs. Thus, by adopting this approach, geophysicists and other petroleum researchers can be able to rapidly estimate the static rock parameters from their dynamic counterparts derived from well logging data. Besides, the results of this approach will aid to reduce uncertainty in mapping and modeling in situ rock elastic parameters. Furthermore, the employed approach could ease the designing and modeling of reservoir hydraulic fracturing.

Keywords: Brittleness index, dynamic and static rock elastic moduli, Canning Basin, Shale gas, Poisson's ratio

Acknowledgments

I would like to acknowledge and sincerely thank the following persons who made the completion of this work possible:

Allah, the Almighty God for blessing me with the gift of life and good health, strength, capability, and patience.

My wife and my family for their unconditional love and supporting me during the entire research period.

My major supervisor, Prof. Reza Rezaee for his continuous guidance and valuable pieces of advice.

My co-supervisor, Dr. Ali Kadkhodaie for his encouragement, corrections, and valuable advice.

My co-supervisor, Dr. Said Amiribesheli for his valuable inputs, encouragement, and advice.

My friends for their moral support and motivation.

Table of Contents

Abstract iii

Acknowledgments v

List of Abbreviations xi

List of Tables xiii

List of Figures xiv

1 INTRODUCTION 1

1.1 Introduction 1

1.2 Research Background and Purpose 1

1.3 Research Objectives 4

1.4 Overview 5

1.5 Study Area 6

1.6 Data Set Overview 6

1.7 Geology of the Canning Basin 7

1.7.1 Geological Setting 7

1.7.2 Geological Formations and Petrology 11

1.7.3 Stratigraphic Analysis 13

1.8 Summary 14

2 LITERATURE REVIEW 16

2.1 Reservoir Characterization 16

2.2 Rock Elastic Properties 19
2.2.1 Young’s Modulus 19
2.2.2 Lateral strain 19
2.2.3 Poisson's ratio 19
2.2.4 Volumetric strain 20
2.2.5 Bulk modulus 20
2.2.6 Static Shear modulus 20
2.2.7 Static Lame’s Constants 20
2.2.8 Dynamic Young’s Modulus 21
2.2.9 Dynamic Poisson’s Ratio 21
2.2.10 Dynamic Bulk Modulus 21
2.2.11 Dynamic Shear Modulus 21
2.2.12 Dynamic Lame’s Constants 21
2.2.13 Porosity 21
2.3 Seismic Attributes 22
2.4 Well Log Evaluation 23
2.4.1 Spontaneous Potential (SP) Logs 23
2.4.2 Gamma Ray (GR) Logs 23
2.4.3 Neutron Porosity Logs 24
2.4.4 Density Porosity Logs 24

2.4.5 Sonic Log 24
2.4.6 Caliper log 25
2.4.7 Petrophysical Analysis Using Cross plots 25
2.5 Seismic Inversion 25
2.5.1 Forward Seismic Modeling 25
2.5.2 Inverse Seismic Modeling 26
2.6 Interpretation of Seismic Data 27
2.7 Previous Work on Sweet Spot Identification 28
2.7.1 Parameters Affecting Sweet Spots Sweet Spots in Unconventional Reservoirs 28
2.7.2 Criteria for the Identification of Sweet Spots 29
2.7.3 Factors Affecting Shale Gas Presence 29
2.7.4 Quantification of Shale Gas 30
2.7.5 Sweet Spot Identification by Analysis of 3D Seismic Data 30
2.7.6 Sweet Spot Identification Using Electric Logs 31
2.8 Summary 33
3 METHODOLOGY & 3D GEOMECHANICAL MODELING 34
3.1 Data 34
3.2 Modeling Tool 35
3.3 Building 3D Model for the Goldwyer Formation 36
3.3.1 Initialization, Data Importation and Quality Control 36

3.3.2 Seismic Data 36
3.3.3 Well Data 37
3.4 Structural Modeling 37
3.5 Geomechanical Property Modeling 39
3.5.1 Scale Up Well Logs 40
3.5.2 Comparison of the Model's Well Log Data with the Original Well Log Data 40
3.5.3 Geomechanical Parameters Modeling 40
3.6 Brittleness Index Modeling 42
3.7 Regression Modeling 42
4 RESULTS OF MODELING ESTIMATION 44
4.1 Elastic Properties Results 44
4.1.1 Graphical Correlations between Dynamic and Static Elastic Parameters 51
4.1.2 Evaluation of Rock Elastic Parameters versus Depth 54
4.1.3 In Situ Inter-well Geomechanical Mapping/Modeling of Determined Rock Deformation Properties 55
4.1.4 In-Situ Reservoir Deformation Parameter Simulations/Models 61
4.2 Brittleness Index Model 62
4.3 Summary 63
5 SEISMIC INVERSION 65
5.1 Seismic Inversion Results 65

5.1.1 Poisson's Ratio 75

5.1.2 Mu.Rho 76

5.1.3 Lambda.Rho 77

5.1.4 Bulk Modulus 78

5.1.5 Shear Modulus 79

5.1.6 Brittleness Index 80

5.2 Summary 81

6 RESEARCH FINDING'S COMPARISONS, SIGNIFICANCE, DISCUSSION, CONCLUSION AND RECOMMENDATIONS 83

6.1 Comparing the Research's Findings to Current Extant Literature, Studies and Results 83

6.2 Result, Discussions and Evaluations 85

6.3 Conclusions 86

6.4 Recommendations 88

References 89

STATEMENT OF ORIGINAL WORK 96

List of Abbreviations

1D: One dimensional

2D: Two dimensional

3D: Three dimensional

AI: Acoustic impedance

API: American Petroleum Institute

ASCII: American Standard Code for Information Interchange

AVO: Amplitude variation with offset

CQ: Completion quality

DT: Delay Time

E&P: Exploration and production

g/cc: grams per cubic centimeter

GPa: Giga Pascal

h: Euclidean distance

LAS: Log ASCII Standard

Ltd: Limited

MQ: Mechanical quality

ms: millisecond

NPHI: Neutron porosity hydrogen index

OQ: Organic quality

Pa: Pascal

PNN: Probabilistic neural network

P-wave: Primary wave

QC: Quality Control

RHO: Bulk Density

R_{mf}: Mud filtrate resistivity

RQ: Rock quality

R_w: Water resistivity

S-wave: Secondary/Shear wave

TOC: Total Organic Carbon

USA: United States of America

V_p: Primary wave's velocity

V_s: Secondary wave's velocity

Q: Quality factor

List of Tables

Table 4.1: Tabulation of results for the static rock elastic parameters obtained from uniaxial compressive strength empirical laboratory tests on plugs of core samples. 44

Table 4.2: Tabulation of results for the dynamic rock elastic parameters obtained from empirical acoustic logs of plugs of core samples..... 45

Table 4.3: Tabulation of computations to empirically determine the coefficients correlating the predicted static to the determined dynamic rock elastic parameters..... 53

List of Figures

Figure 1.1: Map depicting the world's potential of shale gas production from the most explored to the least explored shale gas resources (modified from the International Energy Association as reported by Carstens, 2014) 3

Figure 1.2: The location (top-right inset figure) and tectonic features of the Canning Basin (enlarged bottom figure depicting the wells at the Crossland Platform) (Burt, Champ & Parks, 2002). 10

Figure 1.3: A 3-Dimensional illustration of the main geological features of the Canning Basin, Western Australia..... 11

Figure 1.4: The general stratigraphy of the Canning Basin (GSWA, 2014). 12

Figure 2.1. The estimation the brittle shale from log data. 18

Figure 2.2: Dip Azimuth map (a horizon seismic attribute) of a seismic trace from a depth of 1500m to 4500m (Chopra et al., 2007). 22

Figure 2.3: Illustration of the convolution model. 26

Figure 2.4: Illustration of seismic inversion process. 27

Figure 3.1. Location of the 11 wells in Canning Basin, Western Australia..... 34

Figure 3.2: Study area limited to 5 out of 11 wells whose data were available. 35

Figure 4.1: Static and dynamic Young's modulus variation with depth. 46

Figure 4.2: Static and dynamic Poisson's ratio variation with depth. 47

Figure 4.3: Static and dynamic bulk modulus variation with depth. 48

Figure 4.4: Static and dynamic shear modulus variation with depth. 49

Figure 4.5: Static and dynamic Lambda.Rho variation with depth. 50

Figure 4.6: Static and dynamic Mu.Rho variation with depth. 51

Figure 4.7: Correlations of dynamic versus statistic rock elastic moduli. 52

Figure 4.8: Plots comparing the variations of Young's Modulus (E), Poisson's Ratio (υ), bulk modulus (K), shear modulus (G), Lambda.Rho (λ.Rho) and Mu.Rho (μ.Rho) rock deformation properties versus depth for all the wells. 55

Figure 4.9: The distribution of Young's modulus from the data sample. The distribution of Young's moduli parameters between wells is illustrated be change from high to low and high again. 56

F**igure 4.10:** Depiction of Poisson's ratio between the target wells. a) The model depicts a cross-section of the Poisson ratio over the study area. b) The model depicts one of the 3D average realizations estimated the distribution of the Poisson ratio values. 57

Figure 4.11. The brittleness index parameter and its overall distribution around the reservoir area around the wells (top picture) and the cross-section of the brittle shale model (bottom picture). 58

Figure 4.12: a) Model is an attempt to map the static bulk modulus parameter for the area surrounding the wells. b) is the depiction of the cross-sectional distribution of static bulk modulus instances with the greenish portions showing the areas with the highest values within the predicted in-situ reservoir model. 58

Figure 4.13: The shear modulus of the reservoir area surrounding the wells. (b) was conceived from the data and depicted the best-case scenarios for the shear modulus deformation parameters around the wells..... 59

Figure 4.14: (a) A section of the area immediately surrounding the wells. High Lambda values are mapped to the one side of the area near the Fruitcake-1 and Missing-1 wells. (b) A 3D

model of Lamda parameter and its spatial distribution across the entire reservoir area that includes the wells. 60

Figure 4.15: (a) A 2D section of the Mu.Rho parameter across the reservoir area of the sample wells under consideration. b) The plot is a depiction of the best-fit model that attempted to analyze the spatial distribution of this parameter for the wells under consideration. 60

Figure 4.16: Plots showing the gamma ray, Lambda.Rho, Mu.Rho and brittleness index variations with respect to depth for the targeted formations. 61

Figure 4.17. Graph showing the correlation between Young modulus and Poisson's ratio indicating a complex relationship. 62

Figure 4.18. Brittleness index model of the Goldwyer Formation in the study area 63

Figure 5.1: Example of the P-impedance inversion analysis of one well for the Goldwyer Shale. The blue curve is P-impedance, the red curve is the synthetic seismogram and the black curve is the seismic trace. 67

Figure 5.2: Background model for the Fruitcake-1 well. 68

Figure 5.3: Background model for the Looma-1 well. 69

Figure 5.4: Seismic inversion results for the Fruitcake-1 well. 70

Figure 5.5: Seismic inversion results for the Looma-1 well. 71

Figure 5.6: Seismic inversion results for the Missing-1 well. 72

Figure 5.7: Seismic inversion of the Missing-1well model. The black curve shown at the well location is the gamma ray. 73

Figure 5.8: Seismic inversion of the Looma-1 well model..... 74

Figure 5.9: The model of Poisson's modulus across the study area. 75

Figure 5.10: The model of Young's modulus across the study area. 76

Figure 5.11: The model of Mu.Rho across the study area. 77

Figure 5.12: The model of Lambda.Rho across the study area. 78

Figure 5.13: Model and mapping of bulk modulus across the study area. 79

Figure 5.14: The model of shear modulus across the study area. 80

Figure 5.15: The model of brittleness index across the study area. 81

Figure 6.1: Sweet spot maps for all Goldwyer zones in the Canning Basin Barbwire terrace as reported by Alshakhs (2017). 86

1 INTRODUCTION

1.1 Introduction

A key objective of the upstream petroleum industry, which primarily deals with exploration and production (E&P), is to accurately predict and identify hydrocarbon provinces in a fast and economical manner. This is particularly important for the upstream petroleum industries dealing with the exploration of unconventional resources such as shale gas plays that have lower permeability as compared to conventional hydrocarbon resources. To this end, seismic data have for a long time been used to identify and locate faults, fractures, and karst regions in wells, thus to avoid drilling in such areas. The presence of faults, fractures, and karsts affects the successful completion of wells (Bacon et al., 2007). This research presents a modified approach that facilitates the rapid prediction of static rock elastic parameters from their dynamic counterparts that can successfully be utilized to predict, map, and model the geomechanical properties of in-situ shale gas plays. Such an approach could be of great significance in the E&P industry as it would facilitate faster and accurate identification of preferential drilling locations in unconventional hydrocarbon resources resulting in a significant drop in oil and gas exploration and production costs.

1.2 Research Background and Purpose

The exploration of shale gas reservoirs has already been done extensively in the USA (such as the Barnett, Fayetteville, Eagle Ford, and Haynesville) and interest in exploring unconventional resources spread to Australia in regions such as the Canning and Cooper Basins as depicted in Figure 1.1 (Carstens, 2014; Josh et al., 2012; Warlick, 2006). It is only recently that the exploration

of Western Australia unconventional resources has picked up its pace and the amount of data has increased to the point of facilitating the estimation of inter-well in situ rock petrophysical and geomechanical properties for the 3-Dimensional modeling of the gas-prone shale plays in Western Australia, particularly in the Perth and Canning Basins (Carstens, 2014; Josh et al., 2012). This is attributable to the fact that shale gas reservoirs have low permeability, thus require complex well development procedures such as horizontal drilling and hydraulic fracturing.

The exploration and production of shale gas are expected to increase, especially as the potential risks associated with conventional resources increase (Carstens, 2014; Josh et al., 2012). Figure 1.1 provides an overview of the world's shale gas resources from the most explored (depicted in red) to the least explored shale basins (depicted in white). The Canning Basin is surrounded by the least explored, but potential unconventional hydrocarbon resources (Carstens, 2014). Since well log data from unconventional resources varies from basin-to-basin, this project presents a modified approach that facilitates the rapid prediction of static rock elastic parameters from their dynamic counterparts, thus availing a potential alternative method that can successfully be utilized to predict, map, and model the geomechanical properties of in-situ shale gas plays. The focus on the Canning Basin is supported by a combination of both recent and past surges in well log and seismic data of wells that have been drilled at the Crossland Platform to assess the hydrocarbon carrying potential of the Canning Basin, the biggest sedimentary rock basin in Western Australia, .

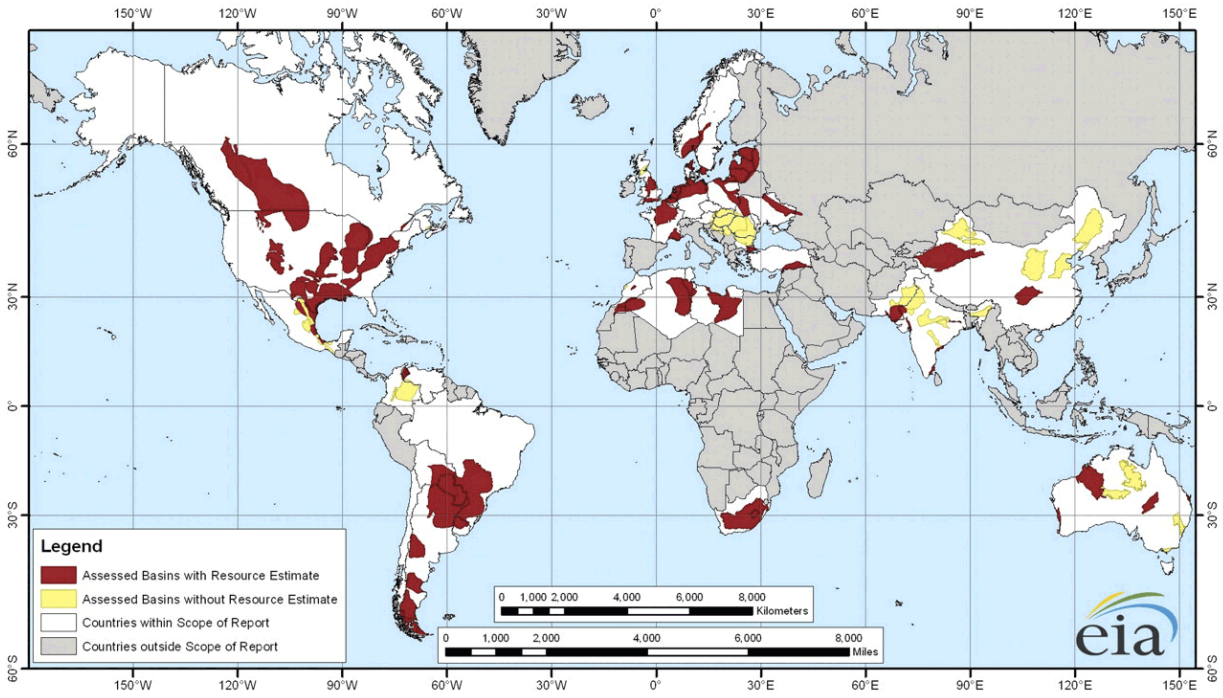

Figure 1.1*: Map depicting the world's potential of shale gas production from the most explored to the least explored shale gas resources (modified from the International Energy Association as reported by Carstens, 2014)*

These data are critical to determining the critical cut-off mechanical values that are important towards increasing the ability to map geomechanical properties andpredict the presence, size, and position of shale gas substructures and their prospectivity with an example from the Canning Basin, Western Australia (Britt & Schoeffler, 2009). Mapping the geomechanical and petrophysical properties of the inter-well in situ shale rock masses of the entire Canning Basin, such as brittleness, offers an increased ability to predict the subsurface that are most likely to contain high hydrocarbon contents. Besides, it simultaneously facilitates the deployment of hydraulic fracturing jobs due to the increased uniqueness and accuracy of predicting the

geomechanical properties of shale formations obtained in one basin (Britt & Schoeffler, 2009; Josh et al., 2012; Rickman et al., 2008).

This undertaking is very important given the potential of Canning Basin's contribution to Australia's total oil production. So far, Canning Basin produces a small amount of oil when compared to Carnarvon, Perth, and Bonaparte basins. The results of this study play a critical role in laying out the potential groundwork that can facilitate future research and exploration endeavors in the Canning Basin shale plays in Western Australia.

1.3 Research Objectives

The principal objective of this study is to develop a modified approach that facilitates the rapid prediction of static rock elastic parameters from dynamic rock elastic parameters. The study further seeks to meet the following specific objectives.

1. Derive correlations between dynamic rock elastic properties for the rapid prediction of static rock parameters (six elastic moduli including Young's Modulus (E), Poisson's Ratio (υ), Bulk Modulus (K), Shear Modulus (G), Lambda.Rho (λ.Rho) and Mu.Rho (μ.Rho) are considered).
2. Utilize the predicted dynamic rock elastic parameters to derive brittleness index.
3. Perform three-dimensional modeling, mapping, and interpretation of rock deformation properties (rock elastic moduli and brittleness index) on the inter-well rock mass of the study area. Interpretations include cross-plots, the correlation equations between rock parameters, and longitudinal sections of the rock elastic moduli versus depth.

4. Perform the simultaneous integration of seismic inversion 3-dimensional models with the pre-determined rock physics models to improve the accuracy of mapping and interpreting rock deformation characteristics.

1.4 Overview

The first activity undertaken in this research project is to analyze and determine the current prospectivity of the entire Canning Basin. This is done by analyzing the general location of the Basin to key infrastructural and physical structures that facilitate the exploration, development, and management of wells. This analysis is supported by an intricate assessment of the geological setting, petrology, and stratigraphy of the Canning Basin. Information to facilitate this analysis is obtained from secondary sources, especially the extant literature on the Canning Basin.

The second activity that forms the fundamental scope of this project is to utilize a method that rapidly predicts static rock deformation parameters from their dynamic counterparts. A total of six elastic parameters are examined and their correlational equations computed. The cored wells include Canopus-1 and Looma-1. The depth of the laboratory derived geomechanical data associated with the different samples include 1508 m for Canopus-1, 1526 m for Looma-1, 1550 m for Fruitcake-1, and 1597 m for Missing-1. These samples were taken from approximately the same depths since Looma-1 is only 18m deeper than Canopus-1. The rest of the wells initially considered are either significantly deeper or shallower.

The scope of the final activity is important towards improving the overall accuracy of mapping and modeling the in-situ rock deformation properties. By relying on seismic data and the exploration reports of the wells, this activity utilizes simultaneous seismic inversion methods that

integrate seismic and well log data to understand the elastic properties, lithology and fluid contents in the subsurface.

1.5 Study Area

The project's study area is located within the South Canning Basin of Western Australia in an area referred to as the Crossland Platform (Figure 1.3). This area occupies a portion of the South Canning Basin and is surrounded by the Fitzroy Trough to the northern margin, the Kidson Sub-basin to the South, the Willara Sub-basin to the northwest, and the Fitzroy sub-basin to the northeast. This project includes Canopus-1, Looma-1 (drilled in 1998), Missing-1 (drilled in 2001), and Fruitcake-1 (drilled in 2001) exploration wells located within the Southern portion of the Canning Basin. Thus, the oldest exploration well and data obtained from the Crossland Platform is Looma-1. All the wells were drilled to investigate the hydrocarbon potential of two sandstone systems within the South Canning Basin (Figure 1.3). Data for these wells was obtained from Shell Development Ltd. and Hughes & Hughes Ltd exploration companies.

1.6 Data Set Overview

This research project utilizes well logs and seismic data provided by Buru Energy Limited. These data were utilized to compute the correlations between static and dynamic rock properties that will be used in constructing a geological model to predict the spatial distribution elastic rock properties and brittleness index.,. The seismic inversion was used to increase the overall accuracy of the model to map the brittleness index and the elastic moduli parameters within the study area. From Figure 1.3 and the approximate locations of the wells, it can be deduced that the subsurface data utilized is inadequate to accurately predict the distribution of the brittleness index and targeted

rock elastic modulii of the underlying strata for the Crossland Platform area towards the South. However, the data can be considered significant in the ability to map and predict the rock elastic parameters and properties of at least 50% of the entire exploration area of Crossland Platform.

In this study, particular attention is paid to the computations that attempt to derive the empirical correlations between static and dynamic rock elastic properties and their ability to facilitate reservoir characterization. Six rock elastic moduli parameters are considered during this empirical correlation attempt comprising of Young's Modulus (E), Poisson's Ratio (υ), Bulk Modulus (K), Shear Modulus (G), Lambda.Rho (λ.Rho), and Mu.Rho (μ.Rho). The current research also attempts to determine the relationship between these empirical correlations in elastic moduli parameters with three petrophysical properties or parameters obtained from well-log data: Neutron Porosity (NPHI), Sonic (DT), and Density (RHOB). Core samples from each of the wells (Canopus-1 and Looma-1) were utilized to derive the static rock deformation parameters using empirically computed correlations in all logged intervals. These static rock deformation parameters were then utilized to estimate the dynamic rock deformation parameters of the wells and the in situ reservoir rocks of the Crossland Platform. The subsurface data set (from both well logs and seismic data) is utilized to estimate and map the distribution of elastic rock properties based on geomechanical and seismic inversion models.

1.7 Geology of the Canning Basin

1.7.1 Geological Setting

The onshore Canning Basin covers an area of about 530,000 km^2 in north-western Western Australia and extends offshore for a total basin area of over 640,000 km^2. The succession in the onshore basin ranges in age from Ordovician to Cretaceous but is predominantly Palaeozoic. The

northwest-trending mid-basin, the Broome Platform, divides the Canning Basin. Also, Broome Platform, in its dissection of the Canning Basin lies in a virtually uninhabited region of the Great Sandy Desert with the major physical features being linear sand-dunes, striking east-west, to form the superficial cover on the Platform. The northernmost of these is the Fitzroy Trough-Gregory Subbasin complex, while the southernmost is the Willara Subbasin-Goldwyer Subbasin complex. The Early Carboniferous Laurel Formation is the main post-salt source rock in the central Canning Basin. Gogo and Anderson Formations, lacustrine, and coal facies within the Grant Group and the Noonkanbah Formation have also source rock potential . However, they are well-positioned in relation to potential petroleum migration pathways, reservoir facies, and structural traps. The rapid deposition associated with the Fitzroy Movement may have resulted in source rocks from the post-salt play passing quickly through the oil generation window with minimal fluid expulsion and producing mainly gas. TOC levels recorded in the shallow marine clastics and carbonates of the Early Carboniferous Fairfield Group suggest good quality hydrocarbon source rocks may be present in this unit.

Furthermore, geochemical data indicate that the most important potential source rocks are in the shallow marine to lagoonal facies of the lower Laurel Formation. Lower Laurel Formation lagoonal shales within the Fitzroy Trough are the likely source of the Yulleroo and Kora hydrocarbons. The Goldwyer Formation is divided into three parts: an upper and lower shale unit with middle limestone unit. The limestones are mostly recrystallized, fine-grained, argillaceous, locally fossiliferous, and generally nonporous. Minor limestones, siltstones, and sandstones are interbedded with the dark carbonaceous and pyritic shales. Complete sections of the Goldwyer Formation occur in Fruitcake-l and Looma-1 (409 and 561 meters thick, respectively). The Willara Formation in its lower part comprises some 200 meters of subtidal interbedded shales and

limestones lying conformably upon the Nambeet Formation. Shallow subtidal and intertidal limestones predominate in the upper part of the section (up to 250 meters thick). Local subaerial exposure, especially at the end of the Willara Formation deposition, resulted in karst weathering, localized dolomitization, and porosity development on the northwest Broome Platform. The Willara Formation is Middle to Late Arenigian in age with diachronous upper and lower boundaries (Figure 1.4).

The Canning Basin is the largest sedimentary basin located in Western Australia. It consists of both onshore and offshore portionsas depicted in Figure 1.3. There are two potential exploration platforms forming part of the Canning Basin that can be accessed by on-land operations: The Broome Platform and the Crossland Platform. Canopus-1 and Looma-1 are located in and around the Crossland Platform whose location can be approximated to be along the Broome/Crossland Platform north-to-south arch. The Crossland Platform is also located to the west of another major geological feature, the Fitzroy Crossing, and in the immediate southeast region of the Broome Platform. Each of these two platforms has its petrological and stratigraphic features, but the scope of this project is oriented towards understanding the features at Crossland Platform where the wells are situated.

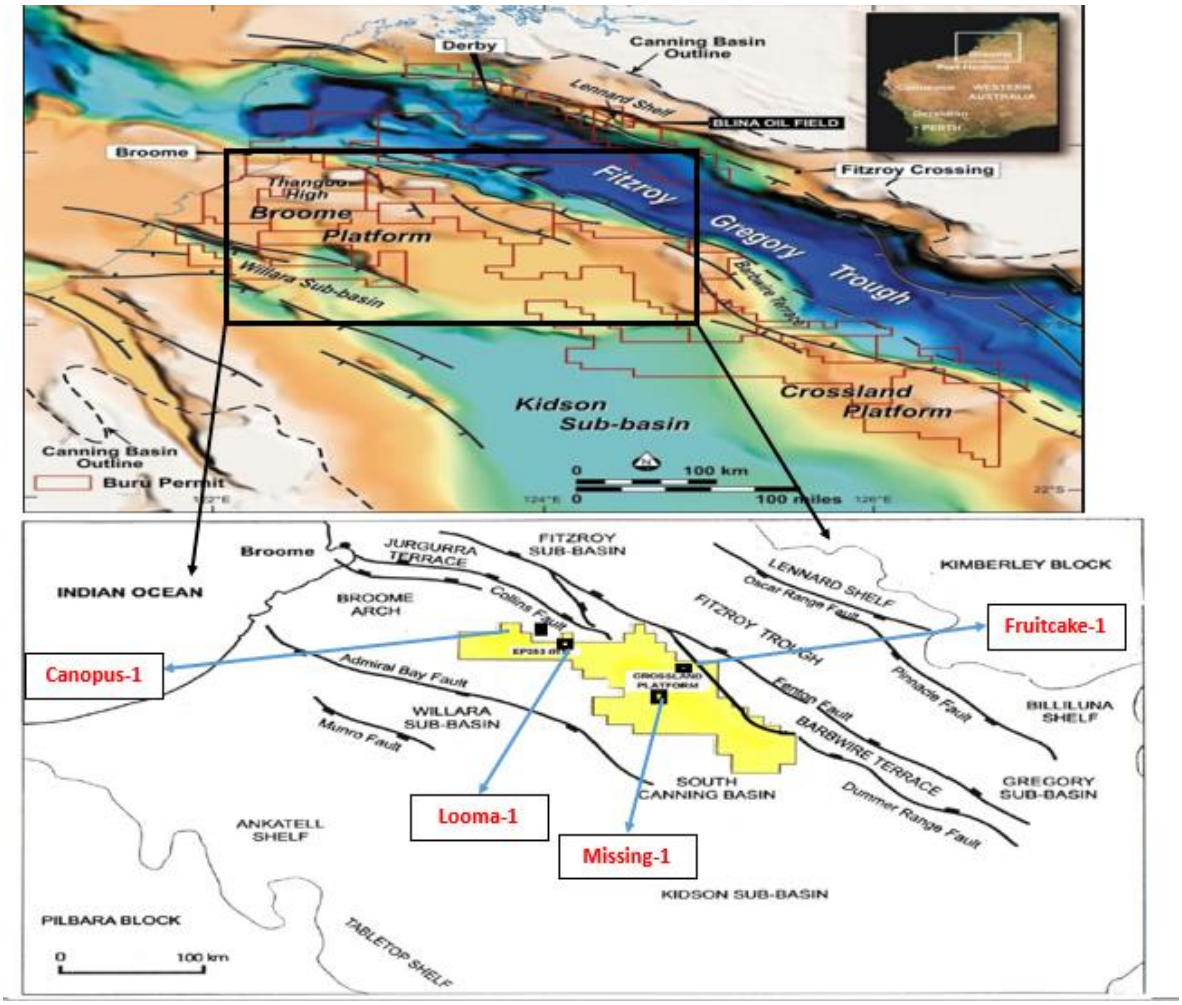

Figure 1.2: *The location (top-right inset figure) and tectonic features of the Canning Basin (enlarged bottom figure depicting the wells at the Crossland Platform) (Burt, Champ & Parks, 2002).*

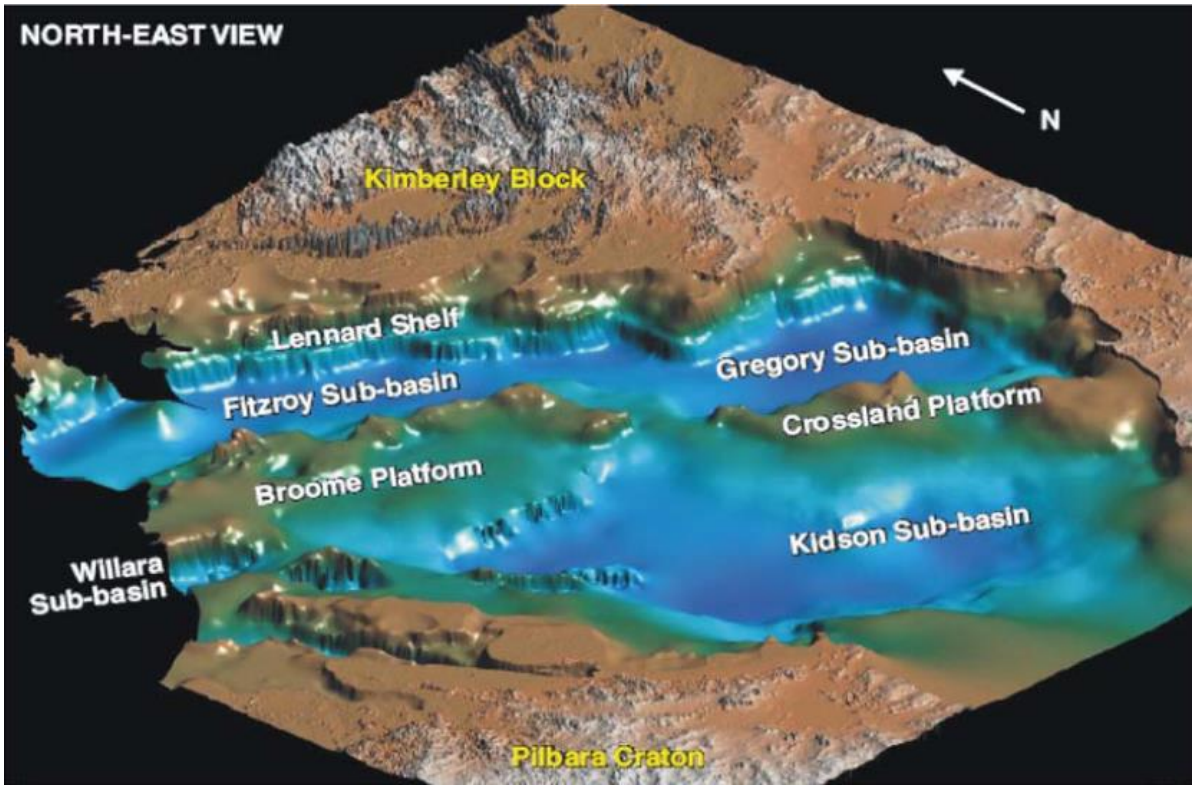

Figure 1.3: *A 3-Dimensional illustration of the main geological features of the Canning Basin, Western Australia.*

1.7.2 Geological Formations and Petrology

The Canning Basin is subdivided into a series of troughs, sub-basins, platforms shelves, and terraces. The Fitzroy Trough and the Gregory Sub-basin which are located on the North, are separated from the Kidson and Willara Sub-basins in the south by the Broome and Crossland Platforms. Most of the initial oil and gas development has been from the Fitzroy Trough and Lennard Shelf in the north, where there are outcrops of Devonian reefs.

In mid-Ordovician times (the oldest rocks in the basin), the basin was in the equatorial region; in the Devonian, a time of major reef formation, the basin was located in the sub-tropics,

and in the Carboniferous, it was sub-polar and glacial, and not part of a coal forming region. Tectonic movement in Devonian times created the proto-Canning Basin.

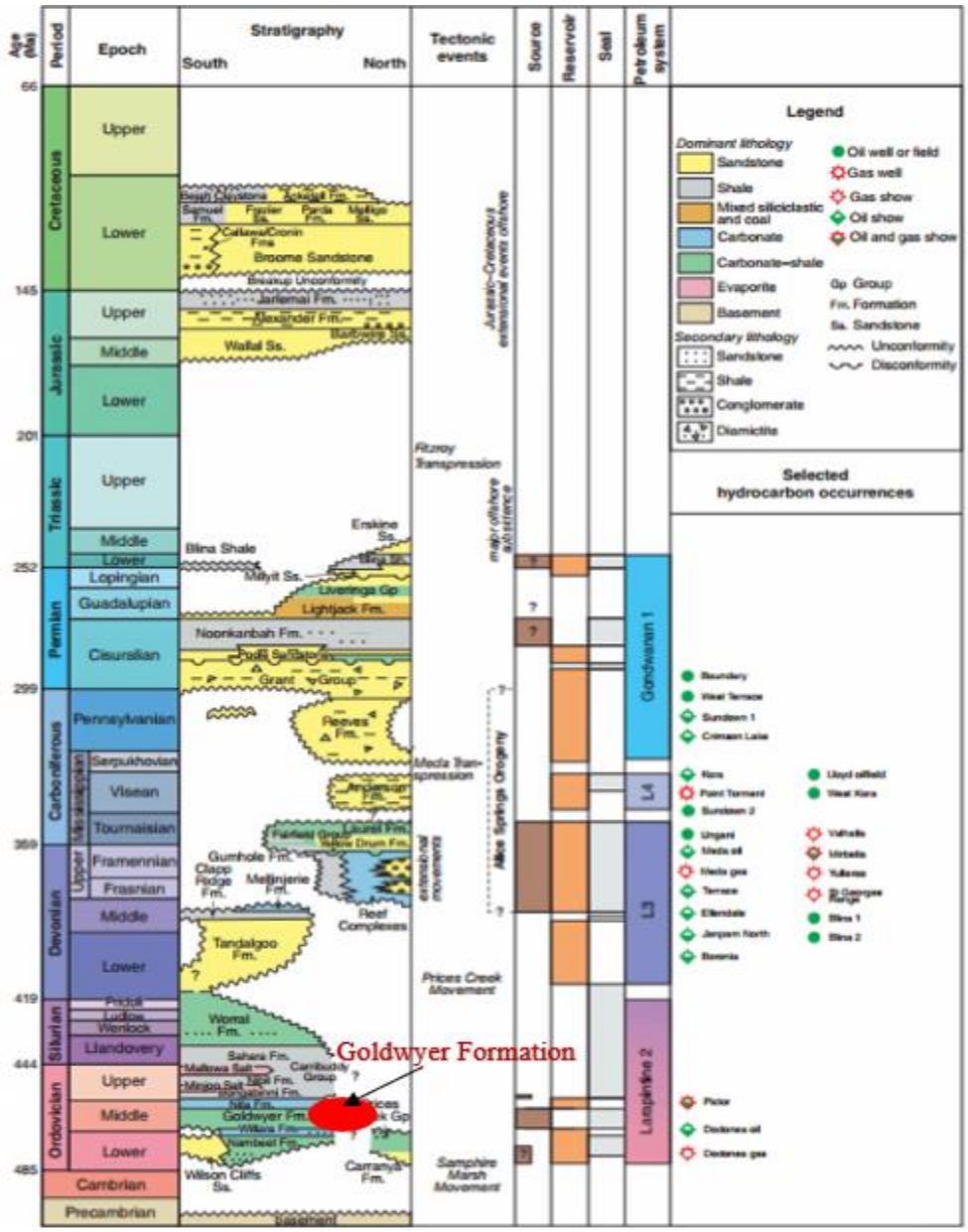

Figure 1.4: *The general stratigraphy of the Canning Basin (GSWA, 2014)*

1.7.3 Stratigraphic Analysis

Figure 1.2 depicts both the location (top-right inset figure) and tectonic features of the Canning Basin (enlarged bottom figure depicting the wells at the Crossland Platform). Figure 1.3 depicts the main geological features of the Canning Basin, Western Australia, while Figure 1.4 shows the Canning Basin's stratigraphy. The basin comprises an onshore and offshore area which is approximately 640,000 km^2 making it the largest sedimentary basin in Australia.

The onshore portion on which the Crossland Platform is located is approximately 530,000 km^2 the area of the Canning Basin. The Crossland Platform consists of the Kidson and the Willara sub-basin. The Canning Basin is a sedimentary basin with intricate geological features and tectonic elements such as complex faulting and compressional forces. On the other hand, the onshore portion is presented with five major tectonic movements and elements. These are:

1. The extension and rapid subsidence of the early Ordovician Section.
2. The cmpression and erosion of the early Devonian Section.
3. The extension and subsidence of the late Devonian Section
4. The compression followed by subsidence of the Carboniferous to Permian Systems
5. The uplifting and subsequent erosion of the Jurassic system.

Despite the foregoing complex tectonic and geological characteristics of the substructural systems of the Canning Basin, the southern portion of this basin is considered to be relatively stable compared to the northern portion. This is because it presents geological features that are less deformed compared to the northern portion of the basin.

1.8 Summary

The need for unconventional hydrocarbon resources is driving the exploration for shale oil and gas in many parts of the world, and Australia is not an exception. There have been explorations in the Canning Basin with little success due to the difficulty of prospecting the shale as it is largely impermeable. This chapter outlined the potential role of establishing cut-offs on geomechanical deformation properties, developing, and producing wells through hydraulic fracturing methods. This requirement together with the non-unique nature of shale gas underscores the need to predict, map, and model rock deformation and petrophysical parameters for locations.

Reservoir characterization that incorporates the mapping of rock deformation properties is fundamental to determining the prospectivity of sedimentary basins such as the Canning Basin, especially unconventional resources. Canopus-1 and Looma-1 form an integral scope of the this agenda to introduce a novel method to rapidly predict and map in-situ rock deformation properties. Most of these wells were spudded at the beginning of the 21st century to investigate the hydrocarbon carrying potential of the Worral and Willara Formations as shown in Figure 1.4.

To postulate the envisioned modified approach to rapidly predict rock deformation parameters, uniaxial laboratory tests were conducted on five core samples obtained from the five wells. Empirical computations were then conducted to correlate six elastic moduli parameters to their dynamic counterparts. The rock elastic properties considered in this project include Young's Modulus (E), Poisson's Ratio (υ), Bulk Modulus (K), Shear Modulus (G), and Brittleness index. The success of the research objective is dependent on four activity categories as schematically summed up and illustrated in Figure 1.2. Well and seismic data reported by Shell Development Ltd and Hughes & Hughes exploration companies are critical to this project's analyses. Seven

models are included to map six elastic modulii and the brittleness index within the study area. The project culminates with the utilization of simultaneous seismic inversion methods and techniques to map the continuous trends of rock deformation properties within the subsurface layers obtained from post-stack seismic data. This last endeavor is geared towards improving the overall accuracy to map and model the predicted and determined rock deformation properties within the the Crossland Platform where the five wells are located.

2 LITERATURE REVIEW

The present study aims at delivering a modified approach for predicting static rock elastic parameters from dynamic rock elastic parameters, particularly through correlation equations. This chapter outlines the literature that is important to the present study. In particular, the topics covered in this chapter include an overview of rock elastic properties, reservoir characterization methods including amplitude analysis with offset, seismic inversion, well-log evaluation, seismic attributes, and 3D seismic data interpretation.

2.1 Reservoir Characterization

Reservoir characterization relies on traditional geophysical methods such as AVO (Amplitude Variations with Offset) to map and predict the distribution of petrophysical and geomechanical properties of in-situ shale gas plays, by integrating well logs and seismic data (Aliouane & Ouadfeul, 2014; Sharma & Chopra, 2016; Zoback, 2010). However, the deployment and utilization of these geophysical methods should carefully be analyzed and managed to avoid errors, particularly during the exploration of shale plays due to the non-unique and largely variant characteristics of these plays (Josh et al., 2012). This is because the anisotropic, heterogeneous, and complex composition of shale plays violate Gassmann's fluid saturation equations and assumptions as utilized and relied upon by reservoir characterization activities that use traditional methods (Chen et al., 2016; Sharma & Chopra, 2016; Dewhurst & Siggins, 2006; Josh et al., 2012; Ghorbani, Zamora & Cosenza, 2009). This is further complicated as the geomechanical and petrophysical properties of world shale plays have been determined to vary from one particular basin to another (Britt & Schoeffler, 2009; Rickman et al., 2008). Avoiding and mitigating the occurrence of errors during the exploration of shale plays is a prerequisite for potentially

improving the ability to precisely detect potential resource shale gas plays or “sweet spots,” and to reduce the overall risks associated with fracking, well-management, and eventually prolong the lifespan of the well. One method that is employed to progressively reduce such errors involves the effective integration of analyses that utilize well-log data with those that employ inverse seismic data manipulation methods to predict, map, and model in-situ reservoir characteristics (Andrä et al., 2013; Ciccotti & Mulargia, 2004; Zoback et al., 2003). Such a method requires the empirical analysis of well-log and seismic data to map, model, and estimate the geomechanical cut-off values critical to determining the prospectivity of shale gas plays (Britt & Schoeffler, 2009; Gray et al., 2010).

According to Josh et al. (2012), three significant factors affect the prospectivity of shale gas plays and the characterization of unconventional resource plays. These are the type, abundance, and thermal maturity of organic contents, including associated other parameters that can be used to determine rock physical properties such as the TOC (Total Organic Carbon) values, porosity-permeability relationship, brittleness characteristics and their influence on shale rock fabric and mineralogical characteristics. Due to the non-unique and largely variant geomechanical properties of shale gas plays from one basin to the other, there should always be a renewed attempt to predict, map, and model these properties in newly explored basins. The Canning Basin in Western Australia is one such basin, which has seen renewed exploration interest, unlike the Barnett Shale of the USA which has extensively been explored (Carstens, 2014).

Determination of the rock brittleness index relies on the derivation of dynamic and static rock elastic properties, especially the Young Modulus (E) and Poisson’s ratio (υ) (Ciccotti & Mulargia, 2004; Mavko, Mukerji & Dvorkin, 2003). From these two elastic properties, other properties such as shear modulus (κ), bulk modulus (G), Lambda.Rho (λ.Rho) and Mu.Rho

(μ.Rho) can be derived (Britt & Schoeffler, 2009; Ghorbani, Zamora & Cosenza, 2009; Jacobi et al., 2008; Josh et al., 2012; Ouenes et al., 2014; Xu et al., 2016). The empirical determination of these rock deformation properties, including the Lambda parameters, is important towards the reduction of computational, mapping, and modeling errors associated with the 3-Dimensional characterization of reservoirs. The current research incorporates a modified approach that utilizes empirical tests on core samples that attempts to correlate dynamic and static rock elastic parameters to enable the efficient prediction, mapping, and modeling of static rock parameters. This is because static rock elastic parameters are predominant over their dynamic counterparts because of their increased ability to represent and predict the actual loading characteristics of the in-situ reservoirs (Andrä et al., 2013; Ciccotti & Mulargia, 2004; Mavko, Mukerji & Dvorkin, 2003).

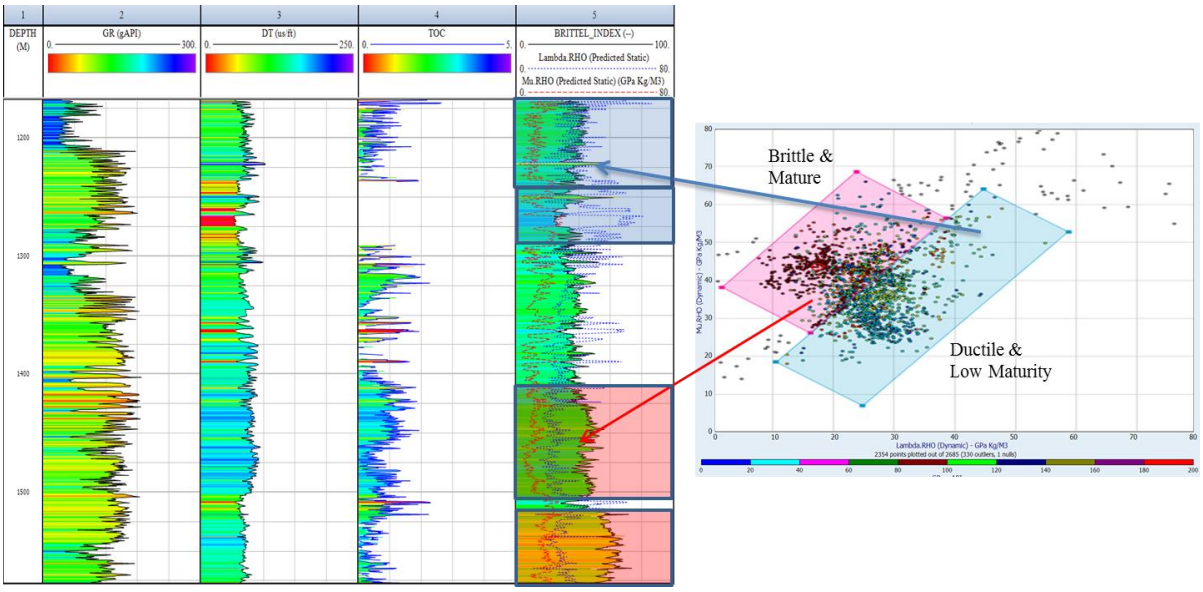

Figure 2.1*. The estimation of the brittle shale from log data along with gamma ray, sonic transit time and TOC representations.*

2.2 Rock Elastic Properties

The seismic and well log approaches are the two major ways in which rock deformation characteristics are theoretically conceptualized. Seismic approaches consider the variations between the P and S wave propagation within the media, while well log data may encompass the measurement of radioactivity and other petrophysical logs on core samples (Chang, Zoback & Khaksar, 2006).

2.2.1 Young's Modulus

Young's Modulus, E, is by definition the ratio of applied stress (σ_{zz}) to vertical strain (ε_{zz})

$$E = \frac{\sigma_{zz}}{\varepsilon_{zz}}$$

E is measured in the units of stress since strain is dimensionless.

2.2.2 Lateral strain

The stress will generally result in a lateral or horizontal deformation, ΔW. The lateral strain can then be defined as

$$\varepsilon_{yy} = \frac{\Delta W}{W}.$$

2.2.3 Poisson's ratio

Poisson's ratio is an important parameter relating the vertical and horizontal strains

$$\nu = -\frac{\varepsilon_{zz}}{\varepsilon_{yy}}.$$

The minus sign is due to the signs of the deformations are opposite for the horizontal versus vertical strains in this simple case.

2.2.4 Volumetric strain

If instead a pressure is applied, it would result in a volumetric strain ε_V

$$\varepsilon_V = \frac{\Delta V}{V}.$$

2.2.5 Bulk modulus

The bulk modulus of a material is then defined as the ratio of applied pressure to volumetric strain

$$K = -\frac{P}{\varepsilon_V}$$

Bulk modulus is equivalent to the inverse of compressibility, β.

2.2.6 Static Shear modulus

Shear modulus, μ or sometimes referred to as G, is defined as the ratio of shear stress to shear strain as follows.

$\mu = \frac{\sigma_{shear}}{\varepsilon_{shear}}$ or $G_s = \frac{E_s}{2\,(1+v_s)}$ GPa ……..……Equation 1

2.2.7 Static Lame's Constants

Lame's constant (λ) is an elastic constant equal to the bulk modulus minus two-thirds of the shear modulus

$$\lambda_s = \frac{E_s v_s}{(1+v_s)(1-2v_s)} \text{ GPa} \ldots\ldots\ldots\ldots\ldots\ldots\ldots\ldots \text{ Equation 3}$$

$$\mu_s = \frac{E_s(1-v_s)}{(1+v_s)(1-2v_s)} \text{ GPa} \ldots\ldots\ldots\ldots\ldots\ldots\ldots\ldots \text{ Equation 4}$$

Also, rock dynamic elastic parameters can be calculated using well log data (compressional wave velocity in km/s), (shear wave velocity in km/s), and ρ (bulk density in g/cm^3) as follows:

2.2.8 Dynamic Young's Modulus

$$E_d = \rho V_s^2 \left(\frac{3V_p^2 - 4V_s^2}{V_p^2 - V_s^2}\right) \text{ GPa} \quad \text{Equation 5}$$

2.2.9 Dynamic Poisson's Ratio

$$v_d = \frac{V_p^2 - 2V_s^2}{2(V_p^2 - V_s^2)} \quad \text{Equation 6}$$

2.2.10 Dynamic Bulk Modulus

$$K_d = \rho V_p^2 - \frac{4}{3\rho V_s^2} \text{ GPa} \quad \text{Equation 7}$$

2.2.11 Dynamic Shear Modulus

$$G_d = \frac{\rho}{V_s^2} \text{ Pa} \quad \text{Equation 8}$$

2.2.12 Dynamic Lame's Constants

$$\lambda_d = \rho^2 (V_p^2 - 2\,V_s^2) \text{ GPa} \quad \text{Equation 9}$$

$$\mu_d = \rho^2 V_s^2 \text{ GPa} \quad \text{Equation 10}$$

2.2.13 Porosity

$$\phi = \frac{Pore\ Volume}{Total\ Volume} \quad \text{Equation 11}$$

2.3 Seismic Attributes

Seismic attributes are mathematical descriptions of the shape or other characteristics of a seismic trace over a specified time interval. Seismic attributes can be used for mapping stratigraphic features. Seismic attributes can help geology interpreters understand the types of environmental deposition. For instance, an anomalous seismic attribute may be associated with the presence of gas or oil. Seismic attributes can be classified as horizon, interval, or surface attributes (Chopra et al., 2007; Misra & Mukherjee, 2018). Seismic attributes can be used for qualitative as well as quantitative analysis. In qualitative application, seismic attributes can be used for evaluating the quality of seismic data, for instance through seismic artifact identification. In quantitative application, seismic attributes can be used to compute, for instance, reservoir thickness or porosity by applying equations that relate rock property changes to changes in seismic attributes.

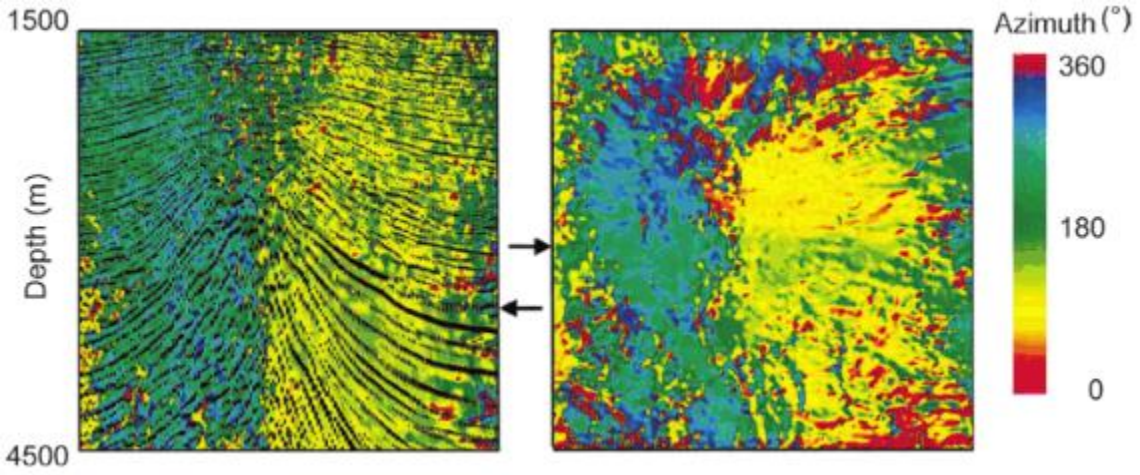

Figure 2.2: *Dip Azimuth map (a horizon seismic attribute) of a seismic trace from a depth of 1500m to 4500m (Chopra et al., 2007).*

2.4 Well Log Evaluation

Well logging technique involves continuous recording of data versus depth of the formation rocks. The logs can then be analyzed for hydrocarbon signatures and cross plots performed. The most common well logs include spontaneous potential, gamma ray, neutron, porosity density, sonic, resistivity, and caliper logs (Darling, 2005; Mussett, Khan & Button, 2000). These logs are described in the following sections.

2.4.1 Spontaneous Potential (SP) Logs

Spontaneous potential log shows the natural electrical charges of underground rock formations and indicates when the logging tool passes from one rock formation to the next. The spontaneous potential logging tool uses two sensors, one located at the surface and another one located down the hole to compare the natural electrical charges at the surface with the electrical charges of the underground rock. Some layers of rocks have a positive charge, while others have a negative charge compared to the surface. If mud filtrate resistivity (Rmf) is less than formation water resistivity (Rw), a shift to the right denotes greater resistance to electricity, thus a positive charge is usually associated with sandstone. Conversely, a shift to the left denotes less resistance to electricity, thus a negative charge is usually associated with shale (Darling, 2005; Mussett, Khan & Button, 2000).

2.4.2 Gamma Ray (GR) Logs

The gamma ray log measures the natural radioactivity of the formation. Because radioactivity tends to be concentrated in shale, the gamma ray normally reflects the shale content of the formations. High gamma readings indicate the presence of shale and cause a deflection to the right. A low reading indicates the presence of clean, non-shaly formations, for instance,

sandstone, limestone, and dolomite; low radioactivity causes a deflection to the left. However, a clean shale-free sandstone may also produce a high gamma ray response if the sandstone contains micas, potassium, or uranium-rich formation waters. Thus, the presence of a clean sandstone can be overlooked if it contains one of the above contaminants. SP and GR logs are used to differentiate potentially porous formations such as sandstone, limestone, and dolomite from non-permeable clays and shales. Besides, SP and GR logs are used to define bed boundaries (Darling, 2005; Mussett, Khan & Button, 2000).

2.4.3 Neutron Porosity Logs

The neutron porosity logging tool counts the number of hydrogen atoms in the surrounding rocks. A shift to the right indicates fewer hydrogen atoms in the formation. Conversely, a shift to the left on the neutron porosity log curve indicates the presence of more hydrogen atoms in the formation (Darling, 2005; Mussett, Khan & Button, 2000).

2.4.4 Density Porosity Logs

The density logging tool measures electron density and transforms it into bulk density. The density porosity log is overlaid the neutron porosity log. A density and porosity curve crossover is significant as it indicates high probability of natural gas. In particular, whereas the neutron curve indicates either tight rock or gas, the density log porosity curve indicates that the rock is more porous and therefore cannot be a tight rock. Such an area indicates a high probability of natural gas (Darling, 2005; Mussett, Khan & Button, 2000).

2.4.5 Sonic Log

The sonic or acoustic log measures the travel time of an elastic wave through the formation. This information can also be used to derive the velocity of elastic waves through the formation. Its main use is to provide information to support and calibrate seismic data and to derive the porosity

of a formation. Sonic logs provide a record of “seismic” velocity and travel time throughout a borehole to calibrate a seismic data set, “seismic” data for the use in creating synthetic seismograms, stratigraphic correlation, and identification of source rocks and over-pressures among others (Darling, 2005; Mussett, Khan & Button, 2000).

2.4.6 Caliper log

The caliper tool measures the variation in size of the well bore. Such variations can affect the accuracy of other logging tools. Therefore, based on the caliper logs, other logs can be recalibrated if necessary (Darling, 2005; Mussett, Khan & Button, 2000).

2.4.7 Petrophysical Analysis Using Cross plots

Cross plots are useful in rock physics as they enable faster evaluation and interpretation of well data. Generally, similar lithological units and fluid contents can easily be identified in a cross plot as they tend to form different clusters. A common practice in log interpretation is to cross-plot various porosity log readings in order to determine formation lithology and accurate porosity. The neutron logs and gamma ray logs complement each other and are often used together. The natural gamma ray log tends to respond to changes in clay mineral content, while the neutron log tends to respond to changes in porosity. Gas identified on neutron logs and gamma ray logs show clear differences (Mussett, Khan & Button, 2000).

2.5 Seismic Inversion

2.5.1 Forward Seismic Modeling

Forward seismic modeling produces a synthetic seismic trace. In particular, blocked velocity and density logs are used to compute reflectivity. The reflectivity is then convolved with a wavelet to produce a modeled seismogram (Cui et al., 2018). Forward seismic modeling is useful

as it allows well markers to be tied to seismic traces. The forward seismic modeling is as illustrated in Figure 2.3.

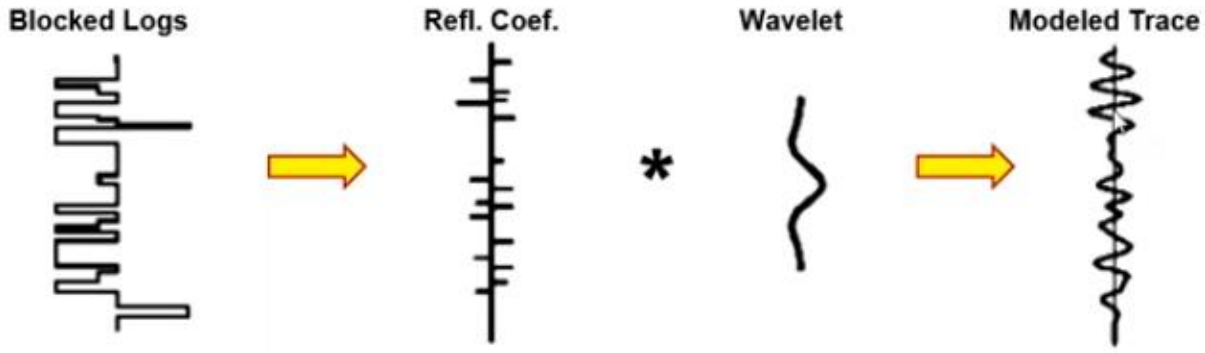

Figure 2.3: *Illustration of the convolution model.*

2.5.2 Inverse Seismic Modeling

In seismic inversion, the original reflectivity data is converted from an interface property (i.e. a reflection) to a rock property known as impedance, which itself is the multiplication of sonic velocity and bulk density. In a conventional seismic reflectivity section the strong amplitudes are associated with the boundaries between geological formations, such as the top reservoir. This type of data is most suited to structural interpretation. In an inverted dataset the amplitudes are now describing the internal rock properties, such as lithology type, porosity or the fluid type in the rocks (brine or hydrocarbons). Inverted data is ideal for stratigraphic interpretation and reservoir characterization (Burianyk, 2019). The seismic inversion process is as illustrated in Figure 2.4.

Seismic inversion can be classified as either post stack or pre stack. Post stack seismic inversion produces a single impedance volume, usually acoustic impedance. On the other hand, pre stack simultaneous seismic inversion generates the acoustic and shear impedance attributes simultaneously (Russell & Society of Exploration Geophysicists, 1988).

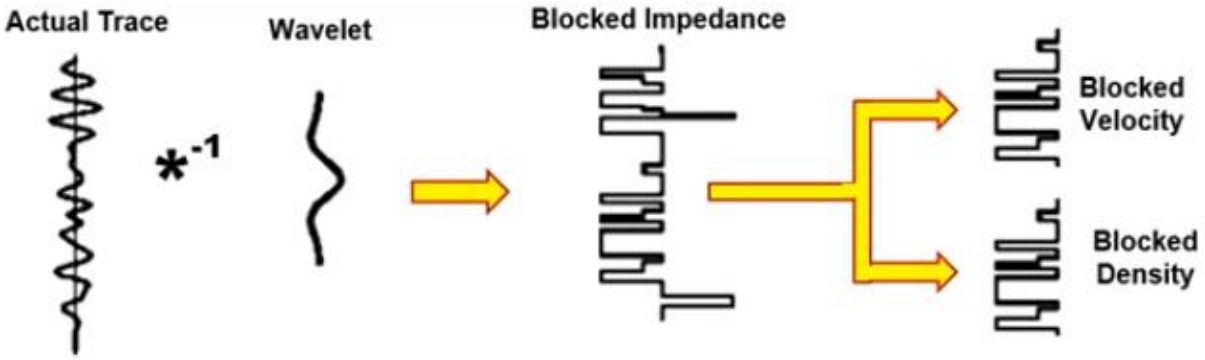

Figure 2.4: *Illustration of seismic inversion process.*

2.6 Interpretation of Seismic Data

The goals of interpreting seismic data include building a geologic framework, identifying prospect elements such as source, migration, reservoir, trap and seals, assessing potential prospects for instance the volume of the hydrocarbons in place and performing economic analysis. In particular, seismic interpretation involves applying the seismology theory to interpret horizons and faults, which are then used to build the geological framework of the present-day structure and stratigraphy (Bacon, Simm & Redshaw, 2007; Yilmaz et al., 2001).

Building a geologic framework involves firstly identifying, mapping and correlating most of the significant fault planes. The second step involves proper identification of horizon-fault and fault-fault intersections. The above steps are termed as structural interpretation. The last step in building a geologic framework involves identifying most of the stratigraphic surfaces, unconformities and depositional sequences. This step is termed as stratigraphic interpretation (Bacon, Simm & Redshaw, 2007; Yilmaz et al., 2001).

2.7 Previous Work on Sweet Spot Identification

2.7.1 Parameters Affecting Sweet Spots Sweet Spots in Unconventional Reservoirs

Sweet spots are areas in unconventional reservoirs with the best production potential. In particular, identification of sweet spots in unconventional reservoirs lowers the risks in the exploration and production of gas as it allows geologists to place wellbores in the most productive areas of the reservoirs. Sweet spots in shale reservoirs can be identified using core analysis, analysis of well log data and analysis of seismic data.

Shale is defined as fine-grained sedimentary rock that was formed as a result of the consolidation of clay and silt into rocks of ultralow permeability. Shale is an example of an unconventional hydrocarbon resource and is characterized by smaller pores as compared to the pores in the conventional reservoirs. In addition, shale is characterized by extremely low permeability, ranging from nanodarcys to microdarcys. Besides, shale is also rich in organic matter as organic matter form the major pore network of some gas shale formations (Rezaee, 2015). Furthermore, a large fraction of the total gas in shale plays is exist as a condensed adsorbed phase. It is difficult to produce from shale resources using conventional methods such as vertical drilling due to the low permeability and low porosity; production from shale resources requires the adoption of techniques such as horizontal drilling and hydraulic fracturing. According to Qian et al. (2018) shale is characterized by low porosity and strong anisotropy. However, Sun et al. (2014) verified the feasibility and effectiveness of the isotropic approximation adopted in high-quality reservoir. Therefore, while still acknowledging anisotropy as a key issue in shale gas plays, this study adopts isotropic assumption in shale gas plays of the Canning Basin, Western Australia.

2.7.2 Criteria for the Identification of Sweet Spots

Geomechanical, geochemical and petrophysical properties are important in the identification of sweet spots in unconventional hydrocarbon resources. Ogiesoba and Eastwood (2013) state that sweet spots are characterized by high total organic carbon (TOC), high acoustic impedance and low water bulk volume. Rezaee (2015) states Young's Modulus and Poisson's ratio as key geomechanical properties in the identification of sweet spots in shale plays. These observations are echoed by Khan et al. (2018) who state that high values of Young's Modulus and corresponding low values of Poisson's ratio indicate brittle zones in unconventional reservoirs. Ogiesoba and Hammes (2014) noted that high-resistivity and high TOC occur in high-quality-factor zones. This in line with Ogiesoba (2016) who noted instantaneous quality factor (Q) as a key factor in the identification of sweet spots in shale plays. In line with the above, this study uses parameters that can be derived from the available data to identity and map sweet spots in the Canning Basin, Western Australia. In particular, the present study uses high acoustic impedance, high-resistivity, high Young's Modulus and low Poisson's ratio values as pointers of potential sweet spots.

2.7.3 Factors Affecting Shale Gas Presence

According to Li et al (2018), hydrocarbon-generation conditions (organic matter type, total organic carbon content, and vitrinite reflectance) and reservoir conditions (reservoir porosity and permeability, reservoir storage-space types, pore-structure characteristics, mineral composition and lithofacies, isothermal adsorption characteristics) play a pivotal role in shale gas reservoirs assessment. The quality of the hydrocarbon-generation conditions plays a critical role in shale gas deposition where the type of organic matter present and its associated organic carbon content are

directly involved in gas formation. On the other hand, the mechanical quality of unconventional reservoir rocks is defined by elastic parameters such as brittleness and stiffness.

2.7.4 Quantification of Shale Gas

Owing to the high cost of exploring unconventional reservoirs, many scholars have attempted to find alternative cheaper methods that could be used for identifying shale gas sweet spots and other unconventional hydrocarbon reservoirs. Aldrich and Seidle (2019) notes that while unconventional reservoirs are influenced by a wide array of factors, including reservoir variables, completion variables, economic and environmental variables, previous sweet spot classification attempts only focused on reservoir variables; other factors such as environmental and operational factors have not been considered in the previous sweet spot classification attempts. The main methods that have so far been applied in the prediction of shale gas sweet spots include analysis of 3D seismic data, electric logs, data mining and integration of multiple data sets. Irrespective of the applied method, the goal has always been to find and present a methodology that could tie a limited set of subsurface parameters to the identification of zones of higher productivity or sweet spots. Aldrich and Seidle (2019) note that the scope of previous studies excluded the quantification of the identified higher productivity zones in unconventional reservoirs.

2.7.5 Sweet Spot Identification by Analysis of 3D Seismic Data

Sena et al. (2011) attempted the identification of sweet spots as well as the estimation of geomechanical properties and in-situ rock principal stresses in shale play resources by integrating the analysis of pre-stack azimuthal seismic data and well logs. Sena et al. (2011) argues that the analysis of pre-stack azimuthal data could yield attributes that are correlated to formation lithology, rock strength and stress fields. In particular, rock elastic properties including Young's modulus and Poisson's ratio could provide valuable information for the identification of

lithological facies, mineral content and rock strength, which could then lead to the identification of sweet spots. Sena et al. (2011) further observed that fractures are likely to propagate in brittle areas, thus pointed out that optimal well placement should target areas that have high porosity, high silica content and high total organic carbon content. To this end, Sena et al. (2011) notes that properties obtained from rock property analysis, such as Poisson's ratio and Lambda.Rho could be useful in the identification of optimal well placement areas.

Perez and Marfurt (2015) investigated the identification of brittle and ductile areas in unconventional reservoirs using seismic and microseismic data. Mineralogy is the key geological factor that controls brittleness in unconventional reservoirs and areas with high quartz and dolomite content tends to be more brittle, whereas areas with high clay content tend to be ductile. Perez and Marfurt (2015) demonstrated how regional brittleness maps could be generated by correlating mineralogical-based brittleness index to elastic parameters measured from well logs. Brittleness index could then be predicted from such correlation from elastic parameters, particularly Lambda.Rho and Mu.Rho derived from surface seismic. Perez and Marfurt (2015) concluded that hydraulically induced fractures are more pronounced in brittle zones and seismic inversion could effectively be used to discriminate between brittle and ductile regions in unconventional hydrocarbon plays.

2.7.6 Sweet Spot Identification Using Electric Logs

Chopra et al. (2018) investigated the identification of organic rich, sweet spots by integrating 3D seismic, well and core data. In particular, the total organic carbon (TOC) was determined from the core samples and then used to determine the organic richness. A relationship between TOC values and the measured density was established through a crossplot analysis. The relationship between the TOC and the measured density was then used to transform the inverted

seismic density into a TOC volume. A probabilistic neural network (PNN) was used to compute density using seismic data. Chopra et al. (2018) observed a correlation of TOC and sweet spots identified based on the seismic data and the core data, thus emphasized the aspect of integration between seismic and other well log data.

Glaser et al. (2013) argue that the economic viability of shale plays is mainly determined by reservoir quality (RQ) and completion quality (CQ). RQ predicts the ability of a reservoir to produce hydrocarbons economically after hydraulic stimulation, whereas CQ predicts whether reservoir stimulation through hydraulic fracturing would be successful. Glaser et al. (2013) further notes that RQ is mainly influenced by mineralogy, porosity, hydrocarbon saturation, organic content, thermal maturity and formation volume. On the other hand, Glaser et al. (2013) showed that CQ is influenced by mineralogy and rock elastic parameters including Young's modulus, Poisson's ratio, bulk modulus, and rock hardness.

2.7.7 Sweet Spot Identification through Data Mining

Tahmasebi et al. (2017) proposed that the best places for hydro-fracking in shale reservoirs could be identified through data mining and machine learning techniques. Such an automatic method could identify shale gas sweet spots using the available reservoir data and can be integrated with reservoir data of different scales and lengths. Besides, such a method could be updated easily whenever new reservoir data are available. Tahmasebi et al. (2017) defines sweet spots as regions that are characterized by high total organic carbon and brittle rocks. Tahmasebi et al. (2017) proposed two data mining and machine learning methods that could be used to identify sweet spots. The first method is based on a stepwise algorithm that determines the best combination of well log data to predict the target parameters, whereas the second method is based on a hybrid machine-learning algorithm that models the complex spatial between the input and target parameters more

accurately. By employing the two methods, a strong agreement between the predicted variables and the available data was reported.

2.8 Summary

In this chapter, a literature pertaining to the present research was reviewed. The topics covered include, reservoir characterization, rock elastic properties, seismic attributes, well log evaluation, seismic inversion, interpretation of seismic data, reservoir modelling and simulation, and previous work on sweet spot identification. The next chapter explores the methodology and 3D geomechanical modeling techniques used in this research.

3 METHODOLOGY & 3D GEOMECHANICAL MODELING

3.1 Data

To build 3D geomechanical models of the Goldwyer gas shale Formation in the Canning Basin, Western Australia, both seismic and well log data were used. The seismic and well log data were received from Buru Energy Limited, a company that had conducted a seismic survey in the Canning Basin. Although 11 wells had been drilled in the Canning Basin, the seismic and well log data was only available for the wellsCanopus-1, Looma-1, Fruitcake-1 and Missing-1. However, only samples from Canopus-1 and Looma-1 are from approximately similar depth range and geographically closer to each other. Therefore, the study area was only limited to the area surrounding the wells,wells Canopus-1 and Looma-1 were used for correlation purposes(Figure 3.1 & Figure 3.2).

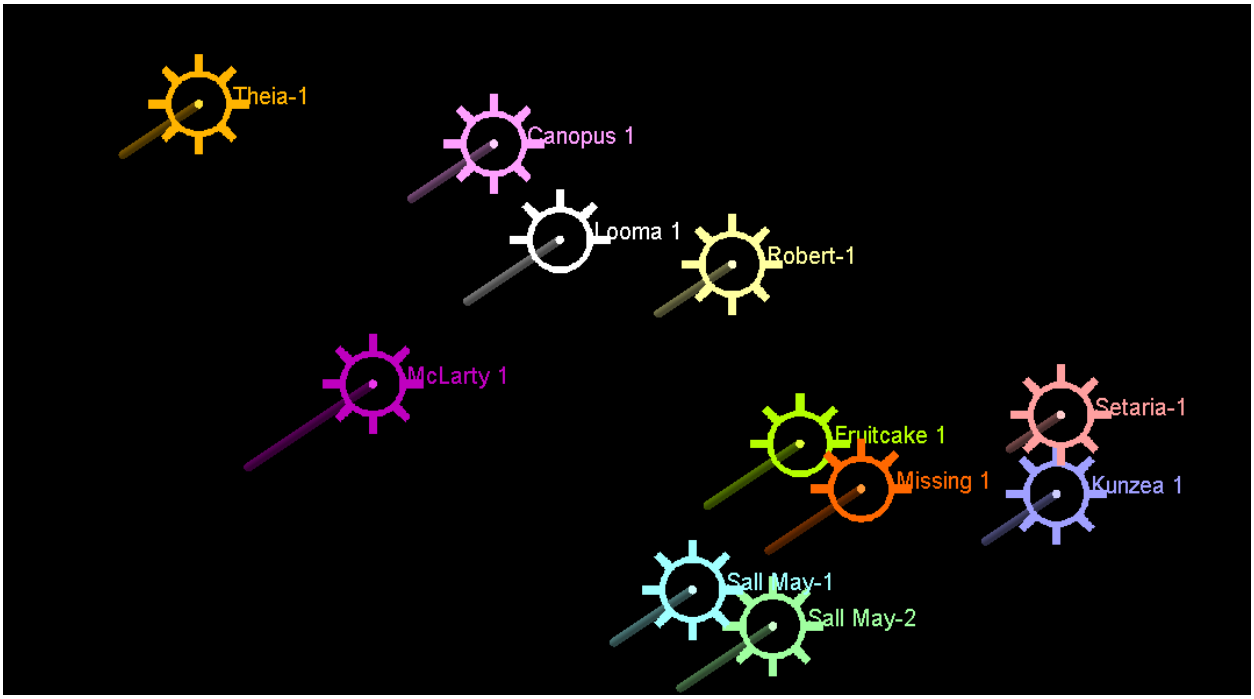

Figure 3.1*. Location of the 11 wells in Canning Basin, Western Australia*

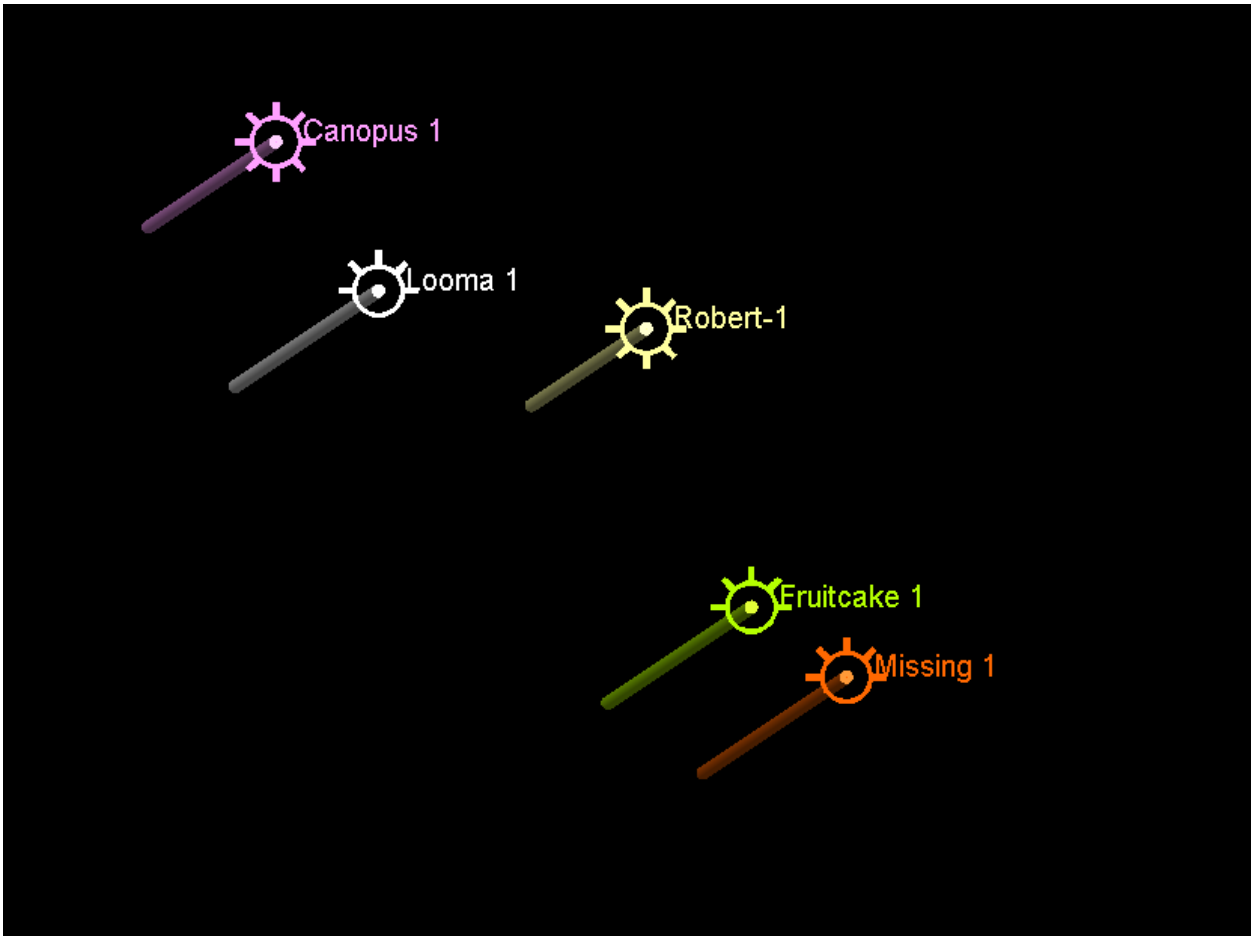

Figure 3.2: *Study area limited to 5 wells out of 11 for which petrophysical data are available.*

3.2 Modeling Tool

Schlumberger's Petrel E&P software platform provides a full range of tools to solve the most complex structural and stratigraphic challenges. It provides a full suite of reservoir characterization tools that enables geoscientists to develop stratigraphic and structural understanding. It also provides workflows that greatly enhances reservoir knowledge. It offers comprehensive capabilities that span from regional evaluations and prospect generation. It is an excellent tool for geoscientists as it allows the interpretation of seismic data while still working with well log information, providing accurate subsurface models. For these reasons, Petrel E&P software

platform was emplyed to build the 3D models of elastic properties of the Goldwyer Formation, Canning Basin, Western Australia.

3.3 3D Elastic Modulus Modeling for the Goldwyer Formation

A key objective of this study was to build a 3D geological model of the Goldwyer Formation in Canning Basin, Western Australia using Petrel E&P software platform. The workflow of building a 3D geological model of a petroleum reservoir in Petrel E&P software platform include, data import, quality control of the input data, well correlation, structural modeling which involves pillar gridding, making horizons & layering, scale up, variography and petrophysical modeling The above steps are described in the following sections.

3.3.1 Initialization, Data Importation and Quality Control

Firstly, a new project was set up in Petrel software and the projection system and unit system defined. This was followed by the importing seismic data of the study area, including well markers, well trajectories and seismic horizons. The input data were validated through a series of cross check comparisons with the original data. In addition, visualization of the imported data was done using cross plots and histograms.

3.3.2 Seismic Data

Seismic data of the Canning Basin were interpreted and the structural elements found include a set of depth surfaces comprising top and base of Goldwyer Formation (in X, Y, Z and ASCII format). These surfaces were loaded to Petrel as set point data set and visually checked for any erroneous data points.

3.3.3 Well Data

Well data was supplied in log ASCII standard (LAS) format and comprised wells Canopus-1, Looma-1, Missing-1, and Fruitcake-1. The imported wells' data contain information on the well Kelly Bushing Elevation, well path, logs and well markers.

Well Marker Data

The two well markers were named as Top-Goldwyer Formation and Base-Goldwyer Formation.

Well Log data

Raw well log data were available in a digital form. In addition, the following geomechanical results were utilized for geomechanical modeling of Young's modulus, Poisson's ratio, Bulk modulus, Mu.Rho, Lambda.Rho, Shear modulus and Brittleness index. Crossplot of dynamic elastic rock properties (Dynamic Poisson's ratio vs Dynamic Young's Modulus) from the results of the geomechanical analysis of well log data on the Goldwyer formation from all depth intervals show the distribution of elastic rock properties resulting from the intercalation laminated shale / sand section. The principle of measuring elastic rock properties in a rock mechanics lab is very different from measuring with a well log. Therefore, it was necessary to convert dynamic to static elastic rock properties (Poisson's ratio and Young's modulus) using the empirical equation proposed by Wang (2000) for Poisson's ratio, and the empirical equation proposed by Eissa & Kazi (1998) for Young's modulus.

3.4 Structural Modeling

Structural modeling is the first step in 3D geomechanical modeling. In particular, structural modeling focuses on the construction of the reservoir architecture. To this end, any structural

feature such faults and folds present in the reservoir are identified. The main steps include fault modeling, pillar gridding, making horizons, making zones and vertical layering. The above steps were implemented one after the other as described below.

Fault Modeling

Fault modeling generates a faulted 3D grid in which the horizons, zones and layers can be inserted into. During fault modeling, the shape of each fault that should be modeled is defined. The faults are defined by a set of key pillars that consist of a set of shape points. The various fault shapes include vertical, linear, listric and curved faults. Based on the seismic interpretation of the Canning Basin, no fault was detected in the seismic sections. Thus, no faults were considered, interpreted or used in geomechanical modeling. With no fault existence, a simple grid generation was adopted.

Pillar Gridding

After fault modeling, the next step involves making grids based on the defined faults. Pillar gridding aims at building a skeleton framework which consists of a top, a mid and a base skeleton grid. Each skeleton grid is attached to the base, mid and top points of the key pillars. Pillar gridding results in the conversion of the faults defined by the key pillars into fault surfaces.

Make Horizons

The make horizons process is the first step in the creation of stratigraphic subdivisions. The stratigraphic horizons are created by inserting the input surfaces into the 3D grid. The input surfaces can include surfaces from seismic or well tops or line interpretations of seismic. Top and base horizons of the Formation were constructed during the pillar gridding process. In addition, two interpreted horizons of the Formation were generated and imported for constructing the reservoir structural framework.

Make Zones

After the horizons have been made, zones are made by inserting additional horizons into the 3D grid. This is achieved by adding isochores to the 3D grids above, below and between the original horizons.

Layering

Vertical layering is the final step in the vertical subdivision of the framework and defines the cell thickness of the 3D grid. The layers are part of the individual zones, but they do not have direct filters as the zones do.

3.5 Geomechanical Property Modeling

Geomechanical property modeling is the process of assigning each cell of the 3D model a value for different rock parameters such as Young's modulus, Poisson's ratio, Bulk modulus, Lambda.Rho, Mu.Rho, shear modulus and brittleness index. In the present study, the Geomechanical property models of the following elastic rock parameters were constructed: Young's modulus, Poisson's ratio, Bulk modulus, Mu.Rho, Lambda.Rho, Shear modulus and Brittleness index.

For all the layers in the Goldwyer Formation, all the geomechanical properties mentioned above were modeled using a stochastic approach due to the following reasons. Firstly, stochastic modeling appreciates inherent heterogeneity in the modeled properties. Secondly, stochastic modeling allows the possibility of quantifying the uncertainty in the modeling process. Thirdly, stochastic modeling allows the possibility of integrating a variety of data, such as seismic acoustic impedance and well log data. Last but not least, unlike the deterministic methods that create smooth models, stochastic methods capture extreme values, resulting in heterogeneous models.

3.5.1 Scale Up Well Logs

The data for scaling up well logs was obtained from Shell Development Ltd and Hughes & Hughes exploration companies. The logging contractor computed the properties for the standard well logs. The role of the author was to randomly check the values if they are legitimate. The first step in property modeling is assigning equivalent well log data to the cells crossed by the well. The scaling up process assigns well log values to the cells in the 3D grid penetrated by the wells. The process is commonly used in post-processing for the distribution of property values between the wells. In geomechanical modeling, the assigned scaled up grid data are called “scaled up well logs”. In the up-scaling process, equivalent average log property is assigned to each cell along the well. For continuous log data like Young's modulus and Poisson’s ratio, an arithmetic average method is chosen for assigning values to each cell of the well block.

3.5.2 Comparison of the Model’s Well Log Data with the Original Well Log Data

In order to control the consistency of the resulting well block data with the original log data and the effect of vertical grid resolution, histograms of the original logs and well block properties were prepared and compared. The best way to check the up scaling is to display the property in the well’s section together with the original well log. The up scaled property is edited directly in the well’s section view and any updates transmitted automatically to the property model.

3.5.3 Geomechanical Parameters Modeling

The following processes were implemented in the stochastic property modeling: transformation of data to a normal distribution, setting anisotropy ellipsoid, setting variogram model, adopting a geostatistical method to generate values for each grid cell, reverse

transformation to original distribution. The above mentioned processes are described in details in the following sections.

Data Transformation

The assumption made in conventional statistical analyses is that the data have a normal (Gaussian) distribution. Therefore, it is necessary to transform the data to a normal distribution before the analysis. To do so, a normal scoring method was applied to the geomechanical data from Shell Development Ltd and Hughes & Hughes exploration companies to transform their distribution to a Gaussian distribution.

Setting Anisotropy Ellipsoid and Variogram Model

Determination of anisotropy ellipsoid is one of the important parts of variography. Based on the sedimentary environment studies in the Canning Basin, it was decided to consider the anisotropy along the direction of N42°, and the results proved by geological and geomechanical concepts of the depositional environment and direction of maximum variation of properties.

Shore Line Direction in Goldwyer Deposits

Variogram is a tool for measuring spatial continuity of data. It is a half of the variance sum of the increment that is the regionalized variables Z(x) at the x and x + h (See Figure 3.3). The lateral parameters of the variograms were determined by the distance between the eastern and western wells of the Canning basin. The Kriging geostatistical method was adopted in the implementation of the geomechanical parameter propagation in the model.

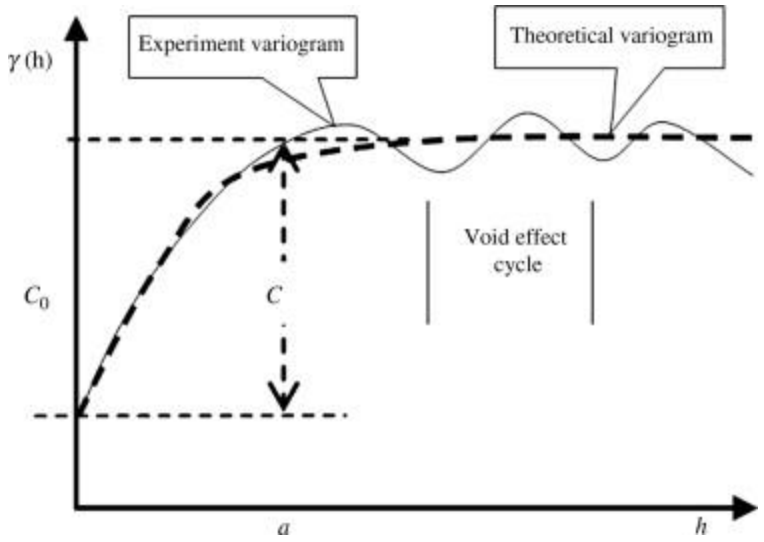

Figure 3.3: *A simple variogram model.*

3.6 Brittleness Index Modeling

The brittleness index model shows the relative brittleness of rocks in particular location in the in situ rock mass. Therefore, shale sweet spots and preferential drilling locations can be easily identified. The brittleness index model was built by combining various weighted rock elastic parameters together. This index can be determined by the following formula:

$I_B = \frac{q_f - q_u}{q_u}$,

Where q_f and q_{fu} are the peak deviator stress and the residual deviator stress, respectively.

3.7 Regression Modeling

One of the objectives of this research was to determine a relationship between dynamic rock elastic parameters and static rock elastic parameters. In particular, such correlation equations could be used to predict dynamic rock elastic parameters from their dynamic counterparts. The predictive correlation equations were generated by running a regressing model between dynamic rock

parameters (the predictors or independent variables) and rock elastic parameters (the outcome or dependent variables).

4 RESULTS OF MODELING ESTIMATION

4.1 Elastic Properties Results

The study aimed at developing correlation equations that show the relationship between the static rock elastic parameters and the dynamic rock elastic parameters. The elastic properties results are as outlined in Table 4.1 and Table 4.2.

Table 4.1: *Tabulation of results for the static rock elastic parameters obtained from uniaxial compressive strength empirical laboratory tests on plugs of core samples.*

Sample	Depth (m)	Elastic Parameters			
		Young's Modulus ($x10^6$ psi)	Poisson's Ratio	Bulk Modulus ($x10^6$ psi)	Shear Modulus ($x10^6$ psi)
A	1467.84	4.77	0.27	3.49	1.87
B	1508.26	1.60	0.18	0.82	0.679
C	1526.23	3.99	0.23	2.44	1.62
D	1550.37	1.58	0.12	0.70	0.702
E	1597.16	3.72	0.18	1.93	1.57

Table 4.2: *Tabulation of results for the dynamic rock elastic parameters obtained from empirical acoustic logs of plugs of core samples.*

Sample	Depth (m)	The Six Elastic Parameters			
		Young's Modulus (x106 psi)	Poisson's Ratio	Bulk Modulus (x106 psi)	Shear Modulus (x106 psi)
A	1467.84	9.31	0.30	7.70	3.59
B	1508.26	4.27	0.19	2.26	1.80
C	1526.23	8.27	0.29	6.48	3.21
D	1550.37	3.82	0.18	1.97	1.62
E	1597.16	8.73	0.28	6.47	3.42

Figure 4.1 compares the variation of static and dynamic Young's modulus with depth in the Goldwyer Formation. Between a depth of 1467.84 and 1597.16 meters, the dynamic Young's modulus is slightly higher than the static Young's modulus. The Young's modulus slightly

decreases with depth indicating that a smaller amount of force would be needed to fracture the rocks located at a depth of between 1508.26 and 1550.37 meters.

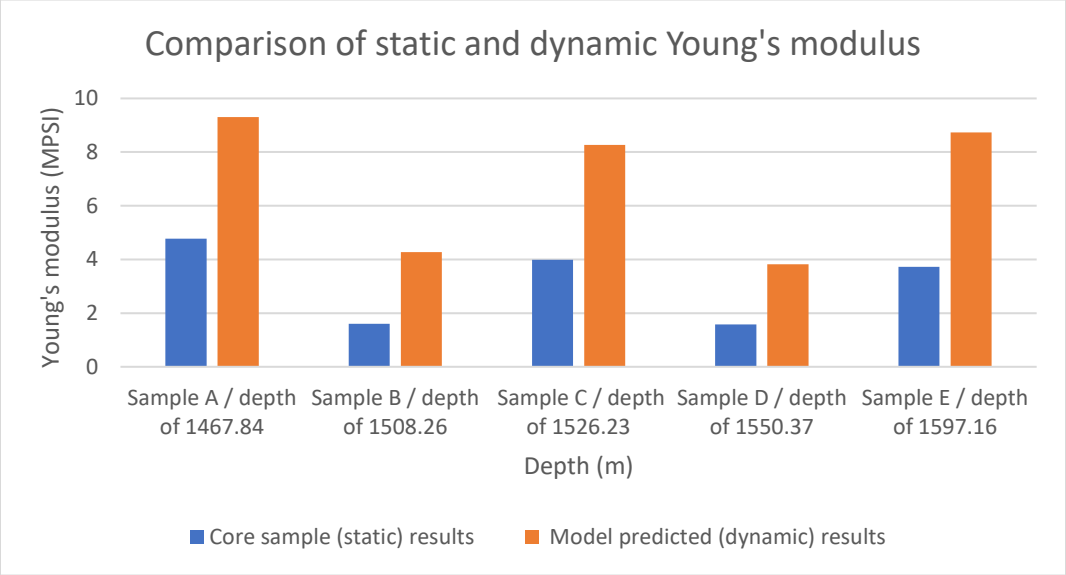

Figure 4.1: *Static and dynamic Young's modulus variation with depth.*

Figure 4.2 shows the variation of static and dynamic Poisson's ratio with depth in the Goldwyer Formation. At each depth, specifically between 1467.84 and 1597.16 meters, the dynamic Poisson's ratio value is relatively higher than the static Poisson's ratio value. The Poisson's ratio values slightly decrease with depth indicating that a smaller amount of force would be needed to fracture the rocks located at depths of 1508.26 meters and 1550.37 meters.

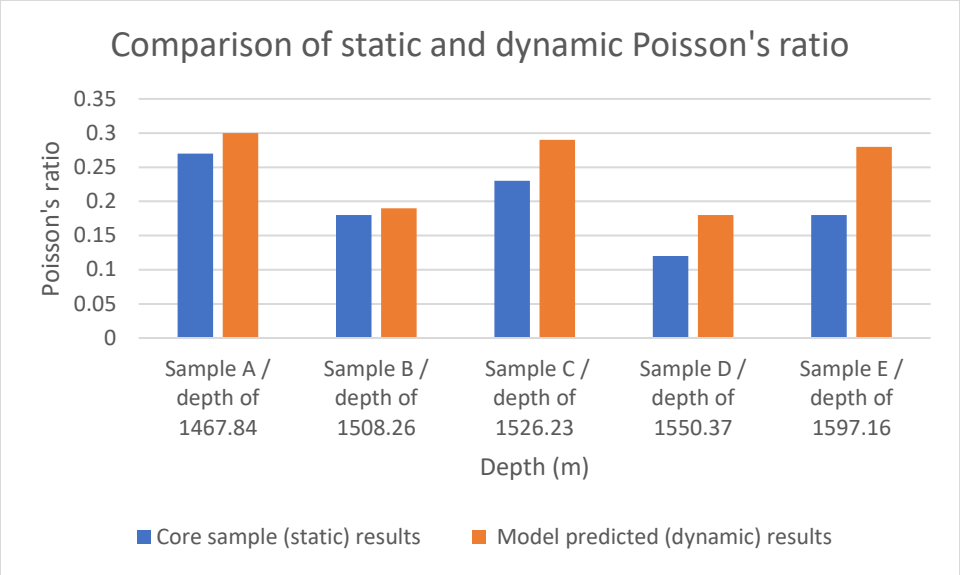

Figure 4.2: *Static and dynamic Poisson's ratio variation with depth.*

Figure 4.3 shows the variation of static and dynamic bulk modulus with depth in the Goldwyer Formation. At each depth, specifically between 1467.84 and 1597.16 meters, the dynamic bulk modulus is slightly higher than the static bulk modulus value. The interval located between a depth of 1508.26 and 1550.37 meters are characterized by slightly lower bulk modulus values indicating a possible location of sweet spots in these rocks as a lower amount of force would be needed to fracture these rocks.

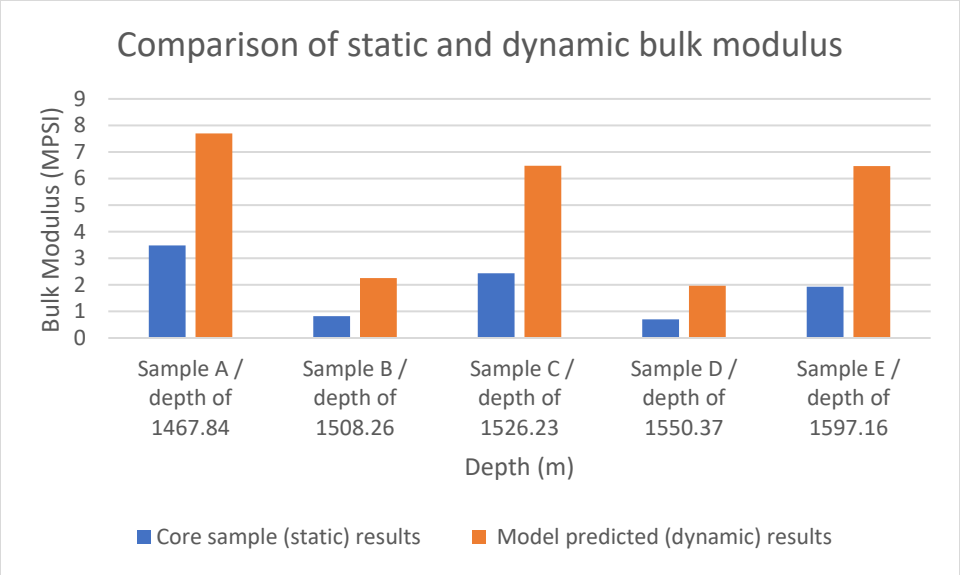

Figure 4.3: *Static and dynamic bulk modulus variation with depth.*

Figure 4.4 shows the variation of static and dynamic shear modulus with depth in the Goldwyer Formation. At each depth, specifically between 1467.84 and 1597.16 meters, the dynamic shear modulus value is slightly higher than the static shear modulus value. The interval located between a depth of 1508.26 and 1550.37 meters are characterized with slightly lower shear modulus values indicating a possible location of sweet spots in these rocks as a lower amount of force would be needed to fracture these rocks.

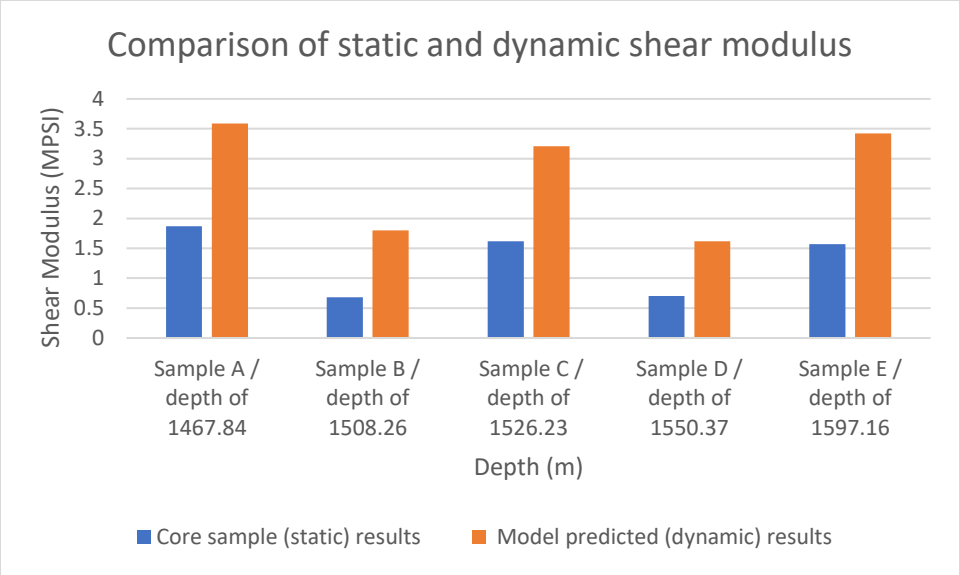

Figure 4.4: *Static and dynamic shear modulus variation with depth.*

Figure 4.5 shows the variation of static and dynamic Lambda.Rho with depth in the Goldwyer formation. At each depth, specifically between 1467.84 and 1597.16 meters, the dynamic Lambda.Rho value is slightly higher than the static Lambda.Rho value. The interval located at a depth of 1508.26 and 1550.37 meters are characterized by lower Lambda. Rho values indicating a possible location of sweet spots in the Goldwyer formation.

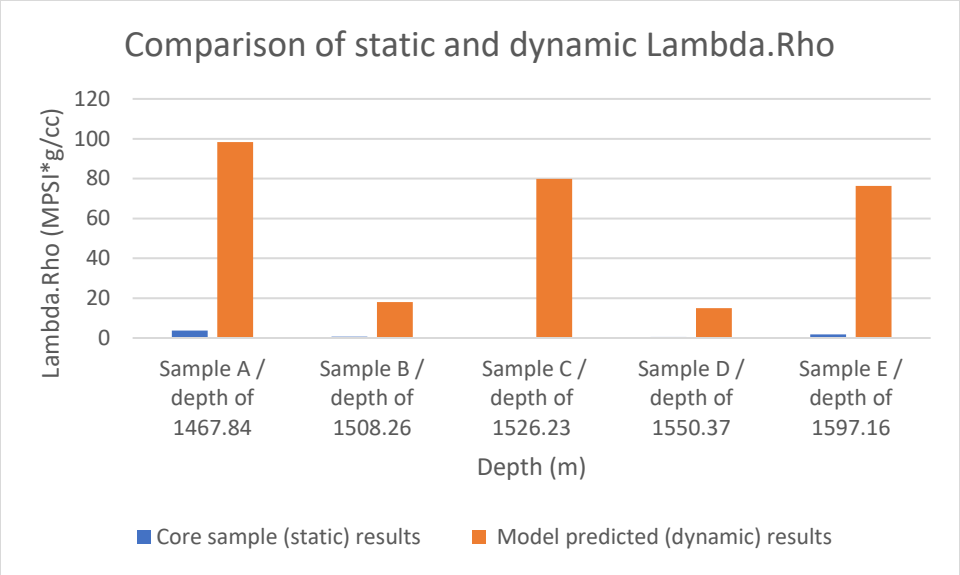

Figure 4.5: *Static and dynamic Lambda.Rho variation with depth.*

Figure 4.6 shows the variation of static and dynamic Mu.Rho with depth in the Goldwyer Formation. At each depth, specifically between 1467.84 and 1597.16 meters, the dynamic Mu.Rho value is slightly higher than the static Mu.Rho value. The interval located at a depth of 1508.26 and 1550.37 meters is characterized by slightly lower Mu. Rho values indicating a possible location of sweet spots in Goldwyer Formations.

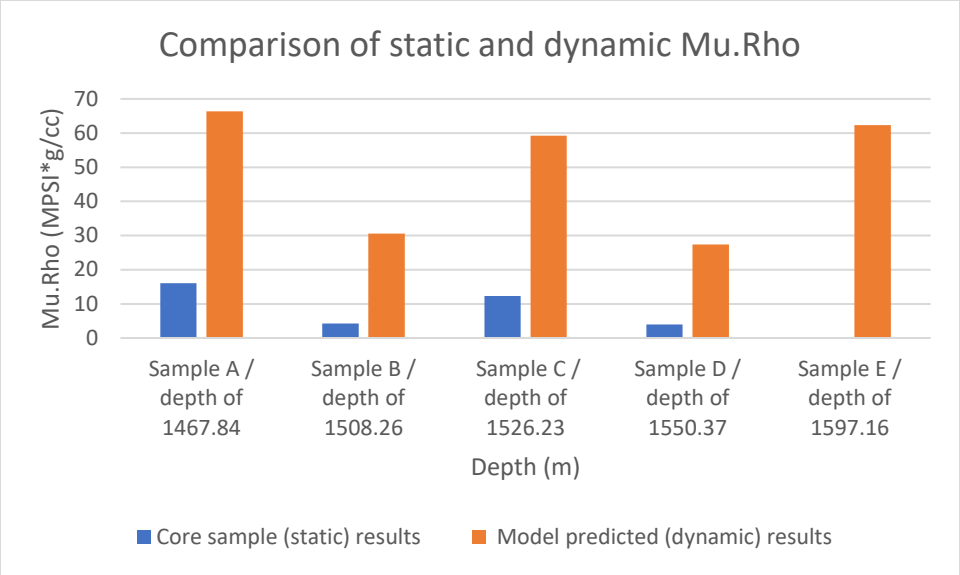

Figure 4.6: *Static and dynamic Mu.Rho variation with depth.*

4.1.1 Graphical Correlations between Dynamic and Static Elastic Parameters

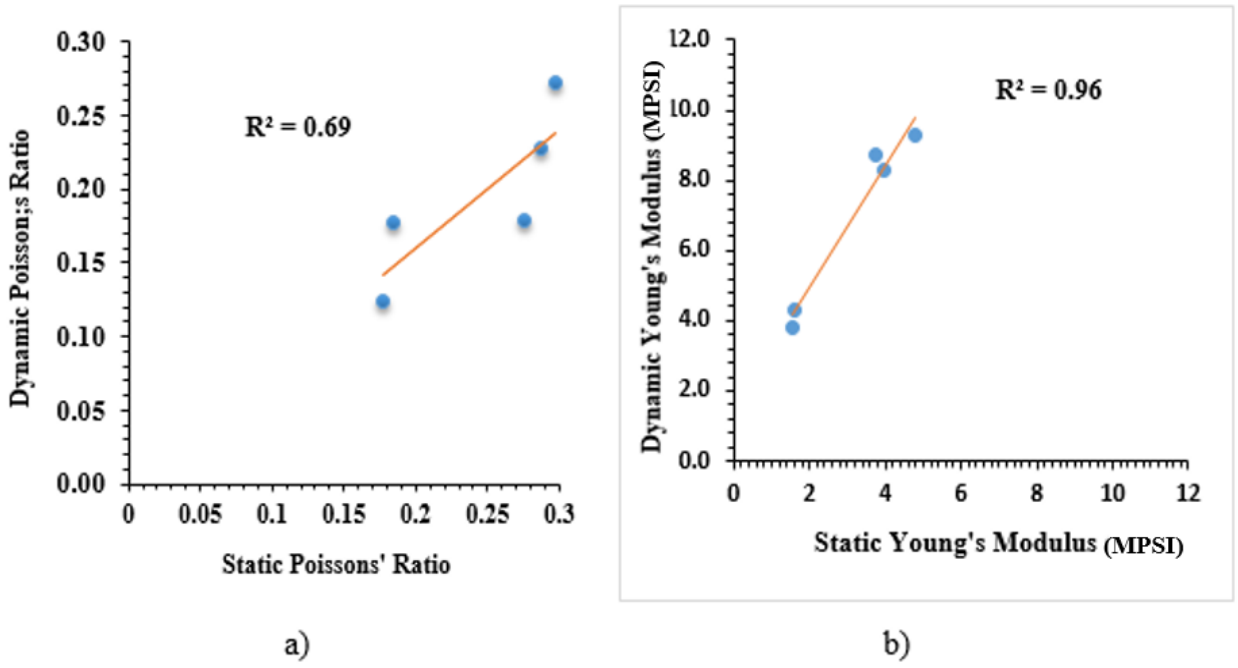

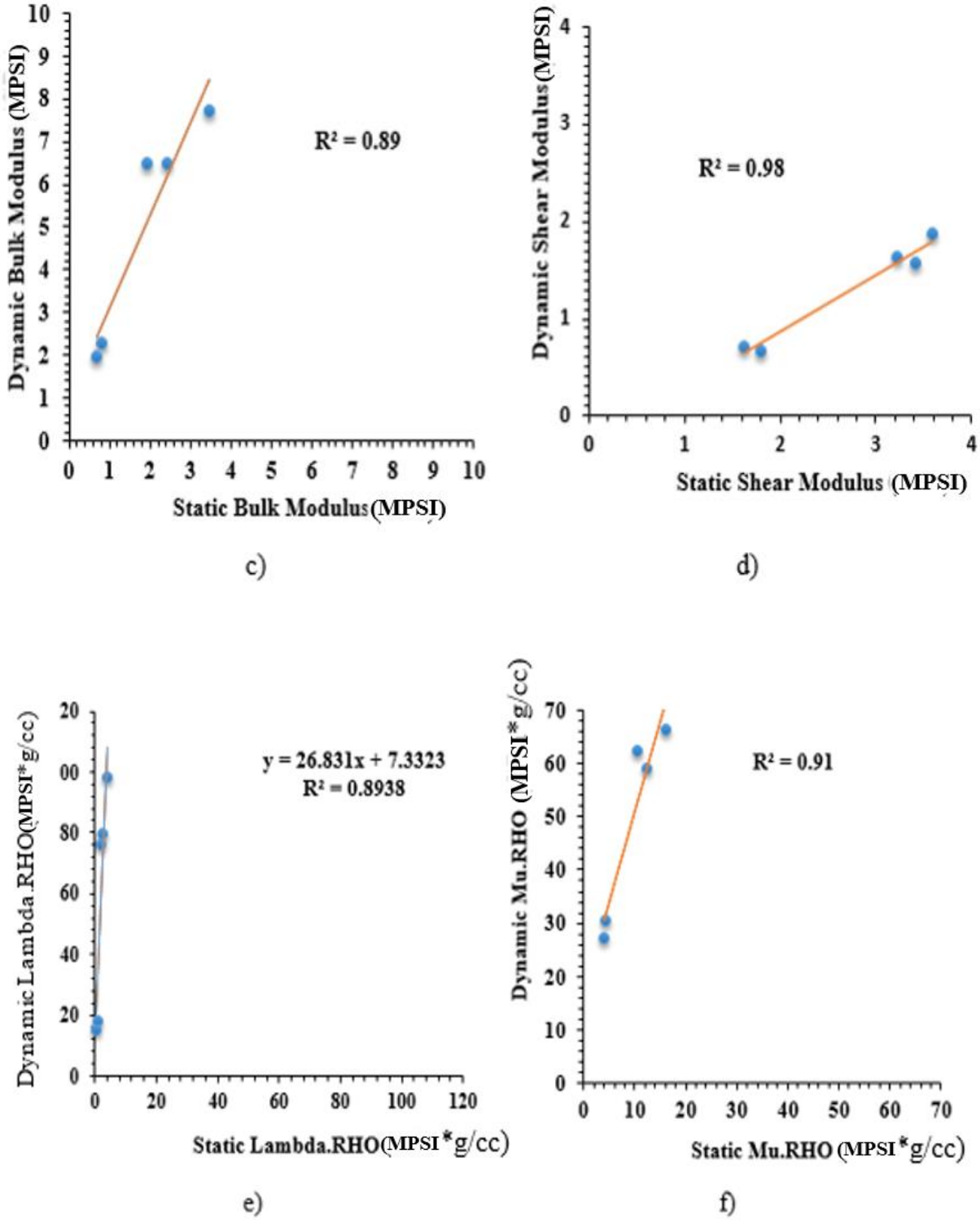

Figure 4.7: *Correlations of dynamic versus statistic rock elastic moduli.*

From Figure 4.7 above we have: a) Graph correlating the static and dynamic values of the Poisson's value with a correltion coefficient of 0.69. b) Graph correlating the static and dynamic values of the Young Modulus (E) elastic properties with a correltion coefficient of 0.96. c) Graph determining the correlation dynamic Bulk Modulus values as a function of Static Bulk Modulus values with a correltion coefficient of 0.89. d) Graph determining the functional correlation between static and dynamic shear modulus values with a correltion coefficient of 0.98. e) Graph depicting the computed correlational relationship that predicts dynamic Lambda.Rho values from their Static Lambda.Rho counterparts (y=26.831x + 7.3323) with a correltion coefficient of 0.89, f) A graphical depiction of the correlation between static and dynamic Mu.Rho parameters with a correltion coefficient of 0.91.

As depicted in Figure 4.7, high R-squared values for the models of the six rock elastic properties were recorded. In particular, the recorded R-squared values range from 0.69 to 0.96. The goodness-of-fit of a linear regression model can be measured using R-squared. High R-squared values indicate a good fit between the regression model and the data (Woodhouse, 2003). Therefore, the high R-squared values indicate the accuracy and reliability of the developed models for predicting static elastic rock properties from dynamic elastic rock properties.

Table 4.3: *Tabulation of computations to empirically determine the coefficients correlating the predicted static to the determined dynamic rock elastic parameters.*

Empirical Correlations	Coefficient of Determination (R^2)
$E_s = 1.76 \times E_d + 1.37$	0.96

$v_s = 0.86 \times v_d + 0.075$	0.69
$G_s = 0.59 \times G_d - 0.31$	0.97
$K_s = 2.16 \times K_d + 0.91$	0.89
$\mu_s * Rho = 3.4 \times \mu_d * Rho + 17.03$	0.91
$\lambda_s * Rho = 2.68 \times \lambda_d * Rho + 7.33$	0.89

4.1.2 Evaluation of Rock Elastic Parameters versus Depth

Figure 4.8 depicts the variation of the brittleness index and the six rock elastic parameters with depth. For each rock property, both the dynamic and the predicted static parameters follow a similar trend with depth. The brittleness index, which is computed from weighted rock elastic parameters is almost constant only with slight variations up to a depth of 1500 meters, beyond which it shifts to the right with an appreciable margin. This indicates the presence of brittle formations in the Canning Basin at depths of about 1520 meters. Brittle rocks fracture easily when subjected to stress, thus shale gas in such brittle and shaly formations could easily be produced through hydraulic fracturing.

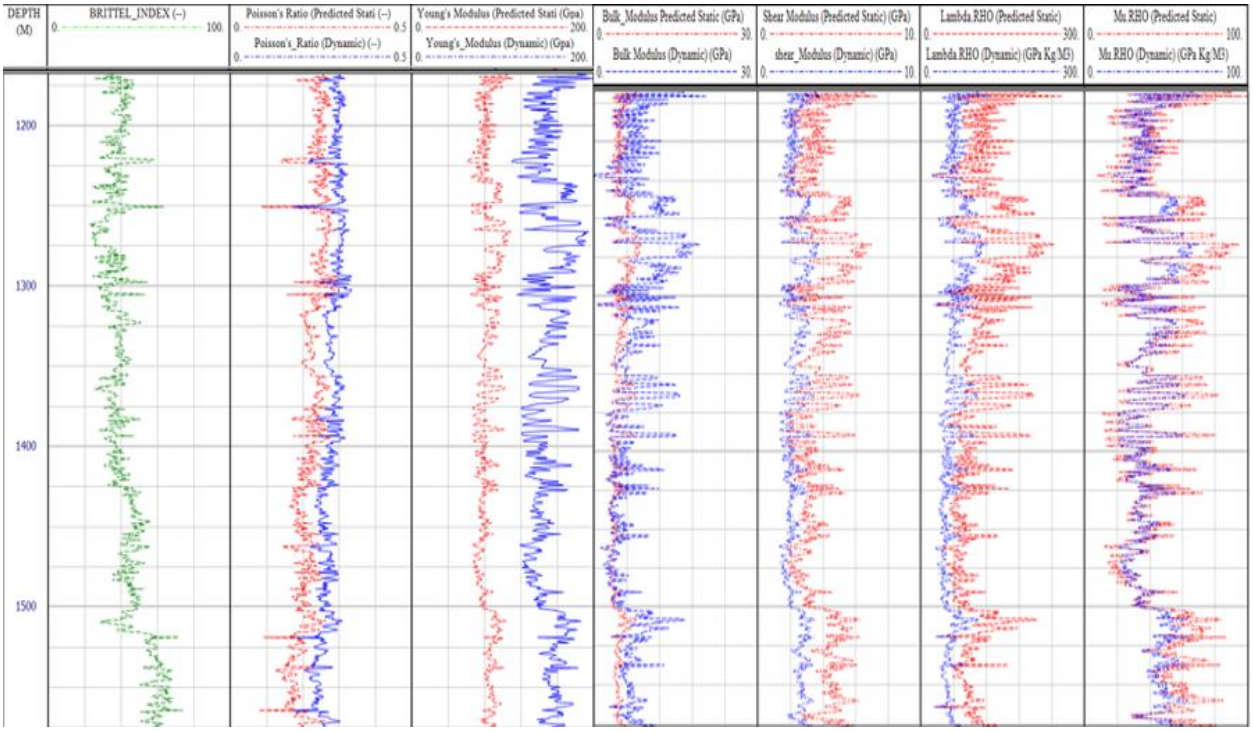

Figure 4.8: *Plots comparing the variations of Young's Modulus (E), Poisson's Ratio (υ), bulk modulus (K), shear modulus (G), Lambda.Rho (λ.Rho) and Mu.Rho (μ.Rho) rock deformation properties versus depth for all the wells.*

4.1.3 In Situ Inter-well Geomechanical Mapping/Modeling of Determined Rock Deformation Properties

Figure 4.9 shows a mapping and distribution of the Young's moduli in the in situ rock mass covered by the wells located in the Canning Basin considered in the present study. The in situ rock masses surrounding Looma-1 are characterized by a high Young's moduli. Conversely, the in situ rock mass surrounding the Canopus-1 well is characterized by lower Young's moduli values. This means higher pressure would be required to fracture the rock masses surrounding Looma-1 as compared to the pressure that would be required to fracture the in situ rock mass surrounding Canopus-1.

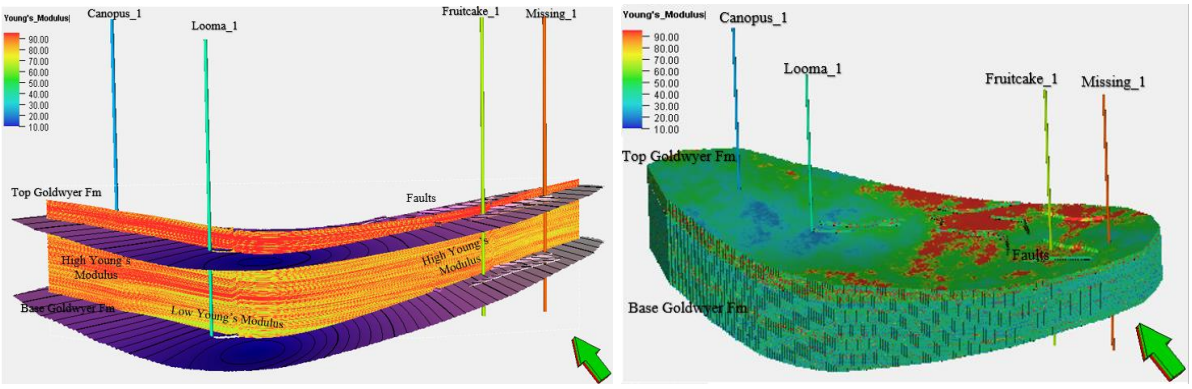

Figure 4.9: *The distribution of Young's modulus from the data sample. The distribution of Young's moduli parameters between wells is illustrated be change from high to low and high again.*

Figure 4.10 shows the distribution of the Poisson's ratio in the study area. The in situ rock mass around the Missing-1 and Fruitcake-1 wells is characterized by higher Poisson's ratio values as compared to the in situ rock mass around Canopus-1 and Looma-1 wells that is characterized by relatively lower Poisson's ratio values. This means that when subjected to the same amount of compression pressure, the strain in the rock masses with higher Poisson's ratio values would be higher as compared to the strain in the rock masses with lower Poisson's ratio values.

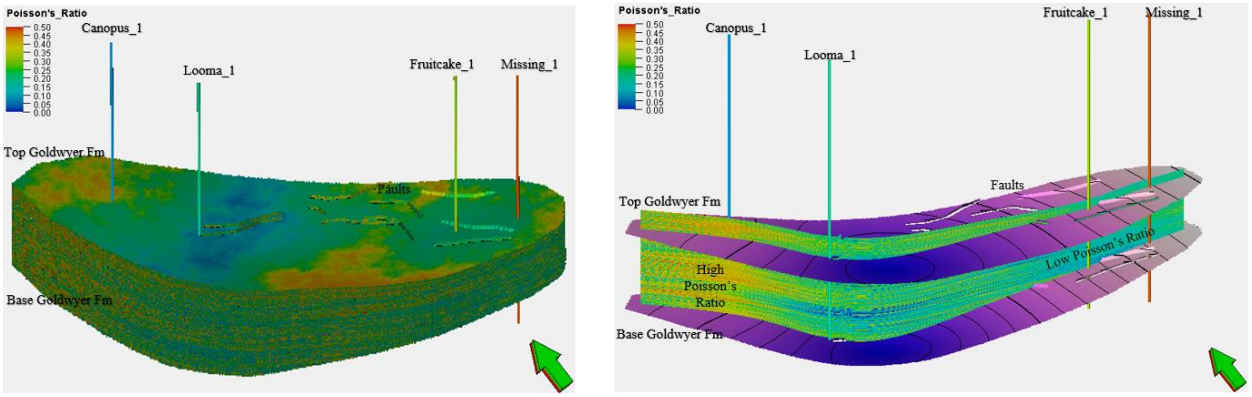

Figure 4.10: *Depiction of Poisson's ratio between the target wells. a) The model depicts a cross-section of the Poisson ratio over the study area. b) The model depicts one of the 3D average realizations estimated the distribution of the Poisson ratio values.*

Figure 4.11 depicts the distribution of brittleness index in the in situ rock mass surrounding the wells. The rock mass around Canopus-1 and Looma-1 wells is characterized by higher brittleness index values as compared to the rock mass surrounding Fruitcake-1 and Missing-1 wells that has lower brittleness index values. This indicates that the in situ rock mass surrounding the former wells is more brittle and lower pressure would be required to fracture it as compared to the latter wells.

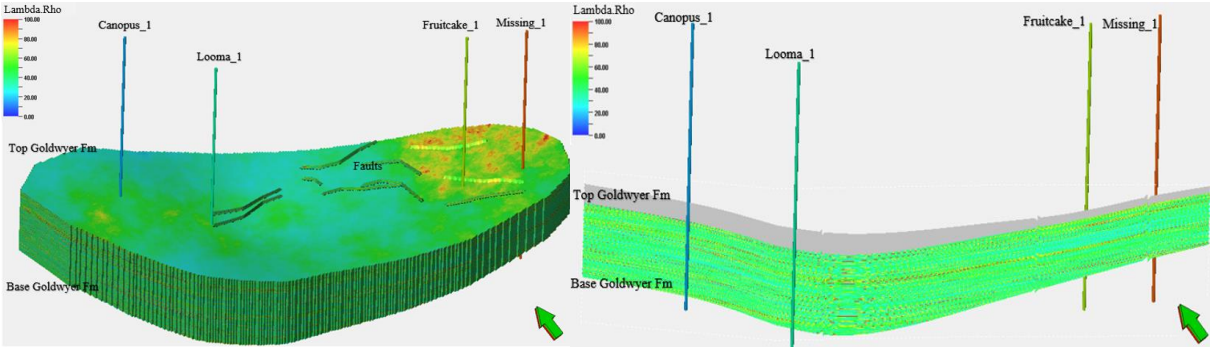

Figure 4.11. *The brittleness index parameter and its overall distribution around the reservoir area around the wells (top picture) and the cross-section of the brittle shale model (bottom picture).*

Figure 4.12 shows the distribution of the bulk modulus in the in situ rock mass surrounding the wells. The rock mass surrounding Looma-1 is characterized by higher bulk modulus values as compared to the rock mass surrounding Canopus-1. Bulk modulus indicates the level of resistance of a material to compression. Therefore, the rock mass surrounding Looma-1 is more resistant to compression as compared to the rock mass surrounding Canopus-1.

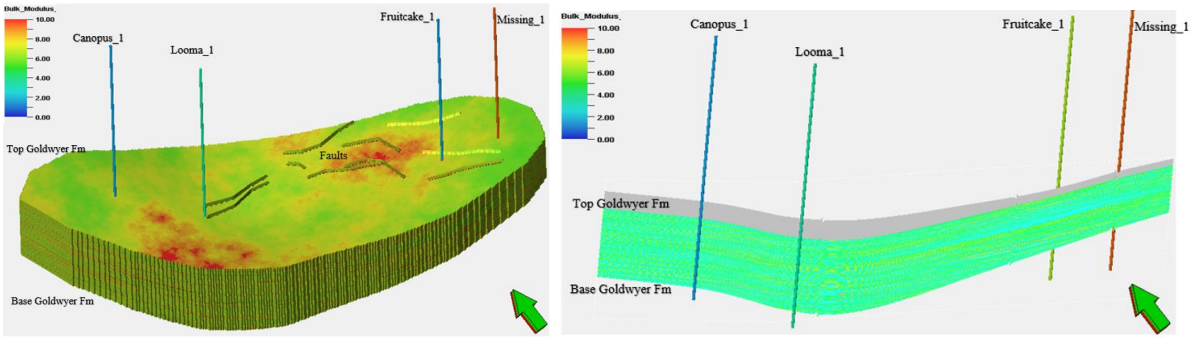

Figure 4.12: *a) A model static bulk modulus parameter for the area surrounding the wells. b) The depiction of the cross-sectional distribution of static bulk modulus instances with the greenish portions showing the areas with the highest values within the predicted in-situ reservoir model.*

Figure 4.13 shows a distribution of the shear modulus in the rock mass surrounding the wells. The modulus of rigidity of a rock indicates the level of resistance of a rock to shear stress. Rocks with higher modulus of rigidity are more rigid as compared to rocks with lower shear modulus values. The rock mass surrounding Missing-1 and Fruitcake-1 well is characterized by

higher shear modulus values as compared to the rock mass surrounding Canopus-1 and Looma-1 wells. This indicates that the rock mass surrounding the former wells is more rigid as compared to the rock mass surrounding the latter wells.

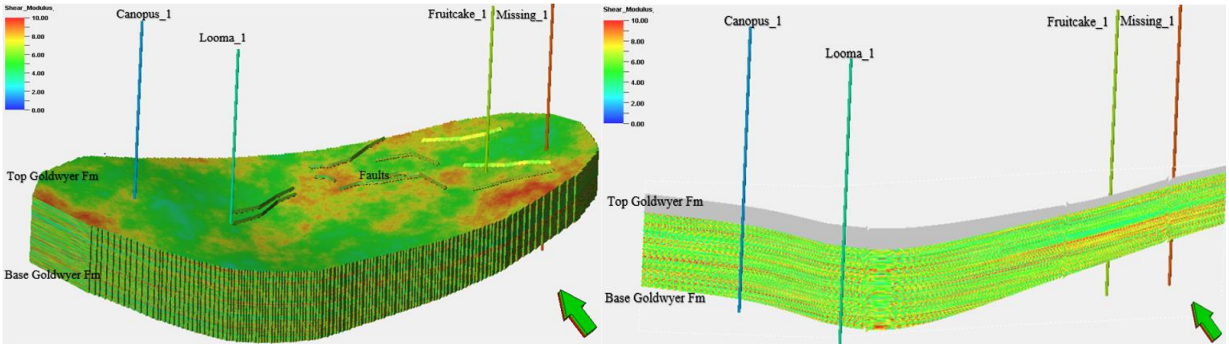

Figure 4.13: *a) The shear modulus of the reservoir area surrounding the wells. (b) was conceived from the data and depicted the best-case scenarios for the shear modulus deformation parameters around the wells.*

Figure 4.14 shows models of Lambda.Rho distribution in the rock mass surrounding the wells. The rock mass surrounding Fruitcake-1 and Missing-1 wells is characterized by higher Lambda.Rho values as compared to the rock mass surrounding Canopus-1 and Looma-1 wells. This indicates that the pore fluid content in the two rock masses is different.

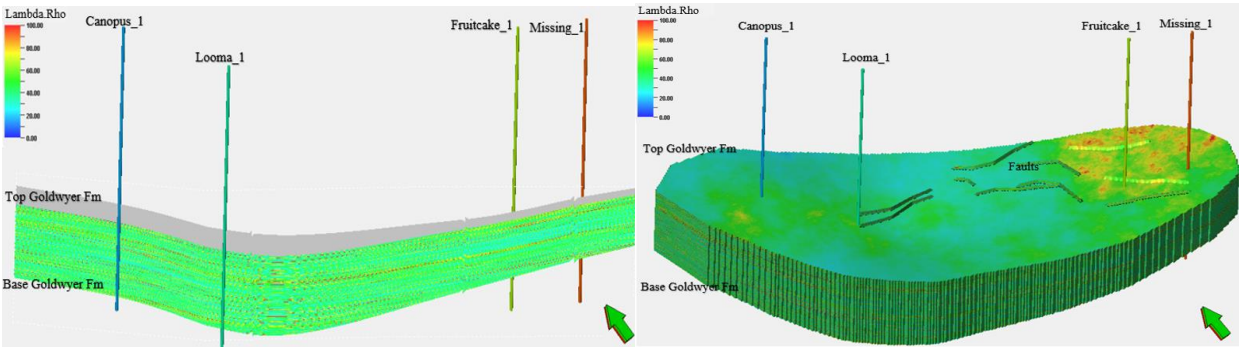

Figure 4.14: *(a) A section of the area immediately surrounding the wells. High Lambda values are mapped to the one side of the area near the Fruitcake-1 and Missing-1 wells. (b) A 3D model of Lamda parameter and its spatial distribution across the entire reservoir area that includes the wells.*

Figure 4.15 depicts models of the Mu.Rho in the in situ rock mass surrounding the wells. According to Goodway, Chen and Downton (1997), Mu.Rho is an indicator of rigidity and can be used to discriminate pore fluid content. The rock mass surrounding Fruitcake-1 and Missing-1 wells is characterized by higher Mu.Rho values as compared to the rock mass surrounding Canopus-1 and Looma-1 wells. This indicates that the pore fluid content in the two rock masses is different. The pore fluid content in the rock mass surrounding the Canopus-1 and Looma-1 is likely to be shale gas due to the low Mu.Rho values.

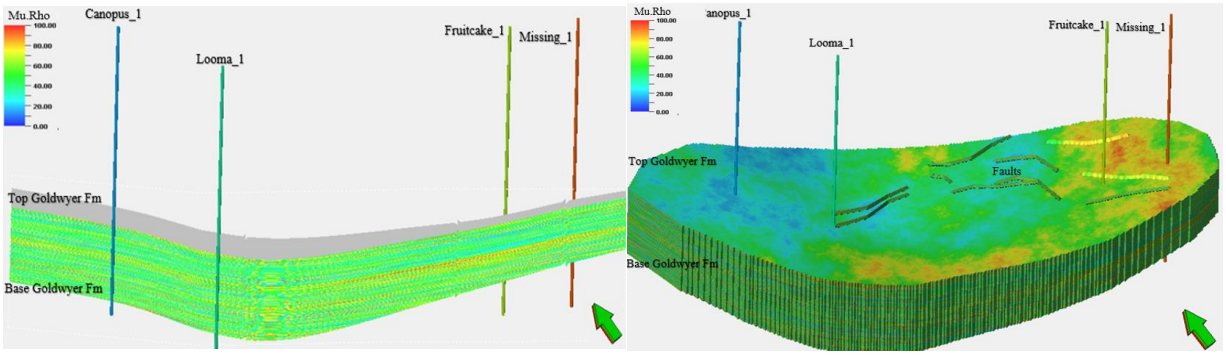

Figure 4.15: *(a) A 2D section of the Mu.Rho parameter across the reservoir area of the sample wells under consideration. b) The plot is a depiction of the best-fit model that attempted to analyze the spatial distribution of this parameter for the wells under consideration.*

4.1.4 In-Situ Reservoir Deformation Parameter Simulations/Models

Figure 4.16 depicts the variation of gamma ray, Lambda.Rho, Mu.Rho and brittleness index versus depth. In Well C, the brittleness index increases gradually indicating the presence of brittle rocks. Conversely, the Lambda.Rho shifts to the left. This is indicative of possible presence of fluids in the formations (Goodway, Chen & Downton, 1997).

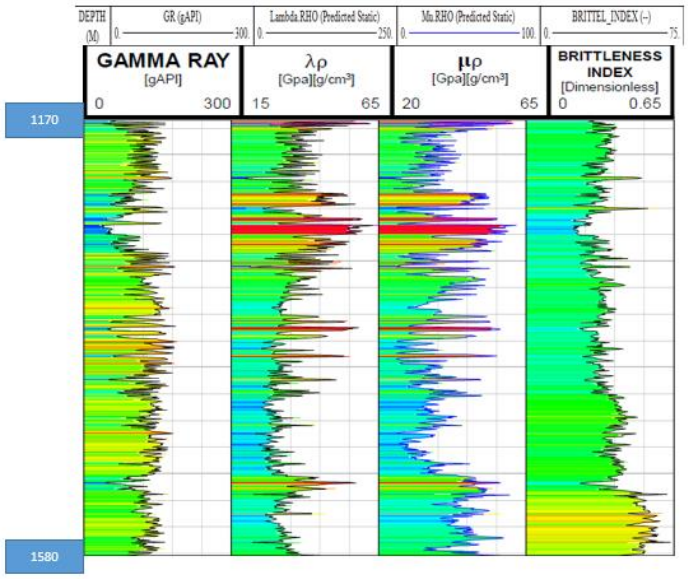

Figure 4.16: *Plots showing the gamma ray, Lambda.Rho, Mu.Rho and brittleness index variations with respect to depth for the targeted formations.*

Figure 4.17 shows a cross plot of Young's modulus versus Poisson's ratio. From this cross plot, it can be seen that most of the formations in the Canning Basin have moderate to high Young's modulus values and moderate Poisson's ratio values. However, there is an anomalous region with low Young's modulus and low Poisson's ratio values. This anomalous region was interpreted as a shale gas sweet spot.

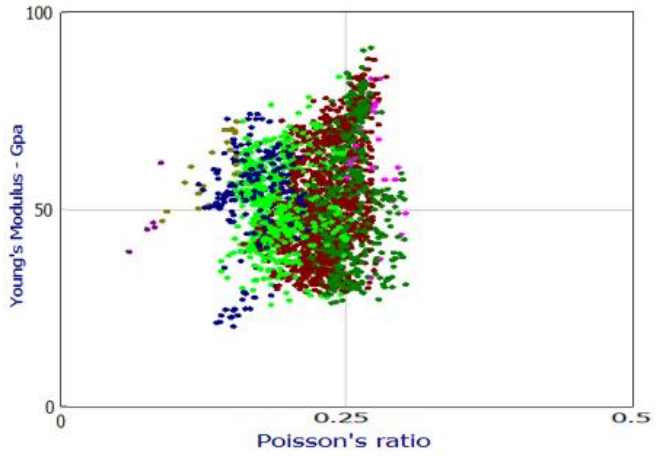

Figure 4.17. *Graph showing the correlation between Young modulus and Poisson's ratio indicating a complex relationship.*

4.2 Brittleness Index Model

Shale plays are unconventional reservoirs that are characterized by low permeability. Therefore, identification of sweet spots in shale plays is crucial to economical drilling operations. In particular, sweet spots help in the identification of the ideal drilling location. Sweet spots in unconventional wells can be identified by determining the reservoir characteristics such as the brittleness index. To this end, a key objective of this study was to model, map and interpret rock deformation parameters including the elastic moduli and the brittleness index of the in-situ inter-well rock mass covered by the wells in the selected study area.

A brittleness index model of the inter-well rock mass covered by the wells considered in this study is as depicted in Figure 4.18. The brittle shale model was built from weighted models of each of the elastic properties. From the brittle shale model, it is clear that the brittle shale is concentrated around the subsurface rock mass covered by the Missing-1 and Fruitcake-1 wells. Conversely, the rock mass around the Canopus-1 and Looma-1 wells is relatively ductile.

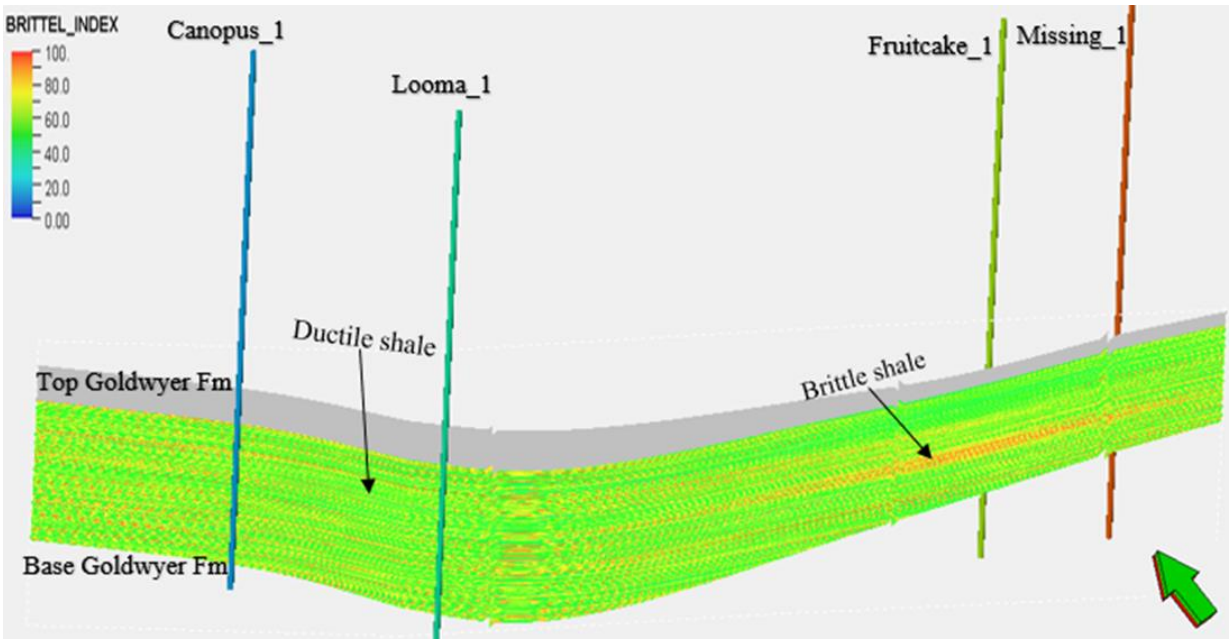

Figure 4.18. *Brittleness index model of the Goldwyer Formation in the study area*

4.3 Summary

In this chapter, the results of the elastic rock parameters were presented. The static rock elastic parameters including Young's modulus, Poisson's ratio, bulk modulus, shear modulus, Lambda.Rho and Mu.Rho were obtained from uniaxial strength empirical laboratory tests of core samples. The dynamic rock elastic parameters were then obtained from empirical acoustic logs. The results for the static elastic rock estimation are summarized in Table 4.1, whereas the results of the dynamic rock elastic rock estimation are outlined in Table 4.2. In line with the objective of this research, correlational equations between the static and dynamic elastic rock properties were established as summarized in Table 4.3. The variation of the computed brittleness index with respect to depth of the five wells is also depicted in Figure 4.18.

In line with the third objective of this research which sought to model, map and interpret rock deformation properties of the in situ inter-well rock mass covered by Canopus-1 and Looma-1, the geomechanical/rock deformation properties were modelled and mapped as depicted in Figure 4.10a to Figure 4.10d. As is seen in Figure 4.10a, the variation of Young's modulus with depth was noted to change from high to low values. Variation of Poisson's ratio values with depth was also modelled and mapped as shown in Figure 4.11. In the considered depth interval, the Poisson ratio values were observed to alternate between high to low values and then from high to low values. High Poisson ratio values were observed around Canopus-1 and Looma-1 wells, particularly in the Goldwyer Formation.

Brittleness index around the five wells was modeled and mapped as shown in Figure 4.9. For the considered depth, the brittleness index transited from high to low and then from high to low; that is, from brittle rocks to ductile rocks. Canopus-1 and Looma-1 had a low brittleness index. Modeling and mapping of the predicted bulk modulus, show high bulk modulus values around the five wells.

From the modeling and mapping of the predicted shear modulus as shown in Figure 4.14, the lower shear modulus values were observed around Canopus-1 and Looma-1 wells. Similarly, lower Lambda.Rho and Mu.Rho values are observed around the Canopus-1 and Looma-1 wells. The values of Lambda.Rho and Mu.Rho are displayed in Figure 4.15 and Figure 4.16, respectively.

5 SEISMIC INVERSION

5.1 Seismic Inversion Results

As pointed out previously, seismic inversion is a key tool in reservoir characterization. Seismic inversion enables the combination of well and seismic data for the prediction of rock properties across a survey such as a lithology, fluid content and porosity that can then be used to help in the identification of hydrocarbon targets and reservoirs. Although many of the rock properties can be identified at the well using the well-log data, rock properties such as fluid content, lithology, and porosity are difficult to obtain away from the well using seismic data. However, with the aid of seismic inversion, rock properties such as impedance and attributes derived from impedance and attributes derived from such as Poisson's ratio, Vp/Vs, Lambda.Rho, Mu.Rho can be obtained. The impedance attributes are directly linked to fluid content, lithology and porosity. In this project RH software was used for seismic inversion.

While well-log data emphasizes rock layer properties, seismic amplitude emphasizes the interface between lithological units. Seismic inversion converts seismic from a boundary property to a layer property such as impedance – impedance attributes emphasize the rock units. Given that impedance is a product of density and velocity, the lithological velocity and density can as well be obtained from seismic inversion. In line with the above, the study endeavored to perform seismic inversion and generate three-dimensional model seismic models of the study area. In order to improve the accuracy of precise mapping and interpreting rock deformation, the study further endeavored to integrate the seismic models with the rock physics properties models. The seismic inversion results are as presented in this section.

Post-stack inversion method was used to generate acoustic impedance volume (AI). This method requires wavelet extraction, which can be achieved using well data or by using a statistical wavelet. The former provides a good evaluation of both the amplitude and phase spectra of the wavelet. In the latter process, the wavelet is extracted from the input seismic data. Both wavelet extraction processes were applied so as to obtain the best correlation between the well log and seismic data. Each of the five wells was tied to the seismic data used to build the inversion model. This allowed for seismic interpretation of the picked horizons. Availability of check-shot data allowed for the establishment of a time to depth conversion model. As shown in Figure 5.1, a high correlation (0.79) was derived between the synthetic trace and the real seismic data.

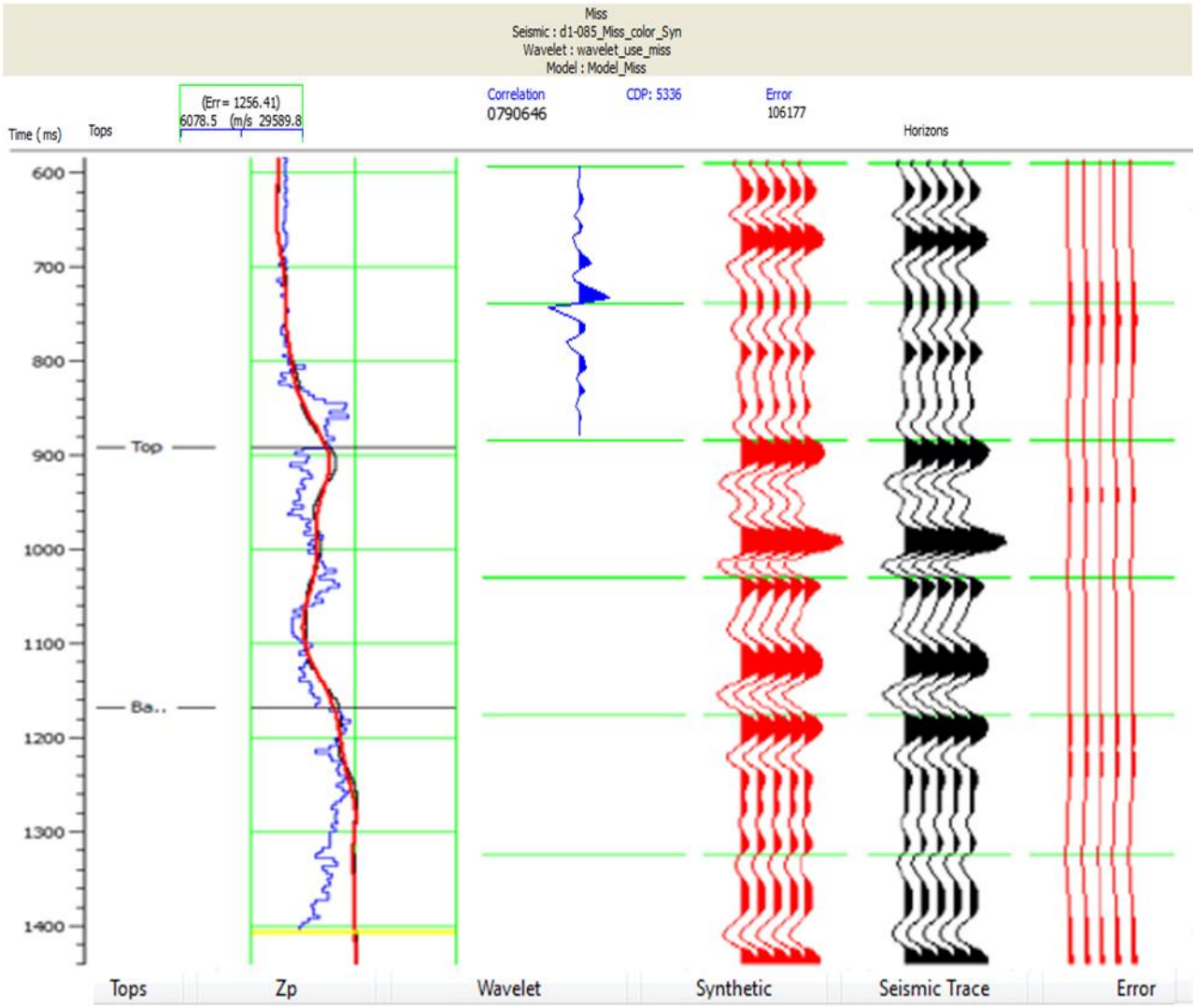

Figure 5.1: *Example of the P-impedance inversion analysis of one well for the Goldwyer Shale. The blue curve is P-impedance, the red curve is the synthetic seismogram and the black curve is the seismic trace.*

The first two seismic inversion steps involve synthetic modeling and wavelet extraction from seismic data and the generation of a background model from well log data tied to the seismic data. The background model contains no seismic information and acts as a guide to ensure that the impedance values obtained from seismic inversion are realistic. Figures 5.2 and Figure 5.3 show

the background models generated using the well log data for Fruitcake-1 and Looma-1 wells, respectively. The high acoustic impedance values around the wells are an indication of shale sweet spots around this area.

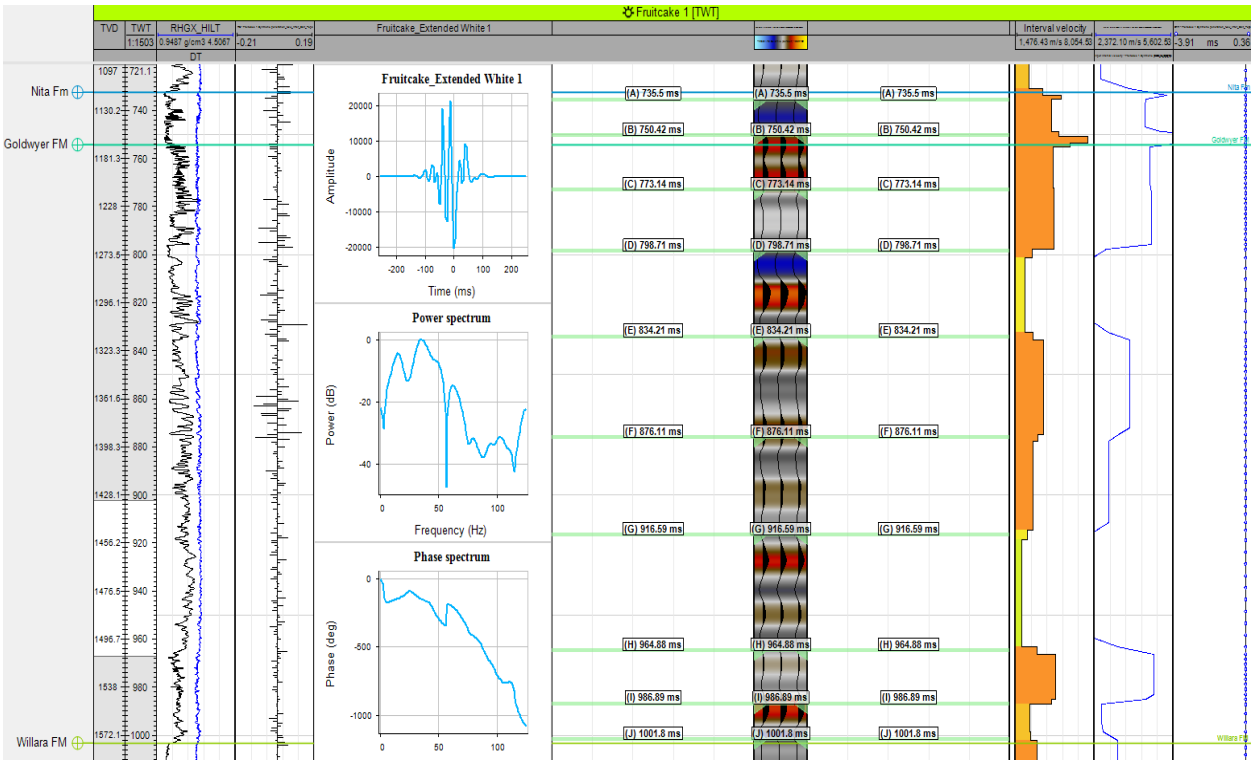

Figure 5.2: *Background model for the Fruitcake-1 well.*

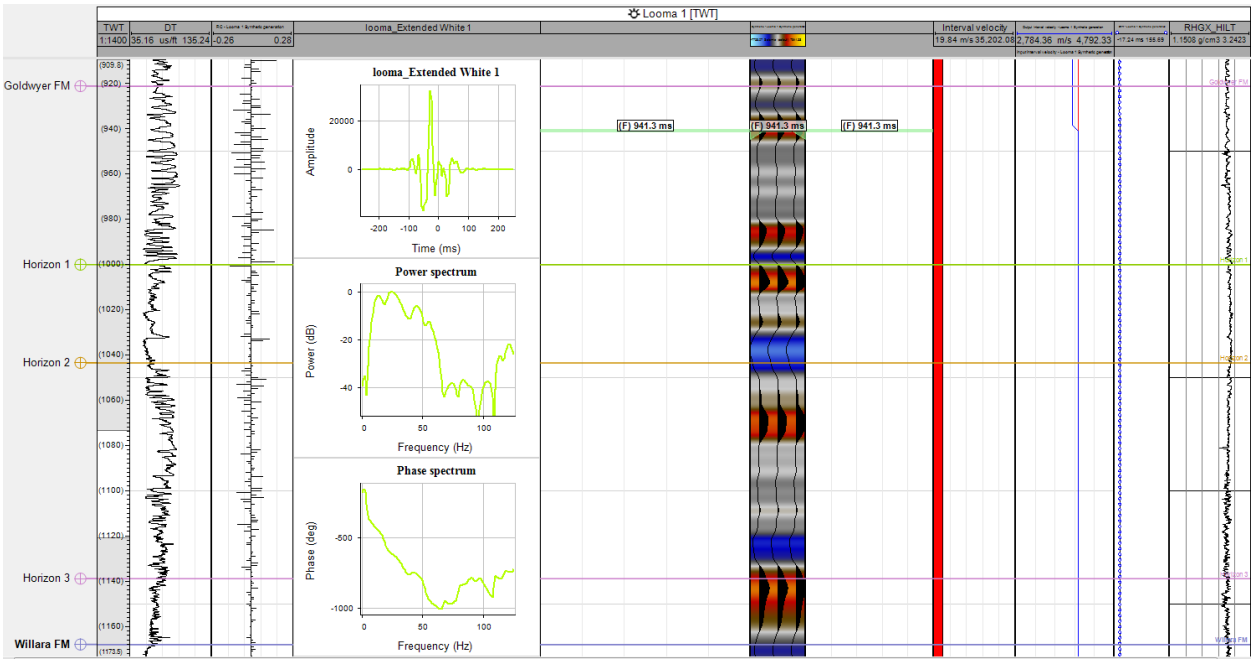

Figure 5.3: *Background model for the Looma-1 well.*

The seismic inversion results for the Fruitcake-1 well are depicted in Figure 5.4. There is an irregular variation of impedance in the subsurface layer. This is an indication of potential shale gas sweet spots around this area. A high correlation (0.89) between the synthetic model and the seismic inversion results is noted.

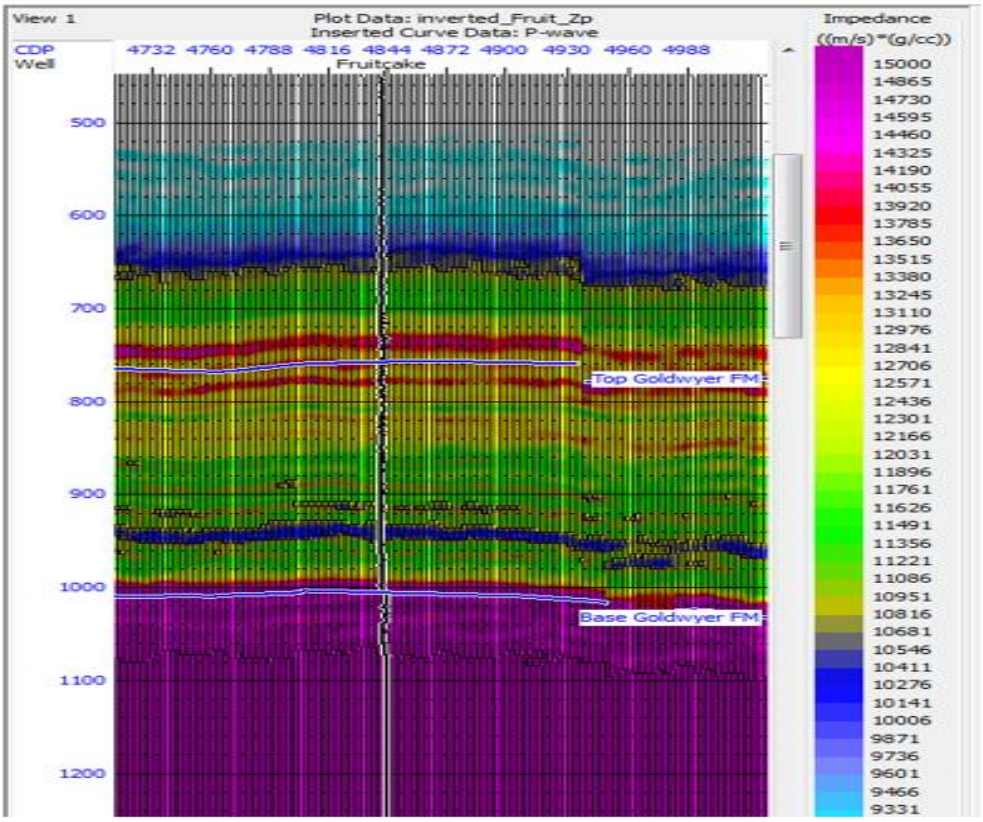

Figure 5.4: *Seismic inversion results for the Fruitcake-1 well.*

Figure 5.5 depicts the seismic inversion results for the Looma-1 well. The impedance eventually increases with depth, but the lithological units between the top and base Goldwyer formation have a low impedance.

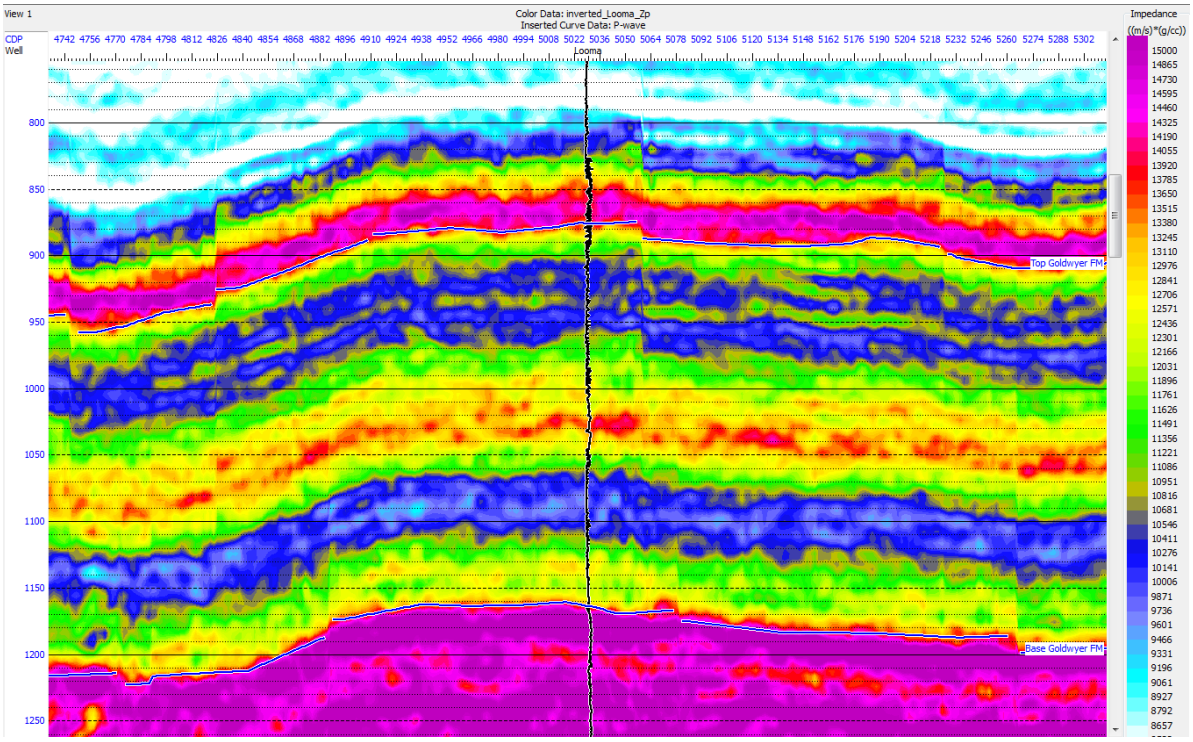

Figure 5.5: *Seismic inversion results for the Looma-1 well.*

Figure 5.6 depicts the seismic inversion results for the Missing-1 well. There is an irregular variation of acoustic impedance in the lithological units between the top and base Goldwyer Formation. However, the acoustic impedance eventually increases with depth. This is an indication of potential shale gas sweet spots in the lithological units between the top and base Goldwyer Formation in the subsurface area around the Missing-1 well.

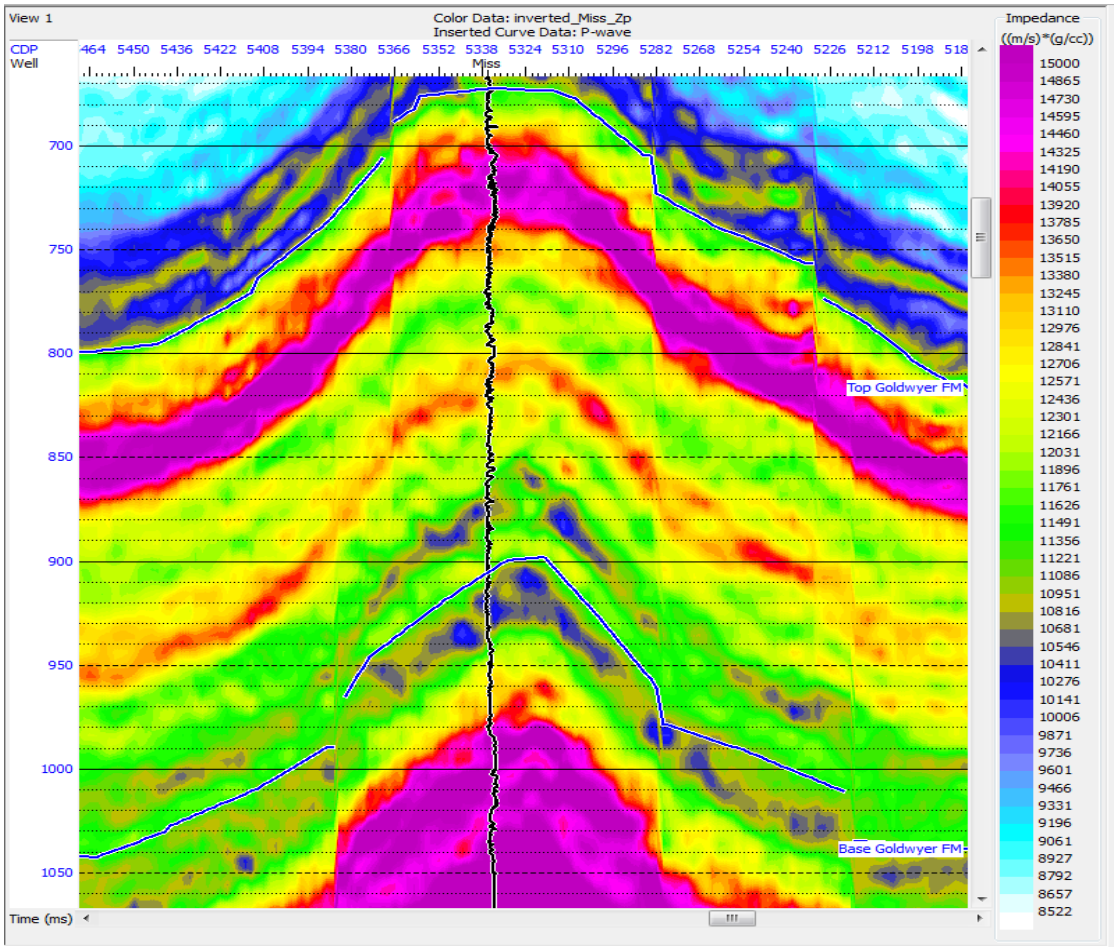

Figure 5.6: *Seismic inversion results for the Missing-1 well.*

Figure 5.7 depicts the seismic inversion results for the Missing-1 well model. In particular, the variation of sonic velocity, density and acoustic impedance with depth in the Goldwyer Formation is shown. The top Goldwyer formation is characterized by a high sonic velocity (approximately 4982 m/s), with the immediate underlying lithological layer having relatively lower sonic velocity. The sonic velocity eventually decreases with the base Goldwyer Formation having the lowest sonic velocity. On the other hand, the top and base Goldwyer formations are denser as compared to the middle lithological units that are characterized by relatively lower density values.

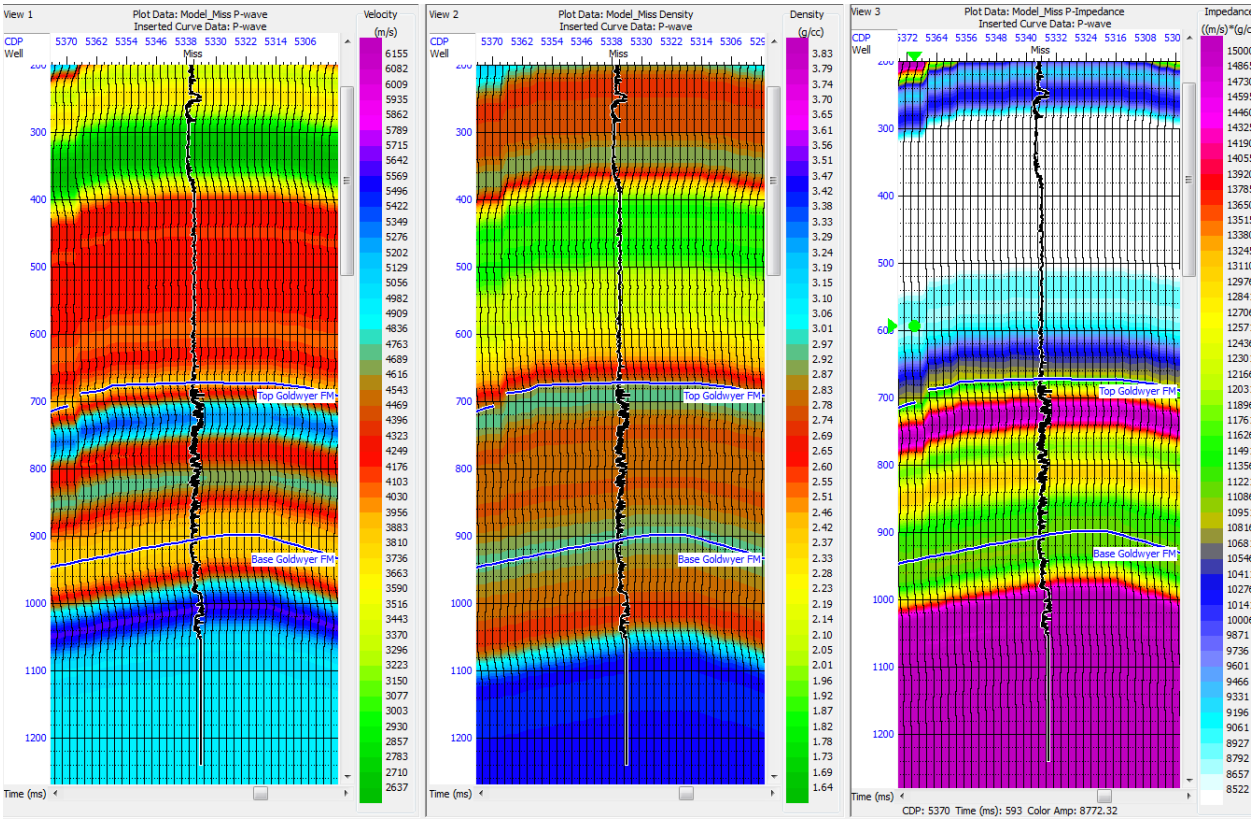

Figure 5.7: *Seismic inversion of the Missing-1well model. The black curve shown at the well location is the gamma ray.*

Figure 5.8 depicts the seismic inversion results for the Looma-1 well model. In particular, the figure shows the variation of acoustic impedance sonic velocity with depth in the Goldwyer Formation. The lithological units near the top and base Goldwyer formation are characterized by lower sonic velocities, whereas the middle lithological layer is characterized by relatively higher sonic velocity values. Similarly, the lithological units near the top and base Goldwyer formation are characterized by higher acoustic impedance values as compared to the middle lithological layer, which is characterized by relatively lower acoustic impedance values.

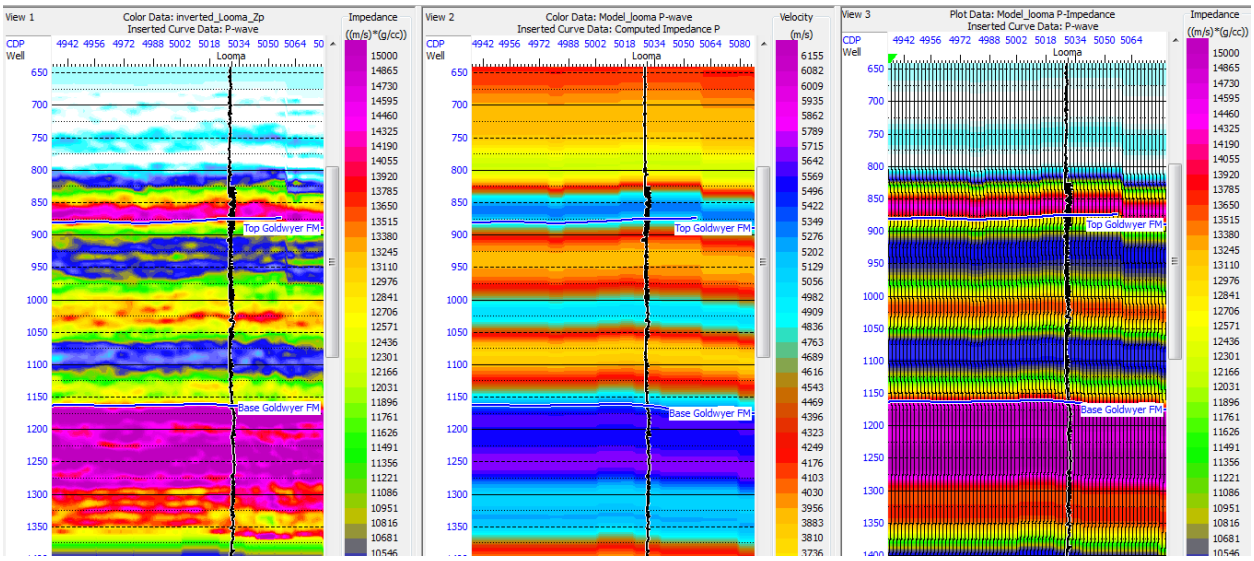

Figure 5.8: *Seismic inversion of the Looma-1 well model.*

The study also sought to develop 3-dimensional models and mapping of the rock deformation parameters derived from seismic inversion. These rock deformation properties include Poisson's ratio, Young's modulus, Mu.Rho, Lambda.Rho, bulk modulus and shear modulus.

5.1.1 Poisson's Ratio

The model of Poisson's ratio across the study area is depicted in Figure 5.10. The lithological units around the Missing-1 and Fruitcake-1 are characterized by low Poisson ratio values as opposed to the lithological units around the Canopus-1 and Looma-1 wells that are characterized by relatively higher Poisson's ratio values. A higher Poisson's ratio indicates a ductile material, whereas a low Poisson's ratio indicates a brittle material. Therefore, the subsurface lithological units around the Fruitcake-1 and Missing-1 wells are brittle.

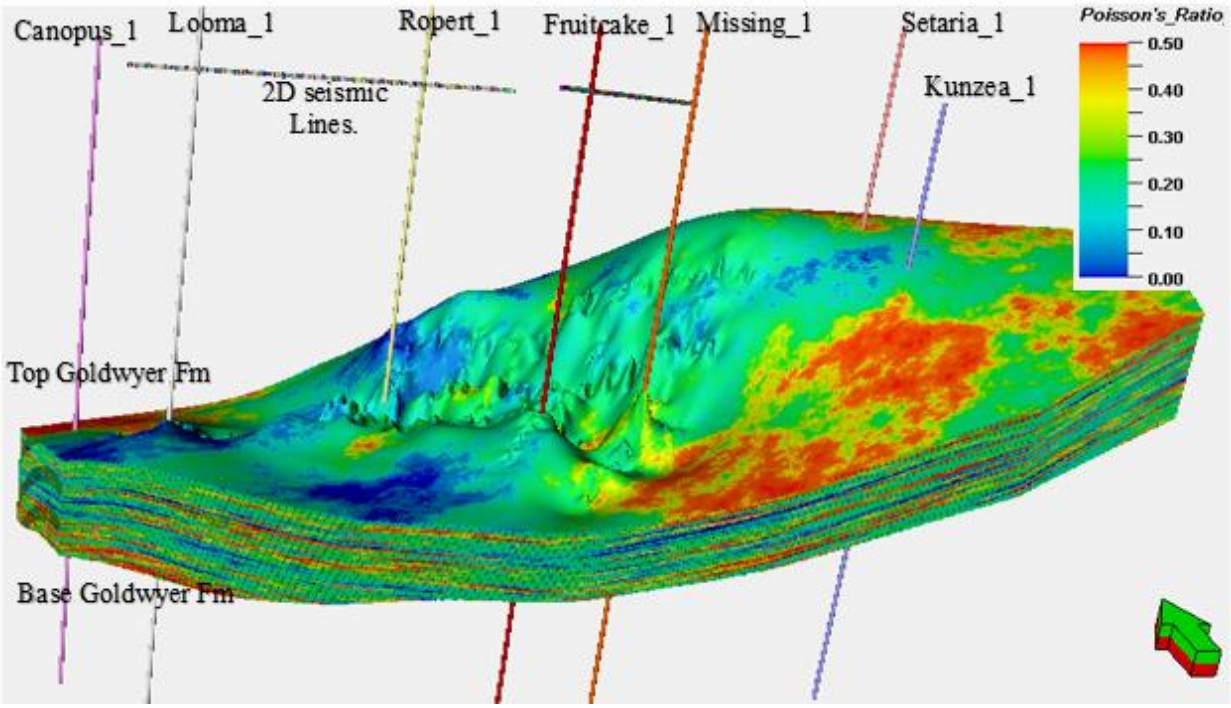

Figure 5.9: *The model of* Poisson*'s modulus across the study area.*

The of Young's modulus across the study area is depicted in Figure 5.11. The subsurface lithological units around the Canopus-1 and Missing-1 wells are characterized by relatively higher Young's modulus values as compared to the subsurface lithological units around the Fruitcake-1

and Missing-1 wells. This means that a lesser pressure would be required to fracture the shale around the latter wells as compared the pressure that would be required to fracture the shale around the former wells.

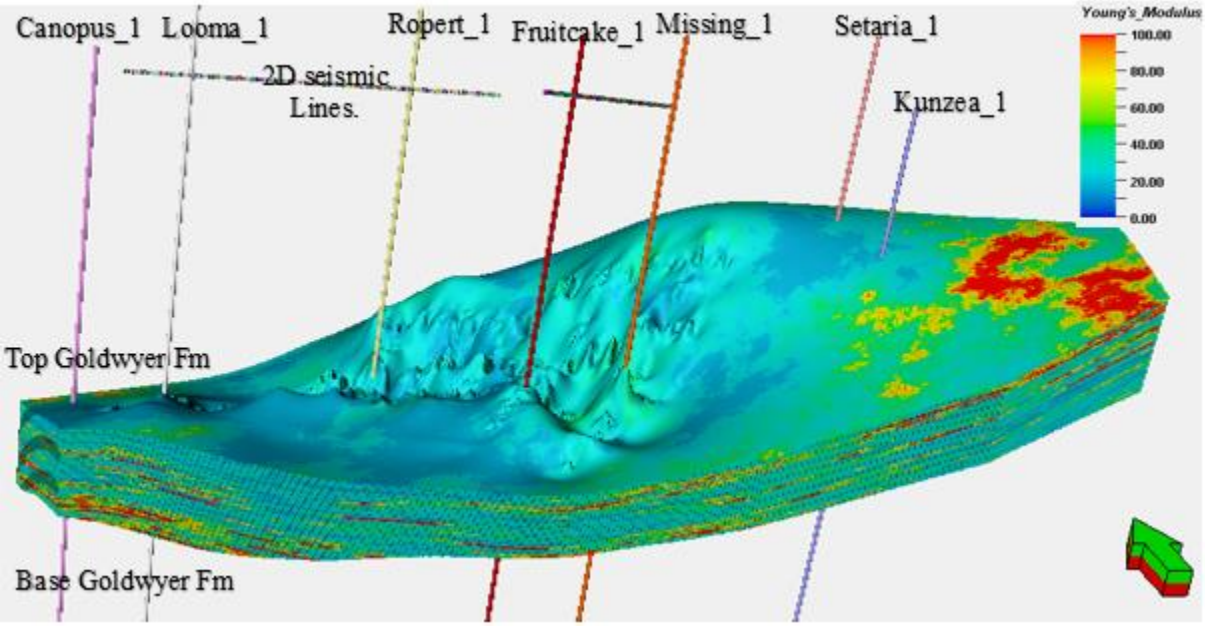

Figure 5.10: *The model of Young's modulus across the study area.*

5.1.2 Mu.Rho

Figure 5.12 depicts a model of the Mu.Rho across the study area. The lithological units around the Canopus-1 and Looma-1 are characterized by higher Mu.Rho values as compared to the lithological units around Fruitcake-1 and Missing-1 wells.

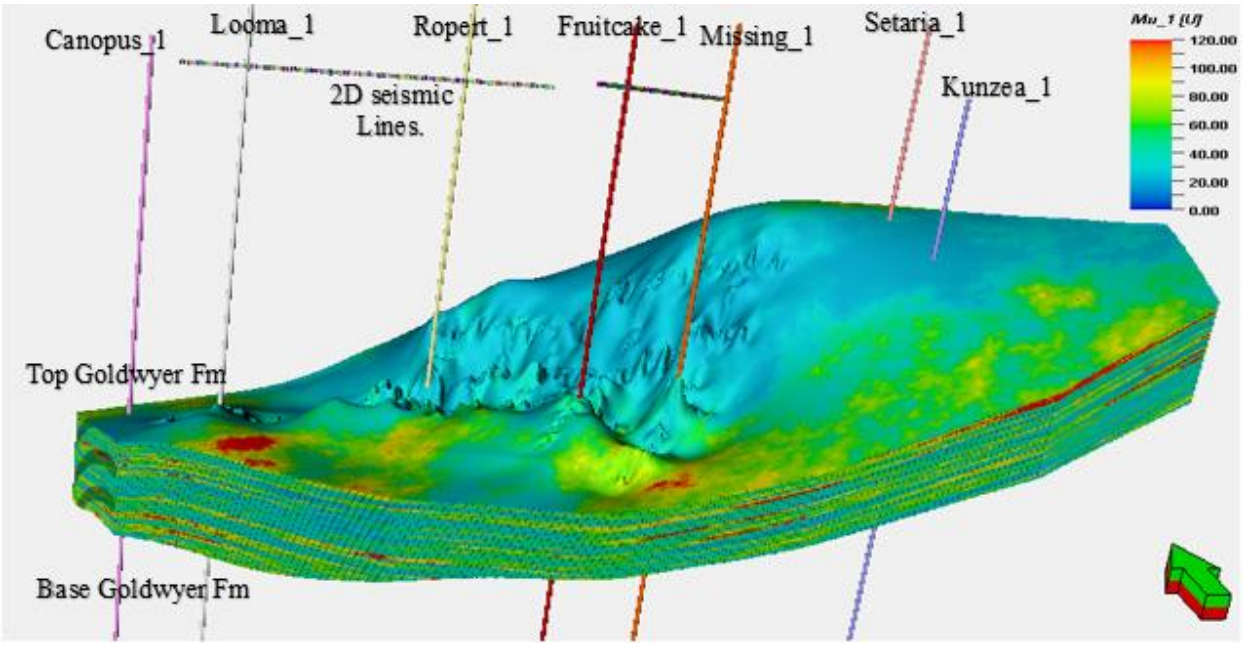

Figure 5.11: *The model of Mu.Rho across the study area.*

5.1.3 Lambda.Rho

A model the Lambda.Rho across the study area is depicted in Figure 5.13. The subsurface lithological units around the Canopus-1 and Looma-1 wells are characterized by higher Lambda.Rho values as compared to the subsurface lithological units around Fruitcake-1 and Missing-1 wells.

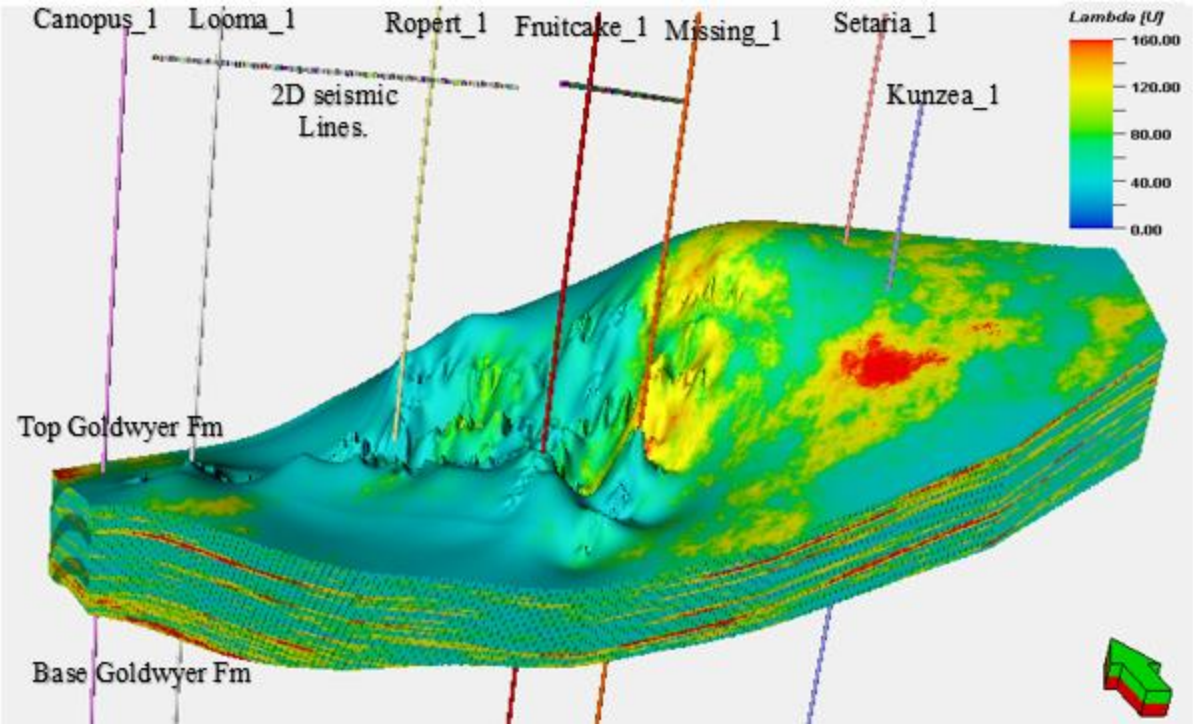

Figure 5.12: *The model of Lambda.Rho across the study area.*

5.1.4 Bulk Modulus

Figure 5.14 depicts a model of bulk modulus across the study area. The lithological units around the Looma-1 and Canopus-1 wells are characterized by higher bulk modulus values as compared to the lithological units around the Fruitcake-1 and Missing-1 wells. Therefore, a lower pressure would be required to fracture the subsurface rocks around the Former wells as compared to the pressure that would be required to fracture the subsurface rocks around the latter wells.

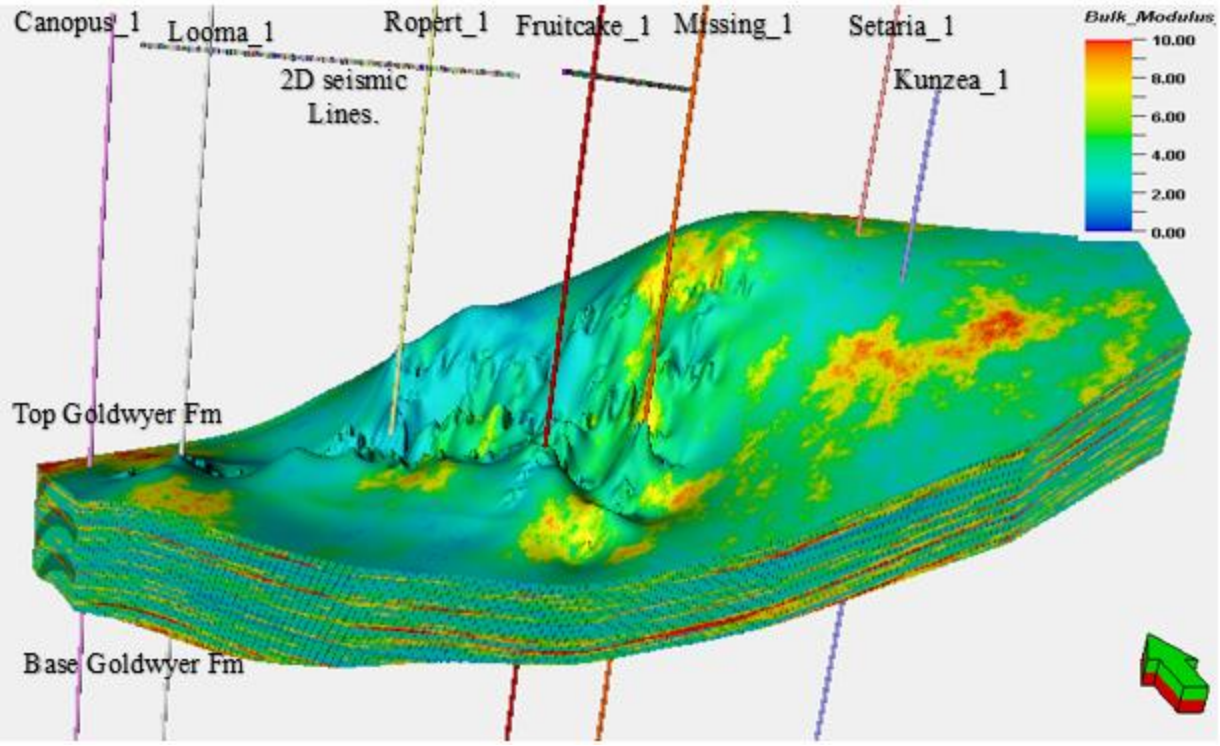

Figure 5.13: *A 3D model bulk modulus across the study area.*

5.1.5 Shear Modulus

A model of shear modulus across the study area is shown in Figure 5.15. The subsurface rocks around Looma-1 and Canopus-1 wells are characterized by higher shear modulus values as compared to the subsurface rocks around the Missing-1 and Fruitcake-1 wells. This means that the subsurface rocks around the former wells are stiffer as compared to the subsurface rocks around the latter wells.

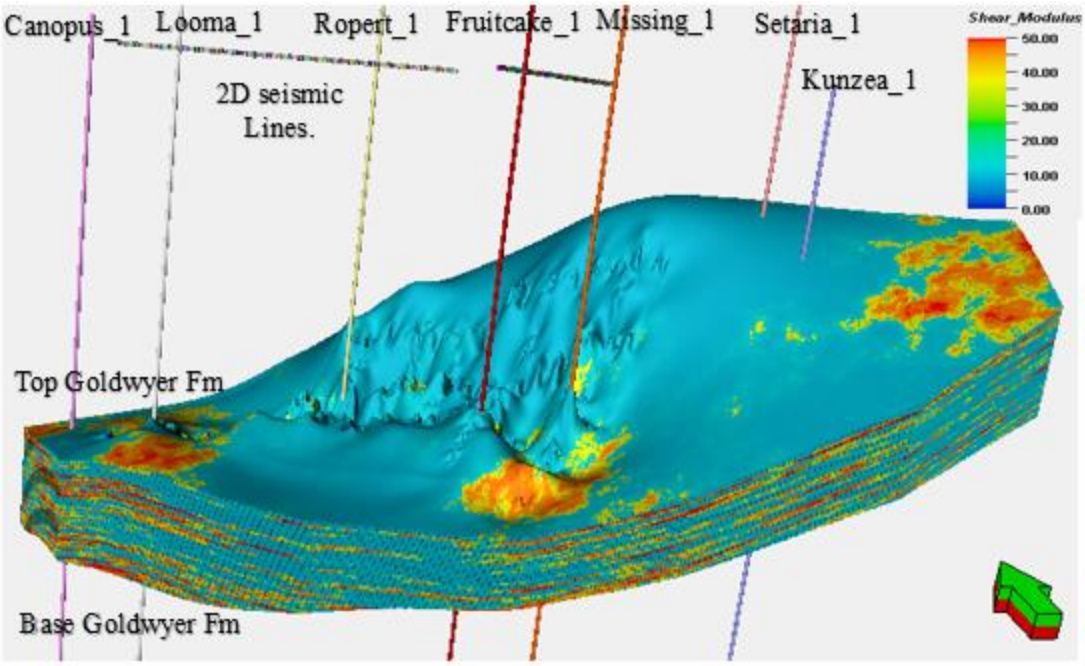

Figure 5.14: *The model of shear modulus across the study area.*

5.1.6 Brittleness Index

A model of the brittle shale index across the study area is depicted in Figure 5.16. The subsurface rocks around the Missing-1 and Fruitcake-1 wells are characterized by a higher brittleness index as compared to the subsurface rocks around the Canopus-1 and Looma-1 wells. Rocks with a higher brittleness index are easier to break as compared to rocks with a lower brittleness index. Equally, shale sweet spots are brittle and characterized by higher brittleness index values. Therefore, the higher brittleness index values around the former wells are an indication of sweet spots in the Goldwyer shale plays.

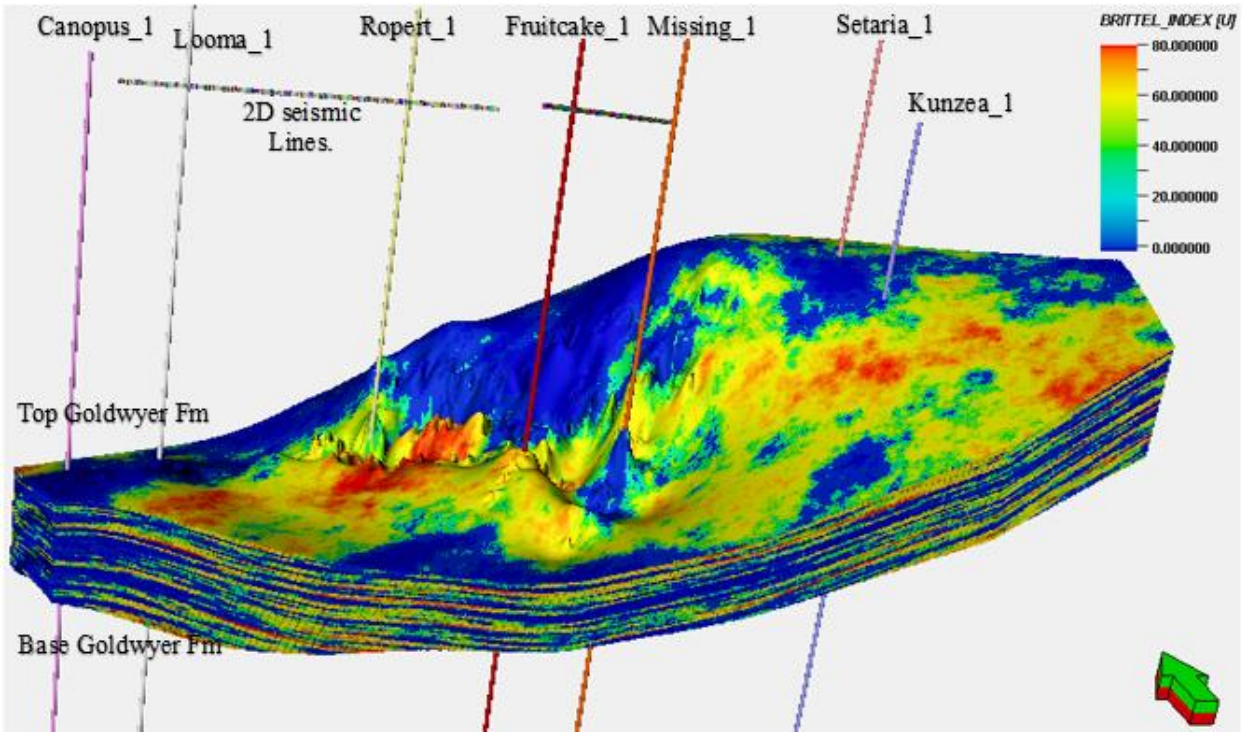

Figure 5.15: *The model of brittleness index across the study area.*

5.2 Summary

The Seismic inversion results for the study area were presented in this chapter. A high correlation (0.89) between the synthetic background models generated from the well log data and the seismic inversion results was noted. The seismic inversion revealed an irregular variation of acoustic impedance with depth in the lithological units between the top and base Goldwyer Formation around the Fruitcake-1 well, whereas the acoustic impedance in the lithological units between the top and base Goldwyer Formation around the Looma-1 well was found to remain constant with depth. However, in all the subsurface rocks below the base Goldwyer Formation, the acoustic impedance eventually increased with depth. The high acoustic impedance values in

the lithological units around the Fruitcake-1 well was interpreted as an indicator of shale gas sweet spots.

Rock deformation parameters determined from the seismic inversion results, including Poisson's ratio, Young's modulus, Mu.Rho, Lambda.Rho, bulk modulus and shear modulus were modelled and mapped across the study area. The lithological units around the Looma-1 and Canopus-1 were found to have relatively higher values of Poisson's ratio, Young's modulus, Mu.Rho, Lambda.Rho, bulk modulus and shear modulus as compared to the lithological units around Fruitcake-1 and Missing-1 wells. In addition, the brittleness index across the study area was modelled and mapped. The lithological units around the Fruitcake-1 and Missing-1 wells have a higher brittleness index as compared to the lithological units around the Canopus-1 and Looma-1 wells. Thus, the shale plays around the former wells have brittle sweet spots that are viable for drilling operations.

6 RESEARCH FINDING'S COMPARISONS, SIGNIFICANCE, DISCUSSION, CONCLUSION AND RECOMMENDATIONS

6.1 Comparing the Research's Findings to Current Extant Literature, Studies and Results

The current study presented a modified approach for mapping in-situ brittleness and other rock elastic properties in shale gas reservoirs. This was achieved by meeting the following objectives. First, deriving correlations and establishing a relationship between dynamic and static rock elastic properties. Here, the static rock properties are obtained from direct measurement of core samples, whereas the dynamic properties are determined from p-velocity, s-velocity and density logs. Second, by predicting the in-situ brittleness index using predicted static and actual dynamic rock elastic properties. Third, by performing a three-dimensional modeling, mapping and interpretation of rock deformation properties on the inter-well rock mass covered by the five wells in the Canning Basin considered in this study. Lastly, performing seismic inversion and integrating the seismic inversion models with the prior determined rock physics models.

Alshakhs (2017) assessed the prospectivity of the Goldwyer Formation in the Canning Basin as a potential unconventional hydrocarbon resource. In particular, this source rock was assessed by estimating key shale play properties including total organic carbon (TOC), total porosity, water saturation and brittleness. Due to the wide separation of the drilled wells penetrating the middle Ordovician unit (Goldwyer formation) in the Canning Basin, the study was limited to the Barbwire Terrace, a sub-division of the Canning Basin.

Alshakhs (2017) used the available well data and testing different estimation methods in estimating each of the key shale play properties outlined above. TOC was estimated from multiple regressions of different well data. Water saturation was estimated using a simplified Archie's equation. Total porosity was estimated using the density porosity method, whereas sonic and density data was used to estimate brittleness index.

Alshakhs (2017) went forward to model each of the four shale properties across the Goldwyer formation in the Barbwire terrace. The models allowed the estimation of the propagation of the above shale gas properties in the Goldwyer formation. Sweet spot maps were generated by combining the average maps of the modelled shale properties in a weighted manner. A similar approach was applied in the present study where rock deformation properties were modelled and mapped across the study area and sweet spot maps generated by combining the rock deformation properties in a weighted manner. However, while Alshakhs (2017) used four shale play properties including TOC, water saturation, total porosity and brittleness to generate sweet spot maps, while the current study focused on six elastic rock properties including Poisson's ratio, Young's modulus, Mu.Rho, Lambda.Rho, bulk modulus and shear modulus to generate the brittleness index and sweet spot maps.

Alshakhs (2017) reported TOC and porosity as the most critical factors in the assessment of shale play prospectivity, particularly the Goldwyer formation. Based on the sweet spot maps, he further reported the upper Goldwyer formation and the lower parts of the lower Goldwyer Formation as the most prospective shale play zones in the Goldwyer source rock. This is confirmed in the present study where the lithological units between the top and base Goldwyer, particularly those around the Fruitcake-1 and Missing-1 wells were found to be the most prospective.

6.2 Result, Discussions and Evaluations

As interest in the exploitation of unconventional hydrocarbon resources continues to increase, there is a great need to develop tools and methods that can be used to aid in the quick assessment of the prospectivity of such unconventional resources. Unconventional resources are characterized by low permeability and are located deep in the earth's crust as compared to the conventional hydrocarbon resources. From the foregoing, modeling of the key shale properties that characterize such unconventional resources and the generation of brittleness index and sweet spot maps is gaining popularity as a quick method for assessing the prospectivity of unconventional hydrocarbon resources.

Alshakhs (2017) may have laid the foundation for the application of the above approach in assessing the prospectivity of the Goldwyer formation in the Canning Basin as a potential hydrocarbon resource. Although different well log data was used, similar prospectivity results were reported in both the latter and in the present study. In the present study, the prospectivity assessment of the Goldwyer formation was enhanced by the availability of seismic data. This highlights the power of the generation of sweet spot maps through shale play's property modeling as a tool for prospectivity assessment.

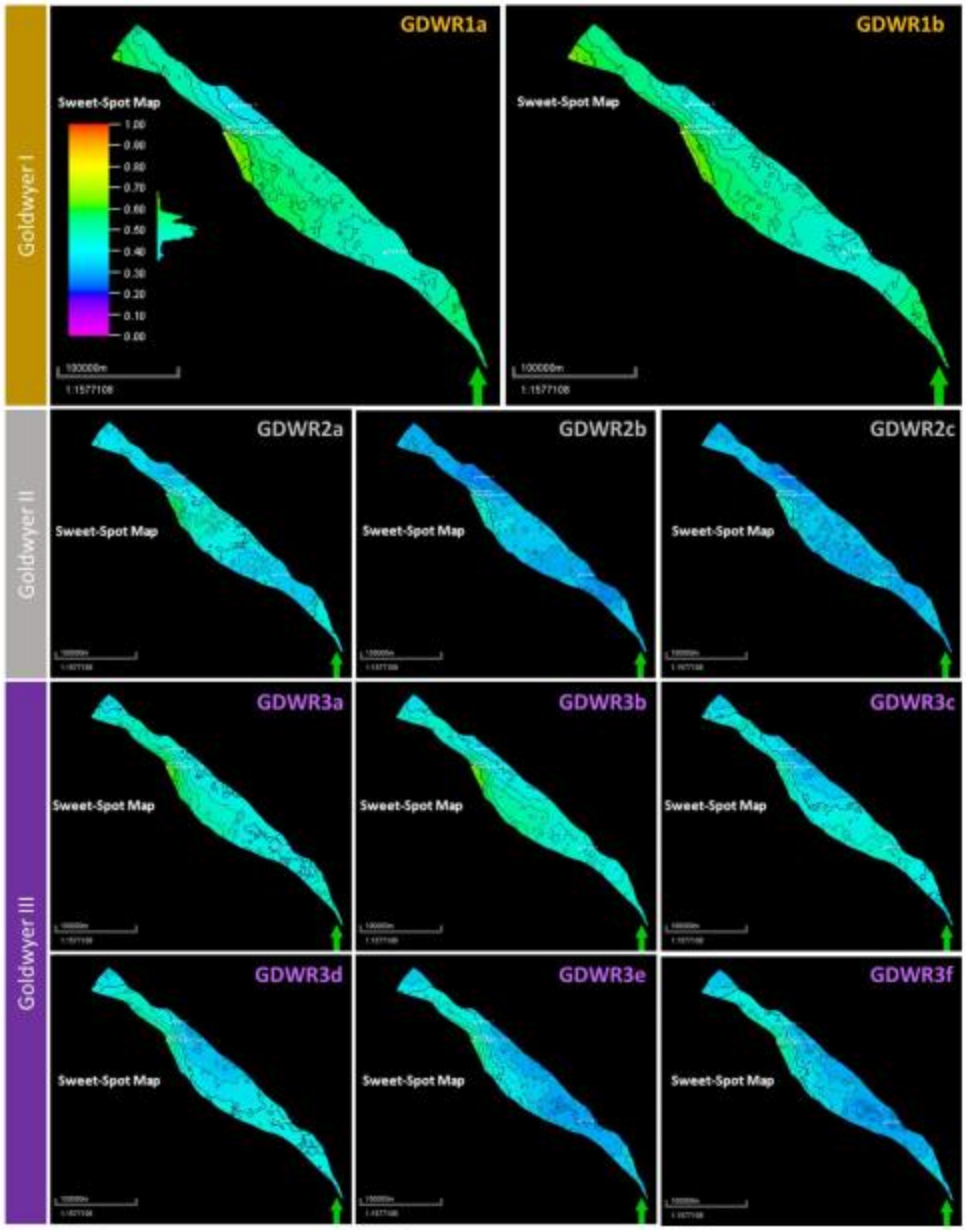

Figure 6.1: *Sweet spot maps for all Goldwyer zones in the Canning Basin Barbwire terrace as reported by Alshakhs (2017).*

6.3 Conclusions

The study has provided a modified approach for mapping the in-situ approach and other rock elastic properties in shale gas reservoirs. The elastic parameters considered include Poisson's ratio,

Young's modulus, Mu.Rho, Lambda.Rho, bulk modulus, shear modulus as well as brittleness index which is derived from the rest of the elastic properties. The Canning Basin in Western Australia was taken as the study area.

The study has provided a method for quickly predicting and estimating the in-situ rock elastic properties, particularly by establishing correlation equations between the dynamic and static rock elastic properties. The dynamic rock properties are determined using sonic logs, whereas the static properties are obtained from direct measurements of core samples. By utilizing the predicted static and actual dynamic rock elastic parameters, in-situ brittleness was predicted.

The study further modelled and mapped the rock deformation parameters across the study area. The modeling allowed for the geostatistical estimation of the propagation of the different properties across the study area. Sweet spots were identified from brittleness index maps that were generated by combining the modelled rock deformation parameters in a weighted manner.

To improve the accuracy of precise mapping and interpreting rock deformation parameters, the study performed seismic inversion and generated models of the different rock elastic properties derived from seismic inversion results. A high correlation was noted between the synthetic models and the actual seismic traces. The rock elastic properties derived from seismic inversion results were then combined in a weighted manner to generate sweet spot maps.

From the sweet spot maps, the lithological units around the Fruitcake-1 and Missing-1 wells in the Goldwyer formation were found to be more prospective as compared to the Goldwyer formation units around the Canopus-1 and Looma-1 wells. This approach was found to be effective in assessing the prospectivity of unconventional hydrocarbon resources as it had been successfully interpreted by previous scholars in similar endeavors. However, the sweet spot maps/brittleness

index maps should not be taken as conclusive tools and they represent the rock defining properties in a weighted. Efforts should be made to interpret the individual shale play properties before making the final decision.

6.4 Recommendations

The current study has presented a modified approach for mapping in situ rock brittleness index and other rock elastic properties in shale gas reservoirs. This allows the generation of brittleness index maps that aids in the identification of potential sweet spots. In addition, a method for quickly predicting in-situ static elastic properties from their dynamic counterparts was presented. This study was limited to the Canning Basin, particularly the Goldwyer formation. Due to the non-uniqueness of shale properties from different basins, this approach is recommended to be extended to other basins containing potential unconventional hydrocarbon resources. In addition, the present study only focused on the modeling and mapping of rock deformation properties across the study area. It would be paramount to understand the economics of production for the Goldwyer shale, thus, production economics for the Goldwyer shale should be investigated in future studies. Future studies could also focus on assessing the possibility of hydraulic fracturing of the Goldwyer shale and the associated risks.

References

Aldrich, J. B., & Seidle, J. P. (2019). Sweet Spot Identification and Optimization in Unconventional Reservoirs. *Mountain Geologist*, *52*(3), 5-12.

Aliouane, L., & Ouadfeul, S. A. (2014). Sweet spots discrimination in shale gas reservoirs using seismic and well-logs data. A case study from the Worth Basin in the Barnett Shale. *Energy Procedia*, *59*, 22-27.

Alshakhs, M. (2017). *Shale Play Assessment of the Goldwyer Formation in the Canning Basin Using Property Modeling* (Doctoral dissertation, Curtin University).

Andrä, H., Combaret, N., Dvorkin, J., Glatt, E., Han, J., Kabel, M., & Marsh, M. (2013). Digital rock physics benchmarks—Part II: Computing effective properties. *Computers & Geosciences*, *50*, 33-43.

Bacon, M., Simm, R., Redshaw, T., & ProQuest (Firm). (2007). *3-D seismic interpretation*. Cambridge: Cambridge University Press.

Britt, L. K., & Schoeffler, J. (2009, January). The geomechanics of a shale play: what makes a shale prospective? In *SPE eastern regional meeting*. Society of Petroleum Engineers.

Burianyk, M. (2019). *Understanding signals: Basic waveform analysis from a geophysical perspective*. Tulsa, OK: Society of Exploration Geophysicists.

Burt, A., Champ, P., & Parks, A. (2002). *Petroleum Prospectivity of the Eastern Canning Basin, WA*. Government of Western Australia: Department of Mineral and Petroleum Resources.

Cannon, S. (2018). *Reservoir modeling: A practical guide*. Hoboken, NJ: John Wiley & Sons, Inc.

Carlson, M. R. (2003). *Practical reservoir simulation: Using, assessing, and developing results*. Tulsa, Okla: PennWell.

Carstens, H. (2014, January 21). A World of Plenty. Retrieved from https://www.geoexpro.com/articles/2013/08/a-world-of-plenty

Chang, C., Zoback, M. D., & Khaksar, A. (2006). Empirical relations between rock strength and physical properties in sedimentary rocks. *Journal of Petroleum Science and Engineering*, *51*(3-4), 223-237.

Chen, Z., Yang, H., Wang, J., Zheng, T., Jing, P., Li, S., & Chen, C. (2016). Application of high-precision 3D seismic technology to shale gas exploration: A case study of the large Jiaoshiba shale gas field in the Sichuan Basin. *Natural Gas Industry B*, *3*(2), 117-128.

Chopra, S., Marfurt, K. J., & Society of Exploration Geophysicists. (2007). *Seismic attributes for prospect identification and reservoir characterization*. Tulsa, OK: Society of Exploration Geophysicists.

Chopra, S., Sharma, R. K., Nemati, H., & Keay, J. (2018). Seismic reservoir characterization of Utica-Point Pleasant Shale with efforts at quantitative interpretation - A case study: Part 1. Interpretation, 6(2), T313-T324.

Ciccotti, M., & Mulargia, F. (2004). Differences between static and dynamic elastic moduli of a typical seismogenic rock. *Geophysical Journal International*, *157*(1), 474-477.

Cui, X., Lines, L., Krebes, E. S., & Peng, S. (2018). *Seismic Forward Modeling of Fractures and Fractured Medium Inversion*. Singapore: Springer.

Darling, T. (2005). *Well logging and formation evaluation*. Amsterdam: Elsevier.

Dewhurst, D. N., & Siggins, A. F. (2006). Impact of fabric, microcracks and stress field on shale anisotropy. *Geophysical Journal International*, *165*(1), 135-148.

Eissa, E. A., & Kazi, A. (1988). Relation between static and dynamic Young's moduli of rocks. *International Journal of Rock Mechanics and Mining & Geomechanics Abstracts*, *25*(6).

Geoscience Australia. (2014, 5) Canning Basin. Retrieved from http://www.ga.gov.au/scientific-topics/energy/province-sedimentary-basin-geology/petroleum/offshore-northwest-australia/canning

Ghorbani, A., Zamora, M., & Cosenza, P. (2009). Effects of desiccation on the elastic wave velocities of clay-rocks. *International Journal of Rock Mechanics and Mining Sciences*, *46*(8), 1267-1272.

Glaser, K. S., Miller, C. K., Johnson, G. M., Toelle, B., Kleinberg, R. L., Miller, P., & Pennington, W. D. (2013). Seeking the sweet spot: Reservoir and completion quality in organic shales. Oilfield Review, 25(4), 16-29.

Goodway, B., Chen, T., & Downton, J. (1997). Improved AVO fluid detection and lithology discrimination using Lamé petrophysical parameters; "λρ", "μρ", & "λ/μ fluid stack", from P and S inversions. In *SEG Technical Program Expanded Abstracts 1997* (pp. 183-186). Society of Exploration Geophysicists.

Gray, D., Anderson, P., Logel, J., AS, T. E. N., Delbecq, F., & Schmidt, D. (2010). Principle stress estimation in shale plays using 3D seismic. *Calgary, Alberta, Canada, GeoCanada*.

Jacobi, D. J., Gladkikh, M., LeCompte, B., Hursan, G., Mendez, F., Longo, J., & Shoemaker, P. (2008, January). Integrated petrophysical evaluation of shale gas reservoirs. In *CIPC/SPE Gas Technology Symposium 2008 Joint Conference*. Society of Petroleum Engineers.

Josh, M., Esteban, L., Delle Piane, C., Sarout, J., Dewhurst, D. N., & Clennell, M. B. (2012). Laboratory characterization of shale properties. *Journal of Petroleum Science and Engineering*, *88*, 107-124.

Khan, I., Ismail, A., & Ali, I. (2018, September). Identification of brittle and ductile zones in sandstone reservoir using well log analysis; a case study, Southern Indus Basin, Pakistan. In IOP Conference Series: Materials Science and Engineering (Vol. 414, No. 1, p. 012021). IOP Publishing.

Mavko, G., Mukerji, T., & Dvorkin, J. (2003). *The rock physics handbook: Tools for seismic analysis in porous media*. Cambridge: Cambridge University Press.

Misra, A. A., & Mukherjee, S. (2018). *Atlas of structural geological interpretation from seismic images*. Hoboken, NJ Wiley Blackwell.

Mussett, A. E., & Khan, M. A. (2000). *Looking into the earth: an introduction to geological geophysics*. Cambridge University Press.

Nicoll, R. S., Laurie, J. R., Kelman, A. P., Mantle, D. J., Haines, P. W., Mory, A. J., & Hocking, R. M. (2009). Canning Basin biozonation and stratigraphy. *Geoscience Australia Chart*, *31*.

Ogiesoba, O. (2016). Application of the Instantaneous Quality Factor (Q) in the characterization of the Austin Chalk and Eagle Ford Shale, South Texas. AAPG Search and Discovery, 41781.

Ogiesoba, O. C., & Eastwood, R. (2013). Seismic multiattribute analysis for shale gas/oil within the Austin Chalk and Eagle Ford Shale in a submarine volcanic terrain, Maverick Basin, South Texas. Interpretation, 1(2), SB61-SB83.

Ogiesoba, O., & Hammes, U. (2014). Seismic-attribute identification of brittle and TOC-rich zones within the Eagle Ford Shale, Dimmit County, South Texas. Journal of Petroleum Exploration and Production Technology, 4(2), 133-151.

Ouenes, A., Bachir, A., & Boukhelf, D. (2014, February). Estimation of stimulated reservoir volume using the concept of shale capacity and its validation with microseismic and well performance. In *SPE/EAGE European Unconventional Resources Conference and Exhibition*.

Perez Altamar, R., & Marfurt, K. J. (2015). Identification of brittle/ductile areas in unconventional reservoirs using seismic and microseismic data: Application to the Barnett Shale. *Interpretation*, *3*(4), T233-T243.

Qian, K. R., He, Z. L., Liu, X. W., & Chen, Y. Q. (2018). Intelligent prediction and integral analysis of shale oil and gas sweet spots. Petroleum Science, 15(4), 744-755.

Rezaee, R. (2015). Fundamentals of gas shale reservoirs. Hoboken, New Jersey: John Wiley and Sons, Inc.

Rickman, R., Mullen, M. J., Petre, J. E., Grieser, W. V., & Kundert, D. (2008, January). A practical use of shale petrophysics for stimulation design optimization: All shale plays are not clones of the Barnett Shale. In *SPE annual technical conference and exhibition*. Society of Petroleum Engineers.

Ringrose, P., & Bentley, M. (2015). *Reservoir Model Design: A Practitioner's Guide*. Springer Netherlands.

Russell, B. H., & Society of Exploration Geophysicists. (1988). *Introduction to seismic inversion methods*. Tulsa, Okla: Society of Exploration Geophysicists.

Schlumberger. (2020). *Petrel geology & modeling*. (n.d.). Schlumberger Software. https://www.software.slb.com/products/petrel/petrel-geology-and-modeling

Sena, A., Castillo, G., Chesser, K., Voisey, S., Estrada, J., Carcuz, J., & Hodgkins, P. (2011). Seismic reservoir characterization in resource shale plays: Stress analysis and sweet spot discrimination. *The Leading Edge*, *30*(7), 758-764.

Sharma, R. K., & Chopra, S. (2016). Identification of sweet spots in shale reservoir formations. *First break*, *34*(9), 43-51.

Simm, R., Bacon, M., & Bacon, M. (2014). *Seismic Amplitude: An interpreter's handbook*. Cambridge University Press.

Sun, Y., Sun, S. Z., Liu, Z., Dong, N., Liu, J., Xia, H., & Du, Z. (2014, June). A New Shale Gas Evaluation Method Using Isotropic Approximation Based on Modified Xu-Payne Model. In 76th EAGE Conference and Exhibition 2014 (Vol. 2014, No. 1, pp. 1-5). European Association of Geoscientists & Engineers.

Tahmasebi, P., Javadpour, F., & Sahimi, M. (2017). Data mining and machine learning for identifying sweet spots in shale reservoirs. Expert Systems with Applications, 88, 435-447.

Wang, Z. (2000). Dynamic versus static elastic properties of reservoir rocks. *Seismic and acoustic velocities in reservoir rocks*, *3*, 531-539.

Warlick, D. (2006). Shale gas and CBM development in North America. *Oil and Gas Financial Journal*, *3*(11), 1-5.

Woodhouse, R. (2003). *Statistical regression line-fitting in the oil & gas industry: A descriptive guide with Microsoft Excel examples*. Tulsa, Okla: PennWell Corp.

Xu, H., Zhou, W., Xie, R., Da, L., Xiao, C., Shan, Y., & Zhang, H. (2016). Characterization of rock mechanical properties using lab tests and numerical interpretation model of well logs. *Mathematical Problems in Engineering*, *2016*.

Yilmaz, O., Doherty, S. M., Yilmaz, O., & Society of Exploration Geophysicists. (2001). *Seismic data analysis: Processing, inversion, and interpretation of seismic data*. Tulsa, OK: Society of Exploration Geophysicists.

Zoback, M. D. (2010). *Reservoir geomechanics*. Cambridge University Press.

Zoback, M. D., Barton, C. A., Brudy, M., Castillo, D. A., Finkbeiner, T., Grollimund, B. R., & Wiprut, D. J. (2003). Determination of stress orientation and magnitude in deep wells. *International Journal of Rock Mechanics and Mining Sciences*, *40*(7-8), 1049-1076.

STATEMENT OF ORIGINAL WORK

The author declares no conflict of interest with the foregoing research activity.